

Imperial College London

University of London

MODAL ANALYSIS OF ROTATING
MACHINERY STRUCTURES

by

ENRIQUE SIMON GUTIERREZ-WING

A thesis submitted to the University of London
for the degree of Doctor of Philosophy

Department of Mechanical Engineering
Imperial College London

September 2003

Abstract

A new method for the modal characterisation of rotating machinery structures is presented. The method accounts for the effects of gyroscopic and other forces related to rotation, which are associated with the asymmetry of the damping and stiffness matrices of rotating machinery. By comparison with other methods with the same feature, the new method has the advantage that it does not require the measurement of a complete row of the frequency response function (FRF) matrix.

The new method is based on the modelling of rotating machines as structural assemblies of rotating and non-rotating components. This approach allows the separation of their damping and stiffness matrices into symmetric and asymmetric portions, which consist of the rows and columns associated with the degrees of freedom of non-rotating and rotating components, respectively. The symmetric portions are used to derive mathematical relationships between the modal parameters. These relationships, in turn, are used to supplement FRF data obtained from modal tests. In this way, the amount of measured data required for a complete modal characterisation is reduced.

It is shown that, in most practical cases, only a small number of the FRFs from one row of the FRF matrix are required, in addition to those from one column. Thus, the difficulties of applying controlled excitation forces onto rotating components, for the measurement of one complete row, may be circumvented.

The theoretical soundness of the method is demonstrated using a numerical example, and its practical application is illustrated through the modal characterisation of an industrial test-rig. Some issues regarding its practical implementation are discussed.

It is concluded that, through the reduction of the required number of FRF measurements, the new method enables the modal characterisation of rotating machinery structures in less time and with less effort than are required with the use of other current methods.

*To my Parents, Juventina and Horacio,
with all my love*

Acknowledgements

I would like to thank my supervisors, Prof. David Ewins and Mr. David Robb, for the guidance and support they provided me with throughout this research project, as well as the many members of the Dynamics Section at Imperial College with whom I had the pleasure of working during the last years. Special thanks to Mr. Anthony Stanbridge for his contributions to the experimental part of the thesis, and to the Section's technicians, Mr. Paul Woodward and Mr. John Miller, for their advise and expertise, which proved so useful in getting things done.

A word of appreciation is due to Dr. Jorge E. Aguirre Romano, with whom I had the fortune of working in the years leading to my Ph.D. course, and who provided me with much of the technical knowledge that has helped me bring this project to a conclusion.

I feel in debt to my colleagues Anantawit Tuchinda, Suresh Nayagam and Gan Chen for their friendship and interesting points of view, research-related or not, that were so valuable in getting me through the difficult stages of this work. Many thanks also to my friends and colleagues: Marija, Gigliola, Sen, Hugo, Ibrahim, Dario and Matthew, who made my College life especially enjoyable.

I would like to express my sincere gratitude to Miss Veronika Wirtz, who through the years encouraged me with her understanding, enthusiasm and hard work, making an enormous difference in every aspect of my life.

Finally, I would like to thank the Consejo Nacional de Ciencia y Tecnología and the Centro Nacional de Investigación y Desarrollo Tecnológico of México for the funding they provided for this research project.

Contents

ABSTRACT	<i>ii</i>
ACKNOWLEDGEMENTS	<i>iv</i>
CONTENTS	<i>v</i>
LIST OF FIGURES	<i>ix</i>
LIST OF TABLES	<i>xi</i>
NOMENCLATURE	<i>xii</i>
CHAPTER 1 – Introduction	1
1.1 Rotating machinery structures	1
1.2 Definition of the problem	2
1.3 Objectives of the research work	5
1.4 Scope of the research	6
1.5 Existing results of research	6
1.5.1 Results of theoretical research	7
1.5.1.1 ‘Loss’ of reciprocity in rotating machinery	7
1.5.1.2 Mathematical models	10
1.5.2 Results of experimental and experimentally-oriented research	11
1.5.2.1 Estimation of modal parameters from measurements	11
1.5.2.2 Excitation of rotating machinery components	13
1.6 Overview of the thesis	15
CHAPTER 2 - Spatial models of rotating machinery structures	18
2.1 Introduction	18
2.2 The damping and stiffness matrices of rotating machinery structures	20
2.3 Nomenclature for rotation-related forces	21
2.4 Representation of circulatory forces	22
2.5 Influence of coordinate frame selection on the matrix representation of non-circulatory and circulatory forces	30

2.5.1	Representation of non-circulatory forces	30
2.5.2	Representation of circulatory forces.....	32
2.6	Orthogonal coordinate frames.....	33
2.6.1	Axes of motion	34
2.6.2	Orthogonality of two axes of motion.....	34
2.6.3	Orthogonality in flexible systems.....	37
2.7	Summary	39
 CHAPTER 3 – Modal and response models of rotating machinery structures ...		40
3.1	Introduction.....	40
3.2	The modal model.....	40
3.2.1	Modal parameters	41
3.2.2	Eigenvector normalisation.....	42
3.3	The response model.....	44
3.4	Relationships between the spatial and modal models	45
3.5	Relationships between the response and modal models	46
3.6	Physical interpretation of the relationships between the spatial and modal models.....	47
3.7	Summary	51
 CHAPTER 4 - Estimation of the modal properties of rotating machinery structures from measured vibration data		52
4.1	Introduction.....	52
4.2	Evaluation of the ‘column-row’ method.....	53
4.3	Rotating machines as structural assemblies	55
4.4	Overview of the proposed characterisation method.....	56
4.5	Equations for the computation of the left eigenvectors	57
4.5.1	Effects of matrix symmetry on the relationships between the spatial and modal models	59
4.5.1.1	Matrix symmetry and partial symmetry.....	59
4.5.1.2	Relationships between the modal parameters	61
4.5.2	Normalisation equation	63
4.5.2.1	Modal parameter estimation	64
4.5.2.2	Derivation of the normalisation equation.....	66
4.6	Computation of the left eigenvectors	67
4.6.1	The Kronecker product.....	68

4.6.2	Transformation of matrix equations into canonical form.....	68
4.6.3	Canonical form of the equations for the computation of the left eigenvectors.....	70
4.6.4	Conditions for the existence of a unique solution	72
4.6.4.1	Total number of equations	73
4.6.4.2	Required number of measurements.....	76
4.6.4.2.1	Description of the trial system models.....	76
4.6.4.2.2	Use of the trial system models	77
4.7	Two special cases.....	78
4.8	Damped gyroscopic systems.....	79
4.9	Use of the characterisation method.....	82
CHAPTER 5 – Case studies		84
5.1	Introduction.....	84
5.2	Case study 1: numerical model of a 4-DOF rigid rotor	85
5.2.1	Required FRFs.....	88
5.2.2	Modal analysis of the FRF data.....	89
5.2.3	Eigenvector normalisation.....	91
5.2.4	Results	93
5.2.5	Discussion.....	93
5.3	Case study 2: the “windmill test-rig”	95
5.3.1	Test plan	96
5.3.1.1	Predictive method approach.....	97
5.3.1.2	Direct identification of the left eigenvectors from measurements.....	97
5.3.2	Scope of the characterisation.....	102
5.3.3	Selection of the speed of rotation	106
5.3.3.1	Factors considered.....	106
5.3.3.2	Effects of rotation on the behaviour of the test structure.....	106
5.3.4	Execution of the tests.....	108
5.3.4.1	Speed control.....	108
5.3.4.2	Excitation	108
5.3.4.3	Response measurement	109
5.3.4.4	Signal conditioning	110
5.3.4.5	Signal processing	110
5.3.4.6	Transducer calibration.....	111

5.3.5	FRF measurements	114
5.3.6	Modal analysis of the measured FRFs.....	115
5.3.7	Data reduction and computation of the left eigenvectors.....	116
5.3.8	Results	118
5.3.9	Discussion.....	120
5.3.9.1	Errors in the prediction of the left eigenvectors.....	120
5.3.9.2	Prediction of FRFs corresponding to unmeasured columns of the FRF matrix	122
5.3.9.3	Simplified prediction of the left eigenvectors.....	126
5.3.9.4	Use of non-optimal DOFs	129
5.4	Summary	131
CHAPTER 6 - Summary, conclusions and recommendations for future work...		133
6.1	Summary	133
6.2	Conclusions.....	135
6.3	Recommendations for future work.....	141
6.3.1	Characterisation of systems with close modes	141
6.3.2	Use of residuals for the analysis of continuous systems	142
6.3.3	Diversification of the experimental trials.....	143
APPENDIX A - Row elements of the FRF matrix required for computation of the left eigenvectors		144
APPENDIX B - Relationship between the modal constants of hysteretically and viscously damped system models		146
APPENDIX C - Modal parameters of the “windmill test-rig”		148
REFERENCES.....		149

List of figures

Figure 2.1	Components of the damping and stiffness matrices.....	23
Figure 2.2	Hydrodynamic bearing with shaft journal in its static equilibrium position.....	25
Figure 2.3	Hydrodynamic bearing with shaft journal displaced along the x_1 axis	25
Figure 2.4	Hydrodynamic bearing with shaft journal displaced along the x_2 axis	27
Figure 2.5	Vector field representation of the stiffness characteristic of a journal-bearing system	28
Figure 2.6	Vector field representation of the (a) non-circulatory and (b) circulatory ‘stiffness’ characteristics of a journal-bearing system.....	29
Figure 2.7	2-DOF spring-mass system	31
Figure 2.8	Coordinate systems for the study of a hydrodynamic bearing.....	33
Figure 2.9	Definition of (a) orthogonal and (b) non-orthogonal axes	35
Figure 2.10	Flexibly-supported rigid ring	37
Figure 4.1	Dynamic stiffness matrix, $[Z]$, of a rotating machine	56
Figure 4.2	Structure of the stiffness matrix	59
Figure 5.1	4-DOF rigid rotor	86
Figure 5.2	FRFs of a 4-DOF rigid rotor	88
Figure 5.3	The “windmill test-rig”	97
Figure 5.4	Point FRFs at two different locations.....	99
Figure 5.5	Point FRFs for two senses of rotation	101
Figure 5.6	Equivalence of inverting the sense of rotation and exchanging the excitation and measurement locations for transfer FRFs	101
Figure 5.7	Point FRFs used for frequency range selection.....	103

Figure 5.8	Enlarged view of the selected frequency range.....	104
Figure 5.9	Variation of the first natural frequency due to exciter attachment.....	105
Figure 5.10	Effect of gyroscopic forces on the behaviour of the test structure.....	107
Figure 5.11	Attachment of the electromagnetic exciter.....	108
Figure 5.12	Transducers used for measurements on (a) stationary, and (b) rotating components of the test structure	109
Figure 5.13	(a) Use of an LDV as a calibration reference,(b) mounting of an accelerometer for calibration.....	112
Figure 5.14	(a) Attachment of the exciter to the force transducer, (b) mounting of the calibrated accelerometer.....	113
Figure 5.15	Test DOFs on the (a) front side and (b) back side of the test structure	114
Figure 5.16	FRFs from one column of the FRF matrix	114
Figure 5.17	Prediction of the accelerance at DOF 25 due to an excitation at DOF 26	124
Figure 5.18	Prediction of the accelerance at DOF 25 due to an excitation at DOF 23	125
Figure 5.19	Prediction of the response at DOF 25 due to an excitation at DOF 24	125
Figure 5.20	Prediction of the response at DOF 25 due to an excitation at DOF 6 ...	126
Figure 5.21	Prediction of the response at DOF 25 due to an excitation at DOF 13	127
Figure 5.22	Prediction of the response at DOF 25 due to an excitation at DOF 26 using the right eigenvectors only	128
Figure 5.23	Prediction of the response at DOF 25 due to an excitation at DOF 26 using the right eigenvectors and their complex conjugates.....	129
Figure 5.24	Prediction of the response at DOF 25 due to an excitation at DOF 26 computed with DOFs 3, 4, 23, 24, 25 and 26.....	130
Figure 5.25	Prediction of the response at DOF 25 due to an excitation at DOF 26 computed with DOFs 3, 4, 9, 12, 25 and 26.....	131

List of tables

Table 5.1	Estimated natural frequencies and hysteretic damping factors.....	89
Table 5.2	Estimated modal constants for a hysteretic damping model.....	89
Table 5.3	Estimated natural frequencies and critical viscous damping ratios	90
Table 5.4	Comparison of modal constants $\times 10^3$, for a viscous damping model...	91
Table 5.5	Estimated elements of the normalised right and left eigenvectors	93
Table 5.6	Comparison of left eigenvector elements	94
Table 5.7	Natural frequencies at 831 rev/min, CCW.....	103
Table 5.8	Comparison of the natural frequencies (Hz) of the test structure in stationary and rotating conditions.....	107
Table 5.9	Evaluation of DOFs based on the effective independence algorithm....	118
Table 5.10	Comparison between two theoretically equivalent sets of eigenvectors	119
Table A.1	Required row elements, q , of the FRF matrix for a 15-DOF system....	145
Table C.1	Modal parameters of the “windmill test-rig”	149

Nomenclature

1. Latin and Arabic symbols

$\{0\}, [0], [0]_{4 \times 6}$	Vector, square matrix and rectangular matrix of zeros
a_{ij}	Element of the i row and the j column of matrix $[A]$
$[A], [B], [U], [V], [W]$	Rectangular matrices
$[A_G]$	Matrix of coefficients for the computation of the left eigenvectors
${}_r A_{jk}$	Modal constant of a viscously-damped system model for the r th mode, j th response measurement and k th excitation locations
${}_r \tilde{A}_{jk}$	Modal constant of a hysteretically-damped system model for the r th mode, j th response measurement and k th excitation locations
$\{b\}$	Non-homogeneous term of a linear system of equations
$[C]$	Damping matrix
d	Effective distance travelled by a force
d_{kk}	Element of a diagonal matrix in the k th row and the k th column
$[D]$	Diagonal matrix
$[D_L]$	Diagonal matrix that relates the normalised and non-normalised versions of the left eigenvectors
$[D_R]$	Diagonal matrix that relates the normalised and non-normalised versions of the right eigenvectors
e	Natural logarithm base
\hat{e}_1, \hat{e}_2	Unit base vectors

\vec{f}	Force vector
$\{f(t)\}$	Time-domain force vector
\vec{F}_R, F_R	Resultant of hydrodynamic pressure forces, magnitude thereof
$\{F(\omega)\}$	Vector of force amplitudes in the frequency domain
$\{g\}$	Vectorised form of matrix $[G]$
$\{g_1\}, \{g_2\}, \{g_3\}$	Column vectors of matrix $[G]$
$\{g_T\}$	Vectorised form of the transpose of matrix $[G]$
$[G]$	Transposed inverse of the normalised left eigenvector matrix
$H_{j,k}$	Accelerance frequency response function corresponding to a response measured at DOF j and an excitation force applied at DOF k
i	Imaginary unit ($=\sqrt{-1}$)
$i, j, k, k_0, k_1, k_2, r$	Integer indexes
$\{i_G\}$	Vectorised form of matrix $[I_G]$
$[I_C], [I_K]$	Symmetry selection matrices for the damping and stiffness symmetric equations
$[I_G]$	Symmetry selection matrix for the normalisation equation
$[I]_{N \times N}, [I]_{2N \times 2N}$	Identity matrices of orders N and $2N$
$[\mathcal{J}(\omega)], [\mathcal{J}_0(\omega)]$	Rate of change of accelerance, or jerk, matrix
k_1, k_2	Spring stiffness coefficients
k_{ij}	Element in the i th row and the j th column of the stiffness matrix
$[K]$	Stiffness matrix
$[K_A], [K_B]$	Support stiffness matrices
$[K]_{CIRCULATORY} \Big _{x_1, x_2}$	Circulatory components of the stiffness matrices in the x_1, x_2 coordinate system

$[K]_S, [K]_{SS}$	Symmetric and skew-symmetric components of the stiffness matrix
$[K] _{x_1x_2}, [K] _{x'_1x'_2}$	Stiffness matrices in the x_1x_2 and $x_1x'_1$ coordinate systems
m	Mass
m, n, p, q	Dimensions of rectangular matrices
$[M]$	Mass matrix
n	Integer number
n_c, n_k	Dimension of the asymmetric regions of the damping and stiffness matrices
N	System order
p_c, p_k, p_m	Number of equations obtained from the symmetric portions of the damping, stiffness and mass matrices
p_g	Number of equations obtained from the normalisation equation
$p_{l.i.}$	Number of linearly independent equations
p_{total}	Total number of equations
$[P]_{N^2 \times N^2}$	Permutation matrix for a matrix of order N
q	Required number of FRF matrix row measurements
r_{21}	Component of vector \hat{e}_2 along the direction of vector \hat{e}_1
t	Time
$[T]$	Coordinate transformation matrix
$[U_C(\Phi_R, \lambda)], [U_C]$	Matrix of the eigenvalue and right-eigenvector components of the mass matrix / simplified notation
$[U_K(\Phi_R, \lambda)], [U_K]$	Matrix of the eigenvalue and right-eigenvector components of the stiffness matrix / simplified notation
$[U_M(\Phi_R, \lambda)], [U_M]$	Matrix of the eigenvalue and right-eigenvector components of the damping matrix / simplified notation

$x_1, x_2, x_3, x_4, x_1', x_2'$	Geometric coordinates
$\{x(t)\}, \{\dot{x}(t)\}, \{\ddot{x}(t)\}$	Time-domain vectors of displacements, velocities and accelerations
$\{X(\omega)\}$	Vector of displacement amplitudes in the frequency domain
$\{y\}$	Vector of unknowns in a linear system of equations
$[Z]$	Dynamic stiffness matrix

2. Greek symbols

$[\alpha(\omega)]$	Receptance matrix
$\alpha_{jk}(\omega), \alpha_{jk}$	Element of the receptance matrix for the j th response measurement and k th excitation locations / simplified notation
β, θ	Angle between two coordinate axes
$[\Phi_G]$	Transposed matrix of rows of the normalised left eigenvector matrix
$\{\Phi_G\}_{k_0}$	k_0 th Column of matrix $[\Phi_G]$
$[\Phi_L], [\Phi_R]$	Normalised left and right eigenvector matrices
$[\tilde{\Phi}_L], [\tilde{\Phi}_R]$	Space-state matrices of normalised left and right eigenvectors
$[\Phi_{L1}], [\Phi_{L2}]$	‘Displacement’ components of the space-state left eigenvector matrix
$(\Phi_L)_{kr}, (\Phi_R)_{kr}$	k th elements of the left and right eigenvectors of the r th mode
$[\Phi_{R1}], [\Phi_{R2}]$	‘Displacement’ components of the space-state right eigenvector matrix
η_r	Hysteretic damping loss factor
$[\lambda], [\tilde{\lambda}]$	Eigenvalue matrix and its state-space representation

$[\lambda_1], [\lambda_2]$	$N \times N$ state-space eigenvalue submatrices
$[\lambda_{KM}], [\lambda_{MK}]$	Matrices of eigenvalues of $([U_K]^{-1}[U_M])^T$ and $([U_M][U_K]^{-1})$
λ_r	Eigenvalue of the r th mode
ω	Excitation frequency
$\omega_r, \bar{\omega}_r$	Undamped and damped natural frequencies of the r th mode
Ω	Speed of rotation
$[\Psi_{KM}], [\Psi_{MK}]$	Matrix of right eigenvectors of $([U_K]^{-1}[U_M])^T$ and $([U_M][U_K]^{-1})$
$[\Psi_L], [\Psi_R]$	Matrix of non-normalised left and right eigenvectors
$[\tilde{\Psi}_L], [\tilde{\Psi}_R]$	Space-state matrices of non-normalised left and right eigenvectors
$\{\Psi_L\}_r, \{\Psi_R\}_r$	Non-normalised left and right eigenvectors of the r th mode
ζ_r	Critical viscous damping ratio of the r th mode

3. Other symbols and operators

$\{ \}$	Vector
$[\]$	Matrix
$^{-1}$	Matrix inversion
T	Matrix transposition
$*$	Complex conjugation
$\text{Re}([\])$	Real part of a complex matrix
$\min(n_c, n_k), \max(n_c, n_k)$	The smallest and largest of n_c and n_k

CHAPTER 1

Introduction

1.1 Rotating machinery structures

Modal models are widely used to describe the dynamic behaviour of non-rotating structures. The methods by which these models are obtained have been refined through many years of use, and have now reached an advanced stage of development [14]. These methods can be extended to the study of rotating machinery dynamics.

For modelling purposes, rotating machines can be considered as structural assemblies of rotating and non-rotating components. The dynamic behaviour of these assemblies is determined by the properties of their individual components and their interactions, as is the case for conventional structures formed by the assembly of purely non-rotating elements.

The use of a structural approach to the study of rotating machinery dynamics allows us to model their dynamic behaviour based exclusively on their response to controlled excitation forces, without focusing on the interactions between their components. Thus, by taking the effects of rotation into account, modal analysis and testing methods that were originally designed for conventional, non-rotating, structures can be adapted for their use with rotating machinery.

The research work reported in this thesis deals with the adaptation of conventional modal analysis and testing methods to the study of rotating machinery dynamics. The systems treated here will be referred to as rotating machinery structures, to highlight the

fact that their study was undertaken using a structural dynamics approach. Attention is focused on the methods used for the derivation of modal models of these systems, a process that will be referred to as modal characterisation.

1.2 Definition of the problem

The adaptation of conventional modal analysis and testing methods to the study of rotating machinery structures requires overcoming some important theoretical and practical limitations. Two of these have been identified in previous research work [15], and constitute the motivation for the work presented here: (a) that parts of the modal analysis theory that applies to conventional structures does not apply to rotating machinery structures, and (b) that the structural models of rotating machinery derived by modal analysis methods are difficult to validate using test data, because of practical difficulties that are inherent to the execution of modal tests on these systems. These limitations will now be explained in more detail.

Conventional modal analysis and testing methods are based on the principles of reciprocity, which apply to non-rotating, linear, structures in general. The mass, damping and stiffness matrices that are used to represent the dynamic properties of these systems are symmetric. This symmetry is usually taken as an indicator that the dynamic behaviour of the system under consideration abides by the principles of reciprocity.

The dynamic behaviour of rotating machinery structures, on the other hand, does not always abide by such principles. This is due to the effects of forces that originate on their rotating components, which may either be of the gyroscopic or the circulatory types [19]. Different circumstances in which these types of force may arise have been reported in the literature [12]. Gyroscopic and circulatory forces are represented,

respectively, by the skew-symmetric components of the damping and stiffness matrices of rotating machinery structures [21].

Since the principles of reciprocity do not apply to rotating machinery structures, conventional modal analysis and testing methods cannot be applied to them without modification. With respect to modal characterisation methods, one of the main factors that need to be accounted for is that the models that describe the dynamic behaviour of rotating machinery structures require the definition of more parameters than for the case of non-rotating structures. This is because the asymmetric damping and stiffness matrices of rotating machinery structures involve more parameters than do the corresponding symmetric matrices of non-rotating structures.

This need for additional parameters is not only reflected in the spatial models, which are based on the mass, damping and stiffness matrices, but also in the modal and response models of rotating machinery structures. For example, the definition of the complete modal models for this type of systems requires determining a left eigenvector for each mode of vibration, in addition to its eigenvalue and its right eigenvector. This is in contrast with the modes of non-rotating structures, for which only the eigenvalue and the right eigenvector, traditionally known as the mode shape vector, are required.

With respect to the response model, the need for additional parameters is due to the fact that the frequency response function (FRF) matrix of rotating machinery structures is asymmetric. Hence, a complete response model requires defining more FRFs than in the case of conventional structures, for which the FRF matrix is symmetric.

The need to determine more parameters in order to build the models of rotating machinery structures affects the way in which modal tests are carried out on these

systems, since it is usually necessary to perform more response measurements in order to obtain the additional parameters.

Several methods to determine the modal parameters of rotating machinery structures have been proposed. They are presented in Section 1.5.2.1. Most of them are only applicable to specific types of systems, such as undamped-gyroscopic systems [48]. However, one of these methods [35] has been widely accepted, mainly because of its simplicity, but also because of its applicability to a wide class of linear systems. We will refer to it as the ‘column-row’ method. It was not developed for rotating machinery structures, which consist of rotating and non-rotating components, but for structures consisting exclusively of rotating components. Nevertheless it may be used for both types of structure, since it allows the identification of all the parameters required to construct the modal models of either type.

The approach of the ‘column-row’ method is to obtain the modal parameters of a rotating system from measurements of one column plus one row of its FRF matrix. Excluding the possibility that a mode may not be excited, any of the measured FRFs may be used to determine the eigenvalues of the system. The FRFs associated with the column of the FRF matrix may be used to determine the right eigenvectors, whereas the left eigenvectors can be obtained from those FRFs associated with the measured row of the matrix.

Although the theory underlying the method is relatively simple, its practical application is hindered by the technical problems associated with the measurement of the FRFs within the row of the FRF matrix [9]. This is because these measurements require applying excitation forces at every point, or more generally every degree of freedom (DOF), of a rotating machine, including those that lie on its rotating components. This

may result in a lengthy measurement procedure, which is further complicated by the need to make reliable measurements of the excitation forces in every case, and by the fact that the rotating components of machinery are usually enclosed in casings and/or exposed to extreme operating conditions.

The solution to these problems has been attempted through the development of measurement and excitation techniques to be used on the rotating components of machinery. However, as will be discussed in Section 1.5.2.2, the use of these methods is still limited to laboratory conditions, mainly because of the difficulties involved with the reliable measurement of the excitation forces and the access to the rotating components of practical systems.

The approach taken for the research work presented in this thesis was aimed at simplifying the modal testing procedure by eliminating the need to measure a complete row of the FRF matrix for the modal characterisation. The implementation of this approach was based on the objectives that are described in the next Section.

1.3 Objectives of the research work

The main objective of the research work presented here is to simplify the modal testing procedure, with respect to existing ones, by means of which the modal parameters of rotating machinery structures are determined from measured response data.

Several intermediate objectives lead to the achievement of the main objective. These are:

- (i) To develop a strategy for the modelling of rotating machinery that facilitates their study through a structural dynamics approach.

- (ii) To derive the mathematical relationships that exist between the spatial and modal parameters of rotating machinery structures.
- (iii) To develop a method for the computation of the left eigenvectors of rotating machinery structures.
- (iv) To determine the conditions in which simpler measurement schemes than the ones currently used for the modal testing of rotating machinery structures can be devised.
- (v) To design a method for the modal characterisation of rotating machinery structures.
- (vi) To evaluate the applicability of the method to practical systems.

1.4 Scope of the research

This study is confined to linear time-invariant systems for which the dynamic behaviour can be modelled through second-order differential equations with constant coefficients. The emphasis is placed on the fact that the matrices contained in the spatial models of rotating machinery structures are not symmetric and on the consequences that this has on the derivation and application of modal analysis and testing methods for such systems. Other conditions that are known to exist in some rotating machinery structures, such as non-linearity, are not considered.

1.5 Existing results of research

This thesis is focused on the methods for the dynamic characterisation of rotating machinery structures. The goal of this Section is to provide the reader with an overview of the results of research that constitute the background for the problem treated in this thesis.

The material presented in this Section is divided into two main categories, according to whether it corresponds to (a) theoretical or (b) experimental and experimentally-oriented research work.

Within the first category, the material has been further divided into two sub-categories. The first of these deals with the non-abidance of rotating machinery structures to the principles of reciprocity, a condition that will be referred to as ‘loss’ of reciprocity. The second sub-category is related to the mathematical models that have been used to represent the dynamic behaviour of rotating machinery structures, taking into account the effects of this ‘loss’ of reciprocity.

The second category consists of the results of experimental and experimentally-oriented research. The material that corresponds to this category has also been divided into two sub-categories. The first of these deals with the estimation of the modal parameters of rotating machinery structures using measurements of their dynamic response. The second sub-category describes the research work that has been conducted to develop a method for the application of excitation forces onto the rotating components of a machine, which constitutes one of the most difficult tasks in the process of modal characterisation of rotating machinery structures.

1.5.1 Results of theoretical research

1.5.1.1 ‘Loss’ of reciprocity in rotating machinery

The dynamic behaviour of conventional, non-rotating, structures usually abides by the principles of reciprocity of Betti and Maxwell [5,31]. On the other hand, one of the features that characterise rotating machinery structures is that they generally do not abide by these principles.

The first links between this ‘loss’ of reciprocity and the dynamic phenomena observed in rotating machinery were established during attempts to determine the origin of the unstable whirling motion of rotating shafts.

Newkirk [34] investigated the behaviour of shafts exhibiting unusual whirling patterns, with the purpose of finding the underlying causes. Based on field observations and experimental work, he found that the occurrence of a specific type of whirling, called whipping, was related to the use of shrink-fitted hubs on a shaft.

In parallel with the analysis and observations of Newkirk, Kimball [25] developed an internal friction theory of shaft whirling, which states that the whirling motion may be caused by the internal damping forces that arise in the shaft. Shrink-fitted components on rotating shafts impede the deformation of some portions of it, much in the same way as internal material damping does. The forces exerted by the shrink-fitted components on a rotating shaft, as well as those associated with its internal damping, are represented by a skew-symmetric component of the stiffness matrix of the shaft [30], when this matrix is defined with respect to a stationary coordinate system.

The asymmetry of the stiffness matrix is considered to be an indicator that the principle of reciprocity does not apply to the stiffness properties of an internally damped rotating shaft.

Because the skew-symmetric component of the stiffness matrix is directly related to the internal damping forces, which can potentially lead to instability [45], it has been recognised that other systems that exhibit similar stiffness properties may possess unstable modes of vibration. For example, Earles and Badi [13] noted that the external friction forces represented in the skew-symmetric components of the stiffness matrix of rotating discs are associated with unstable modes of vibration. Similarly, according to

Tuchinda and Ewins [47], one kind of instability referred to as brake-disc squeal is related to the friction forces that exist between the rotating disc and a stationary pin, which are partly represented by a non-symmetric stiffness matrix. Numerous other cases in which the asymmetry of the stiffness matrix is related to dynamic instability have been cited in the literature [12].

A fact that is often acknowledged is that the forces related to the asymmetry of the stiffness matrix may be either forward- or backward-rotating, according to whether they act in or against the direction of shaft rotation. Forces of a given type are capable of increasing the energy of a shaft that whirls in the same direction. This leads to the possible existence of unstable modes of vibration in the forward- or backward-whirling directions, depending on the type of force that affects the system. Hydrodynamic bearings are most commonly associated with forward-whirling modes [46] while some interactions between rotating and stationary components of a machine, such as rubs, are related to backward-whirling modes [11].

The forces that are associated with the ‘loss’ of reciprocity that occurs in rotating machinery structures are referred to as ‘circulatory’ or ‘follower’ forces [2, 43]. As has been discussed in previous paragraphs, these forces are represented in the skew-symmetric components of the stiffness matrix. However, there exists another type of force associated with a ‘loss’ of reciprocity, which is manifested in the skew-symmetric components of the damping matrices. These are called gyroscopic forces, and are generated in machine components that rotate and vibrate simultaneously [41]. It is important to point out that not all the forces that are associated with the skew-symmetric components of the damping matrix are related to gyroscopic effects. Such is the case, for example, of the forces generated in oil film journal bearings that are related to the

difference between the cross-damping coefficients corresponding to two orthogonal directions that are usually observed in these bearings [12, 26].

1.5.1.2 Mathematical models

Although the damping and stiffness property matrices of rotating machinery structures are generally asymmetric, there exists no experimental evidence of circumstances in which the inertial forces represented in their mass matrices cause them to become asymmetric [1]. However, it has been demonstrated that, as a consequence of the asymmetry of the damping and stiffness matrices, the response matrix, usually defined by frequency response functions (FRFs) in the frequency domain, is also asymmetric [36].

The ‘loss’ of reciprocity that occurs in rotating machinery structures is accommodated in their modal models by the introduction of a set of parameters that are not usually considered in classical modal analysis theory: the left-eigenvectors [27]. Each of these vectors contains information regarding the ability of excitation of forces to produce a vibration corresponding to a specific mode when applied at different points of a structure [17]. The modal models of rotating machinery are defined by its left-eigenvectors, right-eigenvectors and eigenvalues.

The derivation of mathematical models from measurements is usually based on the identification of the modal parameters of the system under consideration from measurements of its frequency response functions (FRFs). The approaches that have been attempted to achieve this are outlined in the next Section.

The identification of the left eigenvectors has been shown to be particularly problematic. Bucher [8] noted that the identification of these parameters is more susceptible to errors than is that of the right-eigenvectors, considering that both groups

of parameters are obtained from the same set of data. There are two reasons for this: first, that the left-eigenvectors represent internal force distributions associated with the excitation of each of the modes, and, second, that both sets of eigenvectors are usually obtained from resonance response data, but in the resonance region the force data is more likely to be affected by errors than are the responses. In the same paper, Bucher proposed a method to reduce the effects of having an ill-conditioned FRF matrix on the estimations of the left eigenvectors.

1.5.2 Results of experimental and experimentally-oriented research

1.5.2.1 Estimation of modal parameters from measurements

The need to determine the left eigenvectors for the complete modal characterisation of rotating machinery structures, has required that the conventional modal testing methods be modified in order to be applicable to these systems.

Nordmann [35] proposed a testing strategy by means of which the modal parameters of a rotating machine can be obtained. The strategy consists of measuring one row plus one column of the FRF matrix. The right-eigenvectors are determined from the FRFs in the column, while the left-eigenvectors are determined from those in the row. The eigenvalues can be determined from any one or several of the measured FRFs.

Measuring the row of the FRF matrix poses serious practical difficulties. This is because it necessitates applying excitation forces at each of the degrees of freedom of the machine. Thus, this can be a difficult and time-consuming process [20]. For this reason, the search for schemes for reducing the number of FRFs required for characterisation has received considerable interest. In general, this is only possible if the mass, damping and stiffness matrices are assumed to have special forms. For example,

if the structure is considered to be undamped but affected by gyroscopic moments, then the left eigenvectors are exactly the complex conjugates of their right counterparts for each mode, and hence it is not necessary to measure the row of the FRF matrix [32]. A further reduction can be obtained in rotor systems for which the principal directions of stiffness coincide in all bearings. In isotropic rotor systems only half of one column of the matrix must be measured [51].

Bucher [7] designed a characterisation method with which it is possible to reduce the number of measurements by applying a helical transformation to emulate a rotor in which the principal directions of stiffness of all bearings are aligned. In this way, it is possible to obtain an almost diagonal stiffness matrix without affecting the mass and gyroscopic matrices. This approach is applicable to rotor-bearing systems with ‘small’ deviations of the principal stiffnesses with relation to their separation along the shaft axis.

Zhang et al [49] established some relationships between the modal parameters of non-symmetric structural models. With these relationships, it is possible to calculate some modal parameters from others. The relationships are based on the assumption that the non-symmetric parts of the spatial property matrices are known.

Lee [29] proposed the use of complex modal analysis as a means to reduce the number of FRFs required for full identification of a system with non-symmetric property matrices. Through the use of complex coordinates and directional FRFs, he demonstrated that with the complex approach only half the number of the FRFs prescribed in the method of Nordmann are required. However, the benefits offered by this testing strategy are offset by the fact that each of the FRFs requires the application of a complex force vector, as well as the measurement of a complex response. Thus, the

number of FRFs processed is reduced, but the technical effort expended in realising the test is practically the same as with the approach of Nordmann.

Although it has been found that in specific cases it is possible to characterise completely the dynamics of a machine with fewer FRF measurements than those prescribed by the characterisation method of Nordmann [35], in a more general case it is still necessary to measure a complete row and a column of the FRF matrix.

The fact that the rotating components of machinery are only associated with a few of the total number of degrees of freedom has not received attention to date. It can be seen that advantage can be taken of it for characterisation purposes, since the gyroscopic and circulatory forces that cause the ‘loss’ of reciprocity can only originate in these components. To date there is no evidence of methods being developed that take advantage of this fact to characterise systems that comprise rotating and stationary components.

1.5.2.2 Excitation of rotating machinery components

As was discussed in the previous Section, one of the main difficulties of performing a modal test on a rotating component is the application of excitation forces onto rotating components. Several approaches have been followed in attempts to overcome these difficulties. The simplest one is the use of hammer impact excitation. Nordmann [35] used this strategy to excite the flexible shaft of a pump supported in oil film bearing. This kind of excitation is very convenient to apply, as it requires no special set-up and can be moved easily throughout the machine. Its drawback is that it is difficult to achieve repeatability and to hit a moving component with accuracy. Also, it applies an undesirable tangential component of excitation by friction which, although unmeasured, affects the response of the test-piece. To overcome this problem, Kessler [24] used a tri-

axial force transducer to apply the excitation. In this way, he was able to obtain an estimation of the applied tangential force in order to correct the measured FRFs, although this is not straightforward.

Another excitation method applicable to rotating shafts consists of mounting an unbalanced disk on a bearing which, in turn, is mounted onto the shaft [33]. With this set-up it is possible to control the speed of the rotating disk independently from that of the shaft using a belt drive. Thus, it is possible to apply a rotating unbalance force of controllable frequency to the shaft. This force is not measured directly, but can be calculated if the unbalance of the disk is known. The inconvenience of this method is that it requires the mounting of the excitation device onto the shaft, which is not always possible. However, it provides the advantage of applying a purely forward- or backward-excitation, which is convenient for complex modal testing.

If a ‘rider’ bearing is mounted onto a shaft, then it is possible to excite it using a shaker attached to the external race of that bearing: a technique which was used in a laboratory model by Rogers and Ewins [40]. It offers the advantage that different kinds of excitation forces can be applied [37], but the clearance between the bearing balls and the races may affect the precision with which the force is measured. The NASA Lewis Space Center spin rig [6] uses this kind of excitation, with the shakers attached to bearings mounted on flexible supports.

The use of active magnetic bearings to apply excitation forces [22] has gained popularity in the last years. The magnetic bearings consist of coils through which an electric current is applied to generate a magnetic field. This field produces an attractive force that acts on the shaft and which can be controlled through the intensity of the coil current. Usually, orthogonal coil arrangements are used to excite a rotor at one or more

stations, thus providing the capability of applying a variety of force patterns, such as forward and backward, unidirectional, etc. The drawback of the use of this system is its size and the difficulty to apply precise excitation forces due to the feedback caused by the movement of the shaft within the magnetic field, especially near the resonances. Advances in this field currently aim at developing the necessary control systems [50].

It should be made clear that, with all of the methods described here, the measurement of the excitation forces still represents a problem, since it is not possible to carry it out without mounting a coupling element between the force transducer and a rotating element. Moreover, the fact that the rotating components of machinery are difficult to access, especially for applying excitation forces onto them, still poses problems for the use of any of the methods that have been developed so far.

1.6 Overview of the thesis

This thesis presents a method for the dynamic characterisation of rotating machinery structures using modal analysis techniques. The material presented here covers the underlying theory used for the formulation of the method, its mathematical derivation and its application to numerical and physical systems. The thesis is organised in the following way:

Chapter 2 starts with a description of the spatial models of rotating machinery structures that are used in the thesis. The models are characterised by the asymmetry of the damping and/or the stiffness matrices. A nomenclature for the types of forces that are associated with the asymmetry of these matrices is presented.

Asymmetric matrices are often related to the effects of gyroscopic or circulatory forces on the dynamic behaviour of rotating machinery components. However, it is argued in

this Chapter that the asymmetry of the matrices can occur even in the absence of forces of these types, when non-orthogonal coordinate systems are used to describe the behaviour of the system under consideration.

In Chapter 3, a brief description of the modal and response models of rotating machinery structures are given. Emphasis is given to (a) the fact that the construction of the modal models of these systems requires the definition of their left eigenvectors, and (b) the asymmetry of their FRF matrices, as these features distinguish their models from those of non-rotating structures. Several relationships between the spatial, response and modal models of rotating machinery are derived analytically and a physical interpretation of them is given in terms of the receptance, mobility, accelerance and jerk characteristics.

In Chapter 4, the analytical derivation of a method for the identification of the modal parameters of rotating machinery structures is presented. The objective of the method is to eliminate the need to measure an entire row of the FRF matrix in order to achieve the complete modal characterisation of these systems. The derivation of the method is based on the relationships that exist between the different types of dynamic models of rotating machinery structure presented in Chapters 2 and 3, and those that exist between their modal parameters.

The application of the method is illustrated in Chapter 5, using two case studies. The first of these is carried out on the numerical model of a 4 DOF rigid rotor. It is used to demonstrate the theoretical soundness of the method. Computer generated FRFs are used to simulate true FRF measurements. The simulated FRFs are free of noise. The eigenvalues and right eigenvectors are determined from these ‘measured’ data and the left eigenvectors are computed using the method presented in Chapter 4. The accuracy

of the identified left-eigenvectors is evaluated using their exact values obtained directly from the spatial property matrices of the rotor.

The second case study illustrates the application of the method to a real rotating machine structure. The test structure used for this study is described and the procedure for the characterisation is presented in detail. The objective of this case study is to evaluate the performance of the method in cases where (a) the system under consideration is continuous and hence possesses an infinite number of DOFs, and (b) the measured response data is considerably affected by noise. The effects of the structure possessing close modes on the accuracy of the identified left eigenvectors are discussed. The selection of an optimal set of DOFs to perform the modal characterisation is also dealt with in this second case study.

Chapter 6 presents the conclusions obtained from this research work and presents some possible research activities that could be carried out as a continuation of the work presented here.

CHAPTER 2

Spatial models of rotating machinery structures

2.1 Introduction

Spatial models describe the dynamic behaviour of mechanical systems in terms of their displacements and their time derivatives. In these models, the properties of a system are represented by three spatial property matrices: the mass, $[M]$, damping, $[C]$, and stiffness, $[K]$, matrices. These matrices relate the response of the system, $\{x(t)\}$, to the external excitation forces applied to it, $\{f(t)\}$, through the following time-domain equation:

$$[M]\{\ddot{x}(t)\} + [C]\{\dot{x}(t)\} + [K]\{x(t)\} = \{f(t)\} \quad (2.1)$$

A particularly useful form of this equation is that which corresponds to a harmonic excitation force. This is because the vibration of many practical systems, and especially that of rotating machinery structures, is usually caused by periodic excitation forces, which consist of a finite number of harmonic components.

The representation of Equation (2.1) for the case of a harmonic excitation force can be derived if two considerations are taken into account: firstly, that a harmonic force can be expressed in terms of a force amplitude vector, $\{F(\omega)\}$, an excitation frequency, ω , and time, t , as:

$$\{f(t)\} = \{F(\omega)\} \cdot e^{i\omega t} \quad (2.2)$$

Secondly, that the steady-state response of a linear, time-invariant, system to this type of force is also harmonic and has the same frequency as the force. Hence, it may be represented as:

$$\{x(t)\} = \{X(\omega)\} \cdot e^{i\omega t} \quad (2.3)$$

where $\{X(\omega)\}$ is the vector of response amplitudes. Using Equations (2.2) and (2.3), Equation (2.1) may be expressed for the case of a harmonic excitation force as:

$$[K - \omega^2 M + i\omega C] \cdot \{X(\omega)\} e^{i\omega t} = \{F(\omega)\} e^{i\omega t} \quad (2.4)$$

This equation may also be expressed in its state-space form which, discarding the exponential terms, is:

$$\left[i\omega \cdot \begin{bmatrix} [0] & [M] \\ [M] & [C] \end{bmatrix} + \begin{bmatrix} -[M] & [0] \\ [0] & [K] \end{bmatrix} \right] \begin{Bmatrix} i\omega \cdot \{X(\omega)\} \\ \{X(\omega)\} \end{Bmatrix} = \begin{Bmatrix} \{0\} \\ \{F(\omega)\} \end{Bmatrix} \quad (2.5)$$

The methods developed in this thesis will be based on this representation of the equation of motion.

Equations (2.1), (2.4) and (2.5) apply to both rotating machinery and non-rotating structures. However, the spatial property matrices for the two types of structure may present significant differences. For example, the matrices for rotating machinery structures usually depend on the frequency of rotation, or even on the angular position of their rotating components, whereas in the case of non-rotating structures this dependency does not exist. However, for the work presented here, the most important difference considered is that, whereas the spatial property matrices for non-rotating structures are symmetric, those of for rotating machinery structures are, in general, asymmetric. This asymmetry is caused by the representation of so-called gyroscopic and circulatory forces [19] as properties of the structure, due to the fact that they depend on the velocities and displacements of the structural DOFs.

The representation of these types of force in the spatial property matrices will be treated in more detail in the next Section.

2.2 The damping and stiffness matrices of rotating machinery structures

The elements of the damping, $[C]$, and stiffness, $[K]$, matrices in Equations (2.1), (2.4) and (2.5) are proportionality coefficients that define, respectively, the linear relationship that exists between the velocities and displacements of a structure at its different DOFs and the forces that affect its dynamic behaviour.

For the case of non-rotating structures, the damping matrix is associated with forces that are capable of reducing the mechanical energy of a system, while the stiffness matrix is associated with elastic forces, which produce a tendency of the system to move towards its static equilibrium configuration without modifying its total energy level.

On the other hand, the damping and stiffness matrices of rotating machinery structures also represent the so-called gyroscopic and circulatory forces, respectively, that arise due to rotation. The damping matrix is used to represent the damping and the gyroscopic forces, both of which have a velocity-dependent characteristic. Similarly, the stiffness matrix is used to represent elastic and circulatory forces, which have a displacement-dependent characteristic.

Although this condensed representation of the properties of a structure may avoid the alteration of the traditional structural models given in Equations (2.1), (2.4) and (2.5), it may also create confusion with respect to the physical interpretation of the spatial property matrices. This is because, with this condensed representation, a single matrix represents forces that have completely different effects on the behaviour of a structure. For example, damping forces produce different effects than do gyroscopic forces, since the latter are not capable of modifying the mechanical energy of a structure. On the contrary, they produce a ‘stiffness-like’ effect, which is manifested in a tendency of the

structure to move towards its static equilibrium configuration [16]. Similarly, elastic forces produce different effects than do circulatory forces. While the former have no effect on the total energy level of the structure, the latter are associated with self-excitation or damping mechanisms [14], which may increase or decrease this level.

Given the mixed nature of the forces represented in each of the matrices $[C]$ and $[K]$, it would seem appropriate to refer to them as the ‘velocity-dependent’ and ‘displacement-dependent’ matrices, respectively, rather than the damping and stiffness matrices, in accordance with the terminology suggested in [14]. However, in order to avoid any possible confusion created by the introduction of a new terminology, the terms ‘damping matrix’ and ‘stiffness matrix’ will be kept, and used throughout the thesis to refer to the matrices that represent forces with ‘velocity-dependent’ and ‘displacement-dependent’ characteristics, respectively.

2.3 Nomenclature for rotation-related forces

As was mentioned in the preceding Section, the forces that arise due to the rotation of machinery components are usually divided into two groups: gyroscopic forces, which have a velocity-dependent characteristic, and circulatory forces, which have a displacement-dependent characteristic. These forces are represented by the skew-symmetric components of the damping and stiffness matrices, respectively.

It is important to notice that, apart from true gyroscopic forces, which are essentially due to the inertia of the rotating components of machinery, the first group also includes others such as those associated with the dissimilar cross-damping characteristics of hydrodynamic bearings [45], that are unrelated to gyroscopic effects. Thus, the use of the term ‘gyroscopic’ to refer to this group of forces seems inappropriate. For this reason, the term “velocity-dependent circulatory forces” will be used in the rest of this

thesis to refer to the forces that are represented in the skew-symmetric component of the damping matrix. These forces will be distinguished from those that are represented in the skew-symmetric component of the stiffness matrix, which will be referred to as “displacement-dependent circulatory forces”. Thus, the term “circulatory forces” will denote forces that are represented in the skew-symmetric components of both the damping and the stiffness matrices.

In Figure 2.1, the nomenclature that will be used in the rest of the thesis is illustrated. As it can be seen, the two defined types of circulatory force, i.e. velocity- and displacement-dependent, are represented in the damping and stiffness matrices, respectively. As was mentioned previously, the first type includes gyroscopic forces and others such as those associated with the dissimilar cross-damping characteristics of hydrodynamic bearings. The second type includes forces that arise due to the presence of internal damping in some rotating components, such as flexible shafts, and other forces such as those associated with the dissimilar cross-stiffness characteristics of hydrodynamic bearings. The damping and stiffness matrices also represent the true damping and elastic forces of the system. These two types of force constitute the class of non-circulatory forces.

2.4 Representation of circulatory forces

Circulatory forces arise due to the effects of rotation on the components of machines. Several examples of this type of force have been quoted in the literature; amongst them are those mentioned in the previous Section, rotor-stator rub forces [14], electromagnetic forces in electric induction motors [18] and forces that arise due to the interaction between fluids and the rotating components of machines [12].

Circulatory forces are usually distributed throughout an area of the machine components in which they originate, as are rotor-stator rub forces or hydrodynamic forces in

bearings, or can also be distributed across a volume, as are gyroscopic and electromagnetic forces. However, their study can usually be simplified by expressing them in terms of their resultant forces.

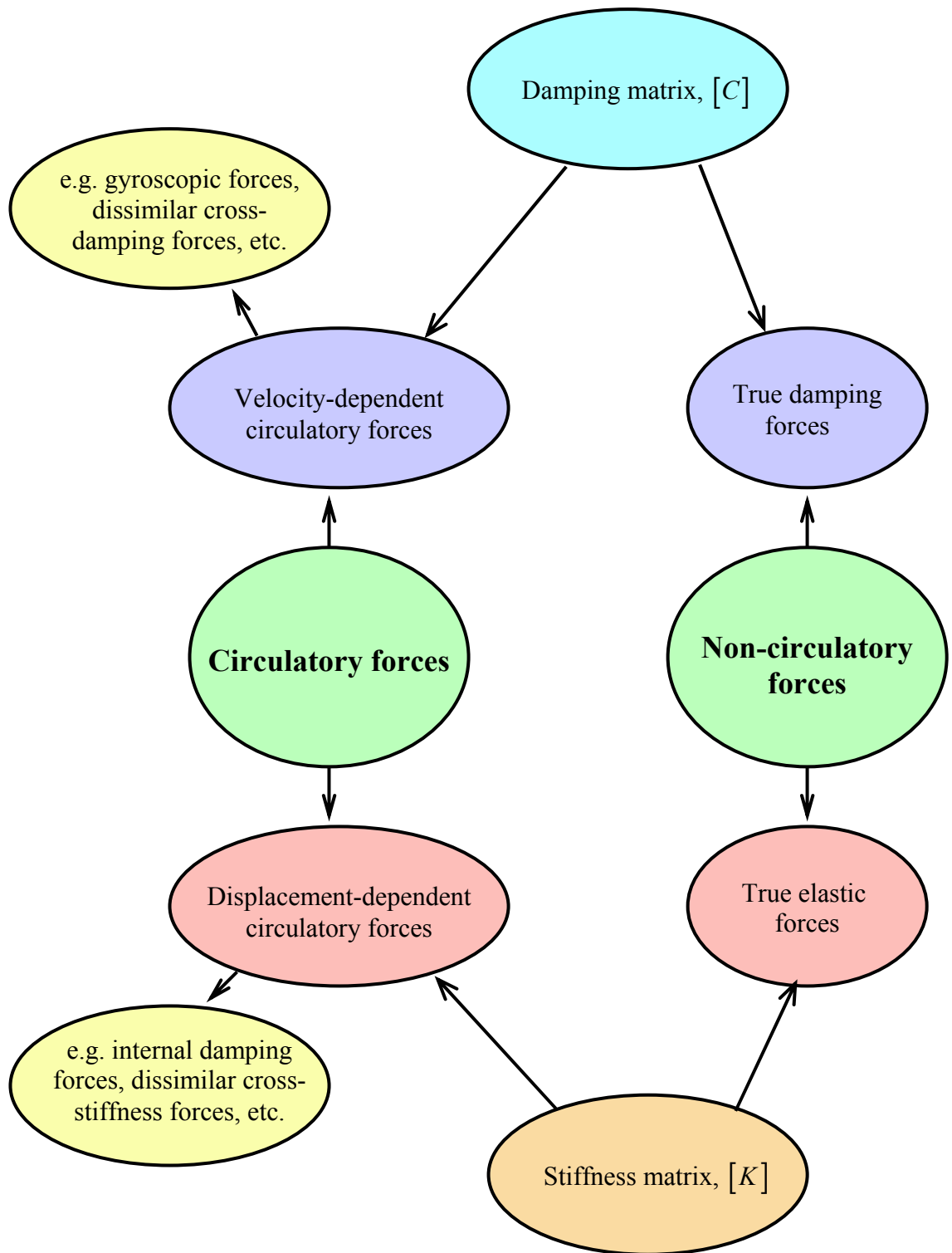


Figure 2.1 – Components of the damping and stiffness matrices

The following discussions are based on the simplest kind of circulatory force, which is represented as a function of the vibration of one point within a plane, and acts only on that plane. This type of representation can be used, for example, for the forces that arise in some hydrodynamic journal bearings. The effects of these forces may be studied in terms of a single resultant force, which acts in a plane that is normal to the shaft axis and is a function of the displacements and/or velocities of the shaft journal in that plane.

The stiffness matrix associated with this type of bearing will now be derived. In doing so, attention is drawn to the fact that each column of the stiffness matrix represents the forces that need to be applied at each DOF in order to produce a static unit displacement of the system at the DOF associated with that column and null displacements at the remaining DOFs. For clarity, the units in which the forces, displacements and stiffnesses are measured will be omitted in this discussion, but are assumed to correspond to a consistent unit system, e.g. Newtons, metres and Newtons per metre, respectively, for the SI unit system.

Figure 2.2 is a schematic diagram of a hydrodynamic journal bearing. The shaft journal is shown rotating clockwise with speed Ω . For clarity, the clearance between the stationary bearing and the shaft journal has been exaggerated and is assumed to be filled with oil. In the first instance, the analysis of the journal-bearing system will be carried out with respect to the x_1x_2 coordinate system.

In Figure 2.2, the shaft journal is shown in its static equilibrium position ($x_1 = x_2 = 0$), in which it is only acted upon by the tangential forces associated with the shear stresses generated in the oil. These forces are uniformly distributed along the surface of the shaft journal and have a null equivalent resultant force.

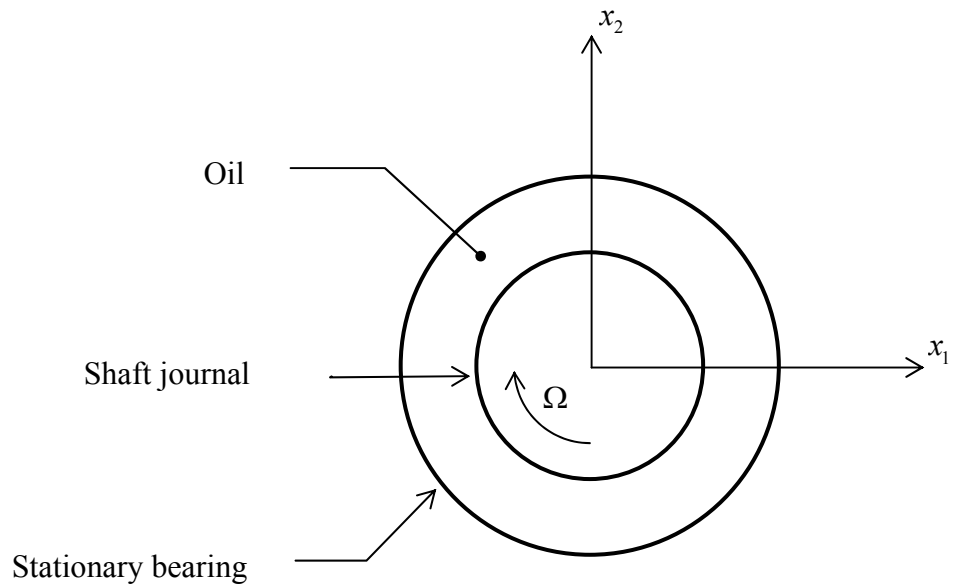


Figure 2.2 – Hydrodynamic bearing with shaft journal in its static equilibrium position.

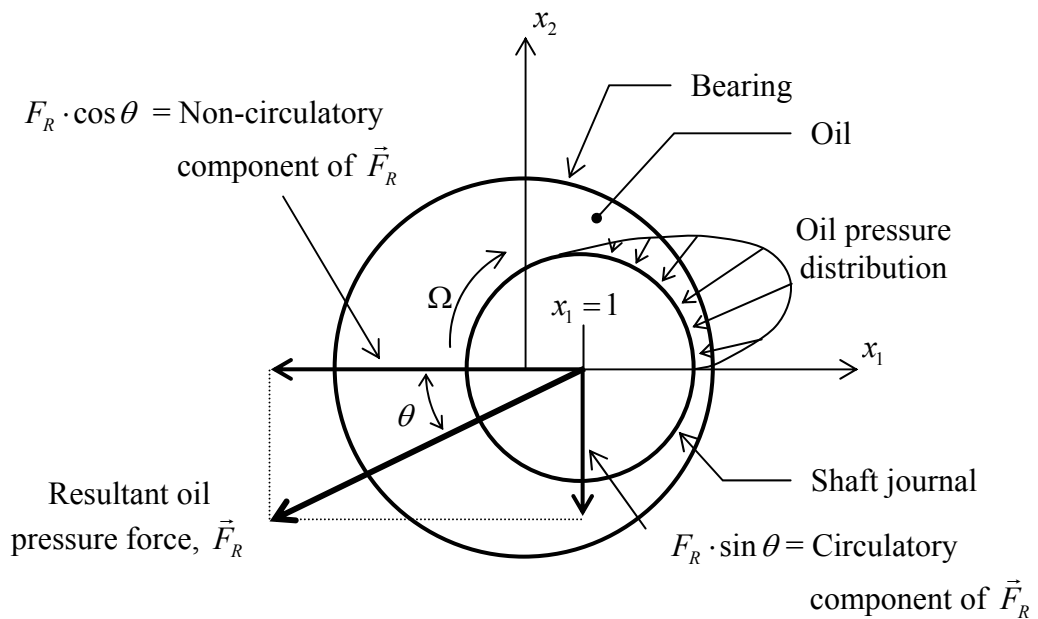


Figure 2.3 – Hydrodynamic bearing with shaft journal displaced along the x_1 axis.

In Figure 2.3, the shaft journal is shown displaced one unit to the right ($x_1 = 1; x_2 = 0$) from its static equilibrium position. This displacement produces a variable pressure distribution of the oil along the surface of the shaft journal [10, 12]. The force that

results from the application of this pressure to the shaft journal is normal to its surface. The line of action of the resultant force passes through the centre of the shaft journal.

In order to produce and maintain the static displacement of the shaft journal shown in Figure 2.3, it is necessary to apply a force to it, such that the resultant of the oil pressure forces, \vec{F}_R , is cancelled-out. The components of the required force will depend on the magnitude, F_R , of \vec{F}_R , as well as on its direction, which is defined by the angle θ . These components constitute the first column of the ‘stiffness’ matrix of the journal-bearing system:

$$\begin{Bmatrix} k_{11} \\ k_{21} \end{Bmatrix} = \begin{Bmatrix} F_R \cdot \cos \theta \\ F_R \cdot \sin \theta \end{Bmatrix} \quad (2.6)$$

In Figure 2.4, the shaft journal is shown displaced upward one unit ($x_1 = 0; x_2 = 1$) from its static equilibrium position. Similarly to the previous case, this produces an oil distribution with an equivalent resultant force that passes through the centre of the journal. The forces that are required to cancel-out this resultant force constitute the second column of the stiffness matrix:

$$\begin{Bmatrix} k_{12} \\ k_{22} \end{Bmatrix} = \begin{Bmatrix} -F_R \cdot \sin \theta \\ F_R \cdot \cos \theta \end{Bmatrix} \quad (2.7)$$

Thus, the complete stiffness matrix for the journal-bearing system may be defined as:

$$[K] = \begin{bmatrix} F_R \cdot \cos \theta & -F_R \cdot \sin \theta \\ F_R \cdot \sin \theta & F_R \cdot \cos \theta \end{bmatrix} \quad (2.8)$$

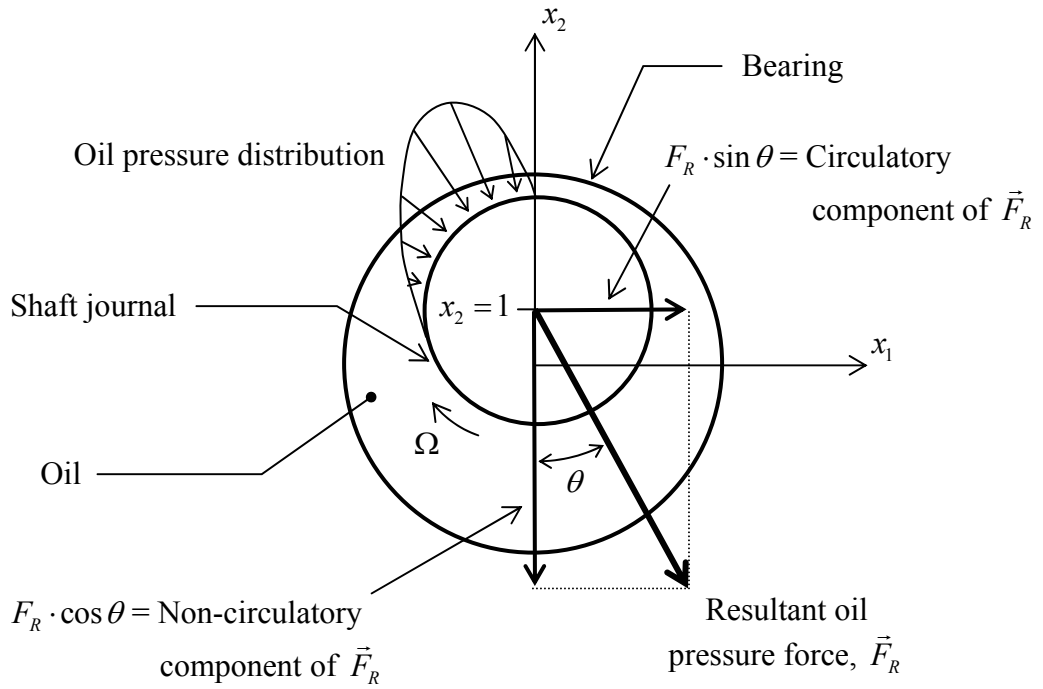


Figure 2.4 – Hydrodynamic bearing with shaft journal displaced along the x_2 axis.

The symmetric, $[K]_s$, and skew-symmetric, $[K]_{ss}$, components of this matrix are, respectively:

$$[K]_s = \begin{bmatrix} F_R \cdot \cos \theta & 0 \\ 0 & F_R \cdot \cos \theta \end{bmatrix} \quad (2.9)$$

$$[K]_{ss} = \begin{bmatrix} 0 & -F_R \cdot \sin \theta \\ F_R \cdot \sin \theta & 0 \end{bmatrix} \quad (2.10)$$

From Figures 2.3 and 2.4 and Equation (2.10), it can be seen that the displacement-dependent circulatory forces of the journal-bearing system are represented in the skew-symmetric component of the stiffness matrix. A similar analysis would reveal the relationship that exists between the velocity-dependent circulatory forces originated in the bearing and the skew-symmetric component of its damping matrix.

Apart from a matrix representation, the relationship between the circulatory forces and the displacements, or velocities, which determine them can be represented graphically

using a vector field diagram. This kind of representation is useful to gain insight into the way in which the circulatory and non-circulatory forces affect the behaviour of a system, but is only practical for simple cases such as the one discussed here.

Figure 2.5 shows the vector field diagram corresponding to the stiffness matrix given in Equation (2.8) for the case of $F_r = 0.5$ and $\theta = 30^\circ$. In this diagram, the forces required to produce static unit displacements of the shaft journal in various directions with respect to its static equilibrium position are represented with blue arrows. The red marks indicate the displacements produced by the force-vectors which originate at each them.

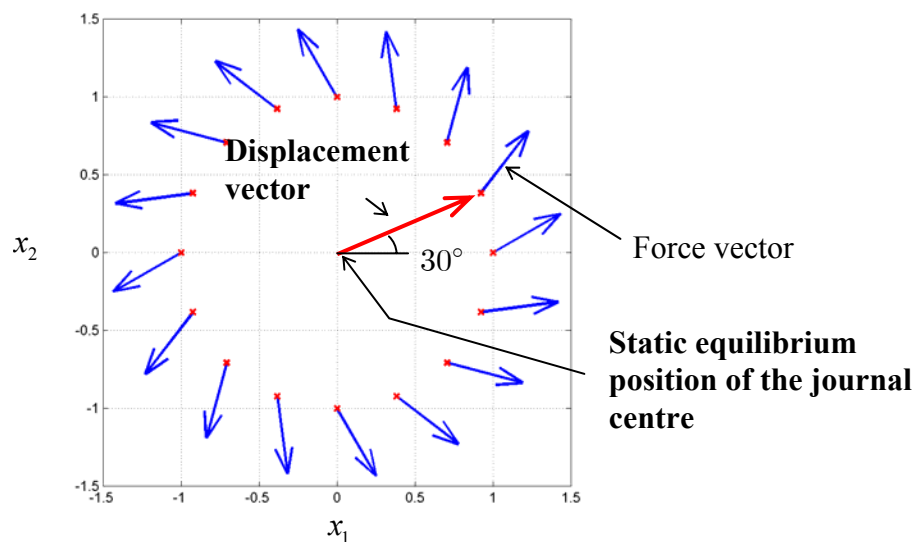


Figure 2.5 – Vector field representation of the stiffness characteristic of a journal-bearing system.

The components of the force vectors associated with displacements along the x_1 and x_2 axes in Figure 2.5 correspond, respectively, to the elements of the first and second columns of the stiffness matrix given in Equation (2.8).

Figures 2.6(a) and (b) present, respectively, the vector field representations of the non-circulatory, or true stiffness, forces and the displacement-dependent circulatory forces associated with the same stiffness matrix.

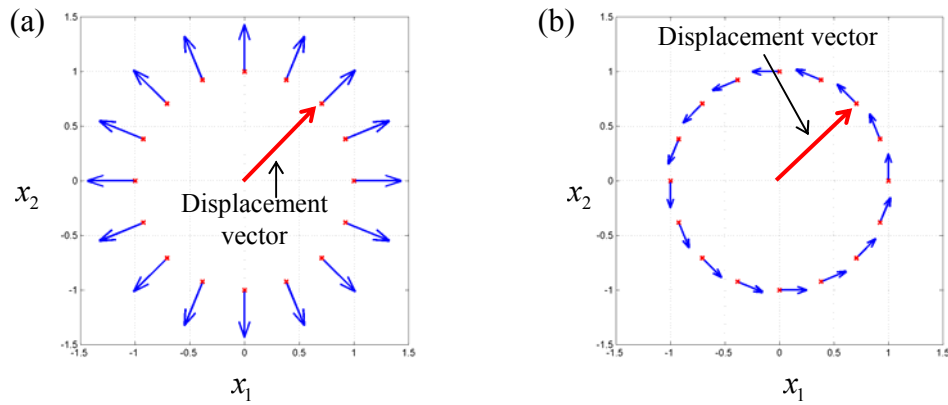


Figure 2.6 – Vector field representation of the (a) non-circulatory and (b) circulatory ‘stiffness’ characteristics of a journal-bearing system.

Figure 2.6(b) demonstrates an important characteristic of displacement-dependent circulatory forces, namely that they are always orthogonal to the displacements that produce them. Similarly, velocity-dependent circulatory forces are orthogonal to the velocities that produce them.

Using the vector field representations of the stiffness matrix components, it can be deduced that circulatory forces would produce a tendency of the shaft journal to move in a circular, whirling, path. Similar diagrams can be drawn for velocity-dependent circulatory forces using the components of the damping matrix, although in this case the coordinates of the points, denoted by the red marks in Figures 2.5 and 2.6(a) and (b), used as origins for the individual force vectors would correspond to the components of the velocities, rather than the displacements, of the shaft journal in the x_1x_2 plane.

For cases of greater complexity, for example those in which more than two DOFs are involved in the mechanism through which circulatory forces originate, the use of vector field diagrams may become impractical for the study of the effects of these forces. For those cases, a matrix representation may be the most suitable alternative.

In using a matrix representation, attention must be paid to the fact that the matrices that represent the dynamic properties of rotating machinery structures, including the effects

of circulatory forces, depend on the coordinate system with respect to which they are defined. This point will be discussed in detail in the next Section.

2.5 Influence of coordinate frame selection on the matrix representation of non-circulatory and circulatory forces

In the example that was used in the previous Section, it was shown that the circulatory forces that affected the stiffness characteristic of the journal-bearing system shown in Figure 2.2 were represented by the skew-symmetric component of its stiffness matrix, whereas the non-circulatory forces were represented by the symmetric component of the same matrix.

However, these associations cannot be taken as a general rule, since the coordinate frame used to define the spatial property matrices affects the way in which the circulatory and non-circulatory forces are represented in them.

In this Section, the influence of coordinate frame selection on the representation of non-circulatory and circulatory forces in the spatial property matrices will be analysed.

2.5.1 Representation of non-circulatory forces

Consider the 2-DOF spring-mass system shown in Figure 2.7. Its stiffness matrix represents exclusively true elastic, i.e. non-circulatory, forces, and may be defined with respect to the x_1x_2 coordinate frame as:

$$[K]_{x_1x_2} = \begin{bmatrix} k_1 & 0 \\ 0 & k_2 \end{bmatrix} \quad (2.11)$$

By applying an orthogonal coordinate transformation to this matrix, the stiffness matrix of the same system may also be defined for the $x'_1x'_2$ coordinate frame as:

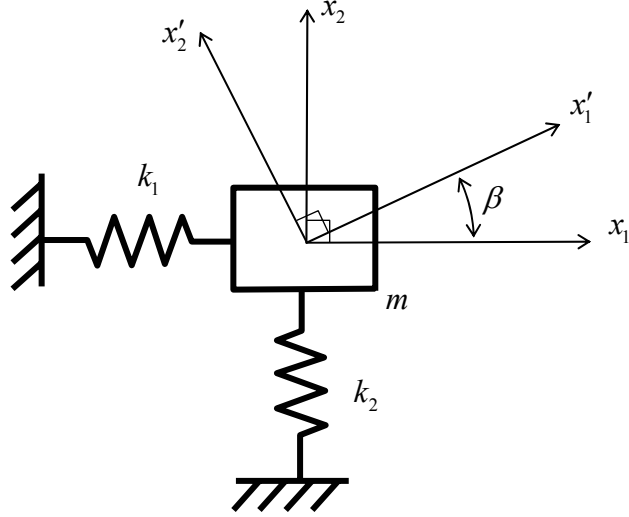


Figure 2.7 – 2-DOF spring-mass system

$$[K]_{x_1'x_2'} = [T]^{-1} [K]_{x_1x_2} [T] \quad (2.12)$$

where:

$$[T] = \begin{bmatrix} \cos \beta & -\sin \beta \\ \sin \beta & \cos \beta \end{bmatrix} \quad (2.13)$$

Thus, we obtain the following matrix:

$$[K]_{x_1'x_2'} = \begin{bmatrix} k_1 \cos^2 \beta + k_2 \sin^2 \beta & (k_2 - k_1) \cos \beta \cdot \sin \beta \\ (k_2 - k_1) \cos \beta \cdot \sin \beta & k_1 \sin^2 \beta + k_2 \cos^2 \beta \end{bmatrix} \quad (2.14)$$

which is symmetric for any value of the parameter β . From this equation, it may be concluded that the stiffness matrix for the system shown in Figure 2.7 is symmetric with respect to any orthogonal coordinate frame in the x_1x_2 plane. This is consistent with the observation made in the previous Section that non-circulatory forces are represented by the symmetric components of the spatial property matrices. However, if we now derive the stiffness matrix of the same system with respect to a non-orthogonal coordinate frame, for example that defined by the x_1 and x_1' axes, we have:

$$[K]_{x_1x_1'} = \begin{bmatrix} k_1 & (k_1 - k_2) \cos \beta \\ 0 & k_2 \end{bmatrix} \quad (2.15)$$

which results from using the following non-orthogonal transformation matrix with the stiffness matrix given in Equation (2.11):

$$[T] = \begin{bmatrix} 1 & \cos \beta \\ 0 & \sin \beta \end{bmatrix} \quad (2.16)$$

Equation (2.15) shows that the matrices that represent non-circulatory forces may be asymmetric if they are defined with respect to a non-orthogonal coordinate system.

Thus, non-circulatory forces may be defined as those that are represented by the symmetric components of the spatial property matrices, **only** when these are derived with respect to an orthogonal coordinate frame.

2.5.2 Representation of circulatory forces

In order to illustrate the influence of the choice of coordinate frame on the matrix representation of circulatory forces, the stiffness matrix given in Equation (2.8) will be used. It will be recalled that this matrix was defined with respect to the x_1x_2 coordinate frame, which is was defined in Figure 2.2 and is shown again in Figure 2.8.

The circulatory forces that arise when the shaft journal rotates inside the bearing are represented by the skew-symmetric matrix given in Equation (2.10):

$$[K]_{CIRCULATORY} \Big|_{x_1x_2} = [K]_{SS} = \begin{bmatrix} 0 & -F_R \cdot \sin \theta \\ F_R \cdot \sin \theta & 0 \end{bmatrix} \quad (2.17)$$

However, if the matrix representation of the circulatory forces is derived for the coordinate frame defined by the x_1 and x_1' axes, we have:

$$[K]_{CIRCULATORY} \Big|_{x_1x_1'} = \frac{F_R \cdot \sin \theta}{\sin \beta} \cdot \begin{bmatrix} -\cos \beta & -1 \\ 1 & \cos \beta \end{bmatrix} \quad (2.18)$$

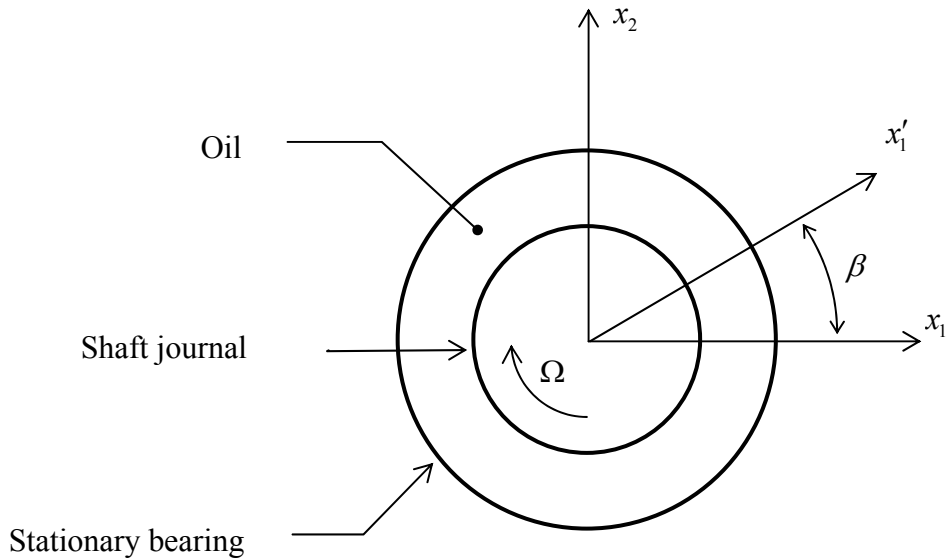


Figure 2.8 – Coordinate systems for the study of a hydrodynamic bearing

which is no longer a skew-symmetric matrix. This Equation demonstrates that, with respect to a non-orthogonal coordinate system, the matrices that represent circulatory forces are not necessarily skew-symmetric.

Thus, circulatory forces may be defined as those that are represented by the skew-symmetric components of the spatial property matrices, **only** when these are derived with respect to an orthogonal coordinate frame.

From the discussions contained in this and the previous Sections, it may be seen that coordinate frame orthogonality plays an important role in establishing a direct relationship between the existence of circulatory forces in rotating machinery structures and the asymmetry of their spatial property matrices. For this reason, the next Section is dedicated to the definition and analysis of orthogonal coordinate frames.

2.6 Orthogonal coordinate frames

The coordinate frames, or coordinate systems, used to study the dynamic behaviour of structures are defined in terms of their DOFs. The DOFs are usually, but not necessarily, associated with a specific structural point and its possible translation (or

rotation) in a predefined direction. With this in mind, each DOF can be interpreted in a geometrical sense as an axis along which (or around which) a structural point, which constitutes the origin of the axis, can move. To facilitate the presentation of the material contained in this Section, the points and the directions of motion associated with the DOFs of a structure will be referred to as ‘origins’ and ‘axes of motion’, respectively.

2.6.1 Axes of motion

Spatial coordinates are numbers by means of which we can determine the position of different points of a structure. Each coordinate is associated with the displacement of a point of the structure in a specific direction. Spatial coordinates have a physical meaning when they are translated into the actual displacements of the structural points. To do this, each point of the structure is made the origin of an axis of motion. The orientation of the axis determines the direction in which the associated coordinate is measured to obtain the corresponding physical displacement of the structure.

Each axis of motion is associated with a base vector, which has the same direction and origin as the axis and usually unit length. This vector represents a unit displacement of the structure at the point corresponding to the origin, and in the direction, of the axis.

2.6.2 Orthogonality of two axes of motion

There exist at least two different approaches to determine whether two axes of motion are orthogonal, depending on whether they share a common origin or not. If they do, then the orthogonality condition can be stated in the sense used by Lathi [28] as follows:

Two axes of motion with a common origin are orthogonal if each of their base vectors is more similar to a null vector than to any multiple of the other base vector.

Figures 2.9(a) and (b) show, respectively, one orthogonal and one non-orthogonal sets of axes of motion. In Figure 2.9(a) the two axes of motion are orthogonal. It can be seen that any multiple of the base vector \hat{e}_1 is a worse approximation of \hat{e}_2 than is a null vector. The axes of motion in Figure 2.1(b) are not orthogonal, since there exists a multiple of \hat{e}_1 that approximates \hat{e}_2 better than does the null vector.

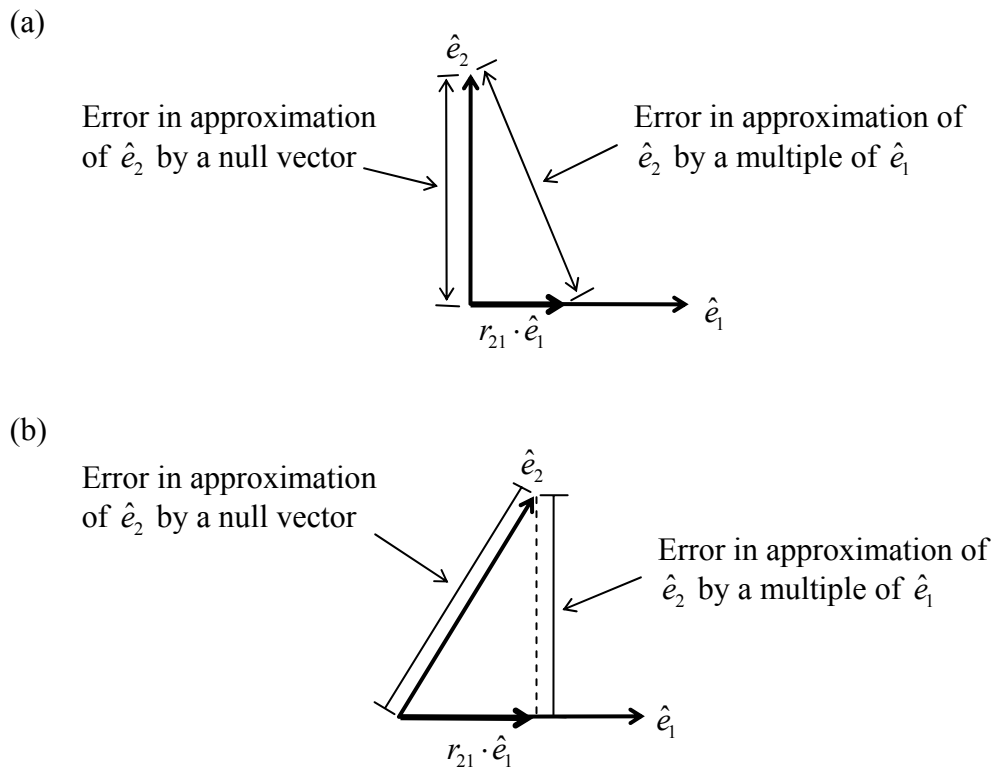


Figure 2.9 – Definition of (a) orthogonal and (b) non-orthogonal axes

Although it is relatively simple to define orthogonality when two axes have a common origin, a more general definition should be applicable to the case in which the origins are different. In this case, orthogonality cannot be assessed only from a geometrical approach. However, a definition more akin to the case of structural dynamics can be used:

Two axes of motion are orthogonal if a force applied along either one of them does no work when the structure undergoes a displacement along the other axis.

This, more general, definition can also be used to assess the orthogonality of axes with common origins.

One fact becomes apparent from this new definition, namely that if the origins of the two axes of motion move independently of each other, then the two axes will always be mutually orthogonal, regardless of their spatial orientation. What is not so immediately evident is under which conditions two axes with different origins are not orthogonal.

One possible case is that of the rigid ring illustrated in Figure 2.10. Point A is the origin of the axis of motion $\overline{AA'}$, and point B is the origin of $\overline{BB'}$. The origins of the two axes are different points of the structure. However, it is clear that a force, \vec{f} , applied in the direction of $\overline{AA'}$ will do a non-zero amount of work on the structure, if it is displaced along $\overline{BB'}$, as it will travel an effective distance, d . Hence, these two axes are not orthogonal. In this example, the fact that the ring is rigid forces the two origins to move simultaneously.

If the ring were not rigid, then it would be possible to prevent the motion of point A while displacing point B . Hence a force applied along $\overline{AA'}$ would do no work when point B were displaced along $\overline{BB'}$. In this case the two axes would be orthogonal.

Thus, the orthogonality of two axes of motion depends on the kinematic conditions that link the motions of their origins. In the first case, these motions are linked because of the fact that the ring is rigid. In the second case this condition is removed and hence the two axes become orthogonal.

Rigidity is an extreme condition. In practice, all systems exhibit some degree of flexibility, and hence different points may be moved independently of each other. On the other hand, during tests and in operating conditions, the deformations of flexible

structures are dominated by only a finite number of modes, and this implies that only a finite, and at most equal, number of points move independently of each other. Since this is the most usual scenario, it will now be discussed in more detail.

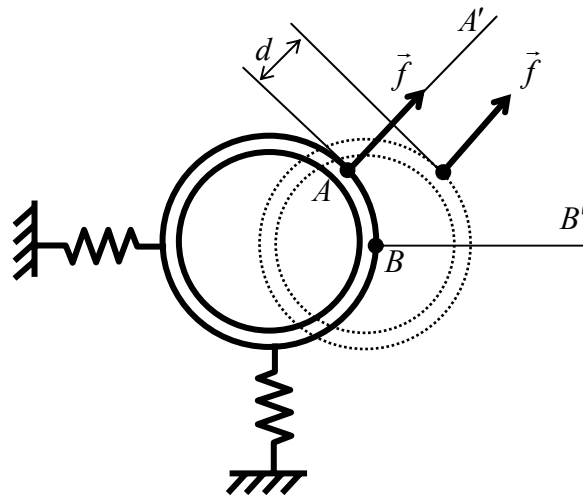


Figure 2.10 – Flexibly-supported rigid ring

2.6.3 Orthogonality in flexible systems

In theory, any two points of a flexible continuous structure may be moved independently of each other. However, in practice, the deformation of a structure is limited to the configurations that can result from the combination of only a finite number of modes. Hence, depending on the modes that determine the possible deformations of the structure, the motions of two different points on the structure may, or may not, be independent of each other.

The orthogonality of the axes of motion of a flexible structure depends on which modes affect its vibration and, of course, also on the origins and orientations of the axes in question.

Each mode shape of a flexible structure associates a displacement vector with each point of the structure. This vector defines the region in space in which that point can

move when only that mode is excited. The vector consists of two displacements: one translation and one rotation. A phase should also be specified for each displacement, but we will consider that all points move in phase for this discussion.

As more modes are considered, the space in which any particular point of the structure can move may also be increased in dimension: a line, a plane or a volume.

The movement of one point along an arbitrary axis forces other points of the structure to move in a limited region. This is because the displacement of one point in a specific direction can only be achieved by exciting each of the modes with specific amplitudes. The combined effect of the modes would yield the desired displacement of the point of interest, but it would also impose a displacement of the remaining points of the structure based on the used modal combination, or would limit their region of motion.

Hence, it can be concluded that the points along a continuous flexible structure do not move totally independently of each other when only a finite number of structural modes are considered. This leads to the possibility of two axes of motion not being orthogonal in spite of their origins lying on different points of the structure.

If two axes with different origins are chosen to describe the behaviour of a flexible structure, then in order for them to be orthogonal it is necessary that at least one of the modal combinations that produce a motion of the first origin along the first axis allows the second origin to move in a direction which is geometrically orthogonal to the second axes. In order to define a complete orthogonal coordinate frame, this criterion must apply between every pair of the axes of motion that define the frame.

2.7 Summary

In this Chapter, the spatial models of rotating machinery structures were introduced. It was highlighted that, in contrast to the models for non-rotating structures, those for rotating machinery structures may involve asymmetric damping and stiffness matrices. This asymmetry is due to the representation of circulatory forces, which were classified into two groups: velocity-dependent and displacement-dependent.

It was shown that circulatory forces are represented in the skew-symmetric components of the damping and stiffness matrices only when these matrices are defined with respect to an orthogonal coordinate system.

A general definition of the orthogonality of a coordinate frame was given, and it was shown that the fact that the DOFs of a continuous system lie on different points of a test structure does not guarantee that the DOFs will be orthogonal. This was illustrated using the case of a rigid ring as an example, and the discussion was extended to the more general case of flexible systems.

CHAPTER 3

Modal and response models of rotating machinery structures

3.1 Introduction

The dynamic characteristics of mechanical systems are usually described using any of three types of model: spatial, modal and response models. However, the three types of model are interrelated.

In this Chapter, a brief description of the modal and response models of rotating machinery structures is given. Based on this description, and that of the spatial models presented in Chapter 2, some relationships that exist between the three types of model are derived analytically. A physical interpretation of these relationships is given.

3.2 The modal model

As in the case of non-rotating structures, the dynamic behaviour of rotating machines may be explained in terms of a superposition of modes of vibration. The number of modes depends on the number of DOFs that they possess.

Rotating machinery structures are continuous systems and as such may have an infinite number of DOFs, and consequently an infinite number of modes. However, in practice, dynamics studies are focused on deriving a model that represents their behaviour only within a limited frequency interval. Within this interval, some of the vibration modes dominate the dynamic behaviour whereas others might only have a small influence.

The most common approach to the dynamic characterisation of practical structures is to build a model based on the predominant modes. Hence, within the limited frequency range of interest, a machine may be considered to behave as a system with only a finite number, N , of DOFs. This makes it possible to express its modal parameters using matrices of finite dimensions.

3.2.1 Modal parameters

Due to the asymmetry of the damping and stiffness matrices, the complete modal models of rotating machinery structures consist of two different sets of modal vectors, the right and left eigenvectors, in addition to one set of eigenvalues. This is in contrast to the case of non-rotating structures, which only consist of the right eigenvectors and the eigenvalues.

For the case of rotating machinery structures, the eigenvalues and right eigenvectors may be determined from the homogeneous part of Equation (2.5) as [32]:

$$\begin{bmatrix} [0] & [M] \\ [M] & [C] \end{bmatrix} \cdot \lambda_r + \begin{bmatrix} -[M] & [0] \\ [0] & [K] \end{bmatrix} \begin{Bmatrix} \{\Psi_R\}_r \cdot \lambda_r \\ \{\Psi_R\}_r \end{Bmatrix} = \begin{Bmatrix} \{0\} \\ \{0\} \end{Bmatrix} \quad (3.1)$$

where $\{\Psi_R\}_r$ is the $N \times 1$ right eigenvector of the r th mode and λ_r is its associated eigenvalue. The left eigenvectors can be obtained from:

$$\begin{bmatrix} [0] & [M] \\ [M] & [C] \end{bmatrix}^T \cdot \lambda_r + \begin{bmatrix} -[M] & [0] \\ [0] & [K] \end{bmatrix}^T \begin{Bmatrix} \{\Psi_L\}_r \cdot \lambda_r \\ \{\Psi_L\}_r \end{Bmatrix} = \begin{Bmatrix} \{0\} \\ \{0\} \end{Bmatrix} \quad (3.2)$$

where $\{\Psi_L\}_r$ is the $N \times 1$ left eigenvector of the r th mode.

For a system of order N there exist $2N$ modes, each with an associated eigenvalue, and right and left eigenvectors. If the mass, damping and stiffness matrices are real, then the right eigenvectors occur in N complex conjugate pairs, as do the left eigenvectors

and the eigenvalues. In this case, the state-space matrices of eigenvalues, and right and left eigenvectors, $[\tilde{\lambda}]$, $[\tilde{\Psi}_R]$ and $[\tilde{\Psi}_L]$, respectively, have the following formats:

$$[\tilde{\lambda}]_{2N \times 2N} = \begin{bmatrix} [\lambda]^* & [0] \\ [0] & [\lambda] \end{bmatrix} \quad (3.3)$$

$$[\tilde{\Psi}_R]_{2N \times 2N} = \begin{bmatrix} [\Psi_R]^* [\lambda]^* & [\Psi_R][\lambda] \\ [\Psi_R]^* & [\Psi_R] \end{bmatrix} \quad (3.4)$$

$$[\tilde{\Psi}_L]_{2N \times 2N} = \begin{bmatrix} [\Psi_L]^* [\lambda]^* & [\Psi_L][\lambda] \\ [\Psi_L]^* & [\Psi_L] \end{bmatrix} \quad (3.5)$$

As for non-rotating structures, the eigenvalues and right eigenvectors of rotating machinery structures define a state of free vibration in which the elements of the right eigenvectors represent the amplitudes and phases of the displacements at each DOF, and the eigenvalues represent their frequencies and decay rates.

These physical meanings of the eigenvalues and right eigenvectors are relatively easy to derive from the equation of motion of a system. However, the meaning of the left eigenvectors cannot be deduced in a straightforward manner. The reason for this is that the equations that define the left eigenvectors do not represent measurable quantities such as forces or displacements, and hence attaching a physical meaning to them is itself a challenge. A physical interpretation of the left eigenvectors is given in references [8], [14] and [17], where they are considered as force patterns associated with the selective excitation of structural modes.

3.2.2 Eigenvector normalisation

The right and left eigenvectors that are obtained from the solutions to Equations (3.1) and (3.2) can only be determined to within an arbitrary scaling factor. This implies that the same set of eigenvectors may be associated with an infinite number of systems, all with different spatial property matrices.

If the eigenvalues and eigenvectors are to be used to characterise specific systems, then it is important to eliminate this arbitrary factor from the definition of the eigenvectors. This is achieved through the process of normalisation.

The normalised right and left eigenvector matrices, $[\Phi_R]$ and $[\Phi_L]$, respectively, are related to their non-normalised representations through the following equations:

$$[\Phi_R] = [\Psi_R] \cdot [D_R] \quad (3.6)$$

$$[\Phi_L] = [\Psi_L] \cdot [D_L] \quad (3.7)$$

where $[D_R]$ and $[D_L]$ are $N \times N$ diagonal matrices chosen so that the state-space property matrices in equation (2.5) are diagonalised through the following transformations [36]:

$$\underset{2N \times 2N}{[\tilde{\Phi}_L]^T} \begin{bmatrix} [0] & [M] \\ [M] & [C] \end{bmatrix} \underset{2N \times 2N}{[\tilde{\Phi}_R]} = \begin{bmatrix} [I] & [0] \\ [0] & [I] \end{bmatrix} \quad (3.8)$$

$$\underset{2N \times 2N}{[\tilde{\Phi}_L]^T} \begin{bmatrix} -[M] & [0] \\ [0] & [K] \end{bmatrix} \underset{2N \times 2N}{[\tilde{\Phi}_R]} = -[\tilde{\lambda}] \quad (3.9)$$

where $[\tilde{\Phi}_L]$ and $[\tilde{\Phi}_R]$ are the state-space matrix representations of the normalised left and right eigenvectors, respectively, and $[\tilde{\lambda}]$ is the corresponding matrix of eigenvalues. Although for a system with complex spatial property matrices the eigenvalues and eigenvectors do not occur in complex conjugate pairs, the entries of the matrices $[\tilde{\Phi}_L]$, $[\tilde{\Phi}_R]$ and $[\tilde{\lambda}]$ are related to each other, as the matrices generally have the following formats:

$$\underset{2N \times 2N}{[\tilde{\Phi}_L]} = \begin{bmatrix} [\Phi_{L1}][\lambda_1] & [\Phi_{L2}][\lambda_2] \\ [\Phi_{L1}] & [\Phi_{L2}] \end{bmatrix} \quad (3.10)$$

$$\begin{bmatrix} \tilde{\Phi}_R \\ \hline \end{bmatrix}_{2N \times 2N} = \begin{bmatrix} [\Phi_{R1}] [\lambda_1] & [\Phi_{R2}] [\lambda_2] \\ \hline [\Phi_{R1}] & [\Phi_{R2}] \end{bmatrix} \quad (3.11)$$

$$\begin{bmatrix} \tilde{\lambda} \\ \hline \end{bmatrix}_{2N \times 2N} = \begin{bmatrix} [\lambda_1] & [0] \\ \hline [0] & [\lambda_2] \end{bmatrix} \quad (3.12)$$

where the block sub-matrices have dimensions $N \times N$. The blocks that constitute the lower rows of the right-hand sides of Equations (3.10) and (3.11) will be referred to as the ‘displacement portions’ of the space-state eigenvector matrices. These will be used extensively in later discussions.

Complex property matrices may be necessary to represent, for example, the properties of systems affected by hysteretic damping forces, whose amplitude may be proportional to the displacement of the system at one of its DOFs, but is in anti-phase with the velocity of the system at that DOF.

The normalisation of the eigenvectors makes it possible to give an arbitrary value to exactly one element of either the right or left eigenvectors of each mode. This is in contrast with the case of stationary structures, for which the condition that the right and left eigenvectors must be numerically identical, due to the symmetry of the spatial property matrices, eliminates the possibility of choosing arbitrary values for any of their elements once the normalisation criteria, e.g. mass-normalisation [14], have been established.

3.3 The response model

The steady-state response of a system, $\{X(\omega)\}$, to a harmonic excitation, $\{F(\omega)\}$, may be computed in the frequency domain using the following equation:

$$\{X(\omega)\} = [[K] - \omega^2[M] + i\omega[C]]^{-1} \cdot \{F(\omega)\} \quad (3.13)$$

or, in terms of the receptance version of the frequency response function (FRF) matrix:

$$\{X(\omega)\} = [\alpha(\omega)] \cdot \{F(\omega)\} \quad (3.14)$$

Using this equation, the receptance matrix, $[\alpha(\omega)]$, may be defined as:

$$[\alpha(\omega)] = [[K] - \omega^2[M] + i\omega[C]]^{-1} \quad (3.15)$$

The receptance matrix constitutes a response model of the system, which describes its dynamic behaviour as a function of the excitation frequency.

3.4 Relationships between the spatial and modal models

For systems with real spatial property matrices, equations (3.8) and (3.9) can be written as:

$$\begin{bmatrix} [\Phi_L]^*[\lambda]^* & [\Phi_L][\lambda] \\ [\Phi_L]^* & [\Phi_L] \end{bmatrix}^T \begin{bmatrix} [0] & [M] \\ [M] & [C] \end{bmatrix} \begin{bmatrix} [\Phi_R]^*[\lambda]^* & [\Phi_R][\lambda] \\ [\Phi_R]^* & [\Phi_R] \end{bmatrix} = \begin{bmatrix} [I] & [0] \\ [0] & [I] \end{bmatrix} \quad (3.16)$$

$$\begin{bmatrix} [\Phi_L]^*[\lambda]^* & [\Phi_L][\lambda] \\ [\Phi_L]^* & [\Phi_L] \end{bmatrix}^T \begin{bmatrix} -[M] & [0] \\ [0] & [K] \end{bmatrix} \begin{bmatrix} [\Phi_R]^*[\lambda]^* & [\Phi_R][\lambda] \\ [\Phi_R]^* & [\Phi_R] \end{bmatrix} = - \begin{bmatrix} [\lambda]^* & [0] \\ [0] & [\lambda] \end{bmatrix} \quad (3.17)$$

since for these systems the eigenvalues and eigenvectors occur in complex conjugate pairs. The spatial and modal parameters in Equations (3.16) and (3.17) may be separated to obtain the following expressions:

$$\begin{bmatrix} [0] & [M] \\ [M] & [C] \end{bmatrix}^{-1} = \begin{bmatrix} [\Phi_R]^*[\lambda]^* & [\Phi_R][\lambda] \\ [\Phi_R]^* & [\Phi_R] \end{bmatrix} \begin{bmatrix} [\Phi_L]^*[\lambda]^* & [\Phi_L][\lambda] \\ [\Phi_L]^* & [\Phi_L] \end{bmatrix}^T \quad (3.18)$$

$$\begin{bmatrix} [M] & [0] \\ [0] & -[K] \end{bmatrix}^{-1} = \begin{bmatrix} [\Phi_R]^*[\lambda]^* & [\Phi_R][\lambda] \\ [\Phi_R]^* & [\Phi_R] \end{bmatrix} \begin{bmatrix} [\lambda]^* & [0] \\ [0] & [\lambda] \end{bmatrix}^{-1} \begin{bmatrix} [\Phi_L]^*[\lambda]^* & [\Phi_L][\lambda] \\ [\Phi_L]^* & [\Phi_L] \end{bmatrix}^T \quad (3.19)$$

from which the some relationships between the spatial and modal property matrices can be established:

$$\text{Re}([\Phi_R][\lambda]^{-1}[\Phi_L]^T) = -\frac{1}{2}[K]^{-1} \quad (3.20)$$

$$\text{Re}([\Phi_R][\Phi_L]^T) = [0] \quad (3.21)$$

$$\text{Re}([\Phi_R][\lambda][\Phi_L]^T) = \frac{1}{2}[M]^{-1} \quad (3.22)$$

$$\text{Re}([\Phi_R][\lambda]^2[\Phi_L]^T) = -\frac{1}{2}[M]^{-1}[C][M]^{-1} \quad (3.23)$$

In the more general case of systems with complex spatial property matrices, equivalent relationships may be defined using the ‘displacement portions’ of the eigenvector matrices defined in Equations (3.10) and (3.11), i.e. the lower row of block submatrices, together with the eigenvector matrix defined in Equation (3.12):

$$\begin{matrix} \begin{bmatrix} [\Phi_{R1}] & [\Phi_{R2}] \end{bmatrix} \\ N \times 2N \end{matrix} \begin{matrix} \begin{bmatrix} [\lambda_1] & [0] \\ [0] & [\lambda_2] \end{bmatrix} \\ 2N \times 2N \end{matrix}^{-1} \begin{matrix} \begin{bmatrix} [\Phi_{L1}]^T \\ [\Phi_{L2}]^T \end{bmatrix} \\ 2N \times N \end{matrix} = \begin{matrix} -[K]^{-1} \\ N \times N \end{matrix} \quad (3.24)$$

$$\begin{bmatrix} [\Phi_{R1}] & [\Phi_{R2}] \end{bmatrix} \begin{bmatrix} [\Phi_{L1}]^T \\ [\Phi_{L2}]^T \end{bmatrix} = [0] \quad (3.25)$$

$$\begin{bmatrix} [\Phi_{R1}] & [\Phi_{R2}] \end{bmatrix} \begin{bmatrix} [\lambda_1] & [0] \\ [0] & [\lambda_2] \end{bmatrix} \begin{bmatrix} [\Phi_{L1}]^T \\ [\Phi_{L2}]^T \end{bmatrix} = [M]^{-1} \quad (3.26)$$

$$\begin{bmatrix} [\Phi_{R1}] & [\Phi_{R2}] \end{bmatrix} \begin{bmatrix} [\lambda_1] & [0] \\ [0] & [\lambda_2] \end{bmatrix}^2 \begin{bmatrix} [\Phi_{L1}]^T \\ [\Phi_{L2}]^T \end{bmatrix} = -[M]^{-1}[C][M]^{-1} \quad (3.27)$$

3.5 Relationships between the response and modal models

If the state-space matrices in Equation (2.5) are diagonalised through the use of Equations (3.8) and (3.9), then the following expressions for the receptance, $[\alpha(\omega)]$, and mobility, $i\omega \cdot [\alpha(\omega)]$, matrices can be established:

$$\begin{matrix}
\left[\alpha(\omega) \right] & = & \begin{bmatrix} \left[\Phi_{R1} \right] & \left[\Phi_{R2} \right] \end{bmatrix} & \begin{bmatrix} \left[i\omega I - \lambda_1 \right]^{-1} & [0] \\ [0] & \left[i\omega I - \lambda_2 \right]^{-1} \end{bmatrix} & \begin{bmatrix} \left[\Phi_{L1} \right]^T \\ \left[\Phi_{L2} \right]^T \end{bmatrix} \\
N \times N & & N \times 2N & 2N \times 2N & 2N \times N
\end{matrix} \quad (3.28)$$

$$\begin{matrix}
\left[i\omega \cdot \alpha(\omega) \right] & = & \begin{bmatrix} \left[\Phi_{R1} \right] & \left[\Phi_{R2} \right] \end{bmatrix} \cdot \dots \\
& & \begin{bmatrix} \left[\lambda_1 \right] \left[i\omega I - \lambda_1 \right]^{-1} & [0] \\ [0] & \left[\lambda_2 \right] \left[i\omega I - \lambda_2 \right]^{-1} \end{bmatrix} & \begin{bmatrix} \left[\Phi_{L1} \right]^T \\ \left[\Phi_{L2} \right]^T \end{bmatrix} \\
& & & & (3.29)
\end{matrix}$$

where I represents an $N \times N$ identity matrix and the remaining block sub-matrices are as defined in Equations (3.10)-(3.12). For the particular case of a system with real spatial property matrices, the receptance matrix is:

$$\left[\alpha(\omega) \right] = \left[\Phi_R \right] \left[i\omega I - \lambda \right]^{-1} \left[\Phi_L \right]^T + \left[\Phi_R^* \right] \left[i\omega I - \lambda^* \right]^{-1} \left[\Phi_L^* \right]^T \quad (3.30)$$

and its elements are defined as:

$$\alpha_{jk}(\omega) = \sum_{r=1}^N \left(\frac{(\Phi_R)_{jr} \cdot (\Phi_L)_{kr}}{i\omega - \lambda_r} + \frac{(\Phi_R^*)_{jr}^* \cdot (\Phi_L^*)_{kr}^*}{i\omega - \lambda_r^*} \right) \quad (3.31)$$

3.6 Physical interpretation of the relationships between the spatial and modal models

The relationships between the spatial and modal models presented in Section 3.4 are independent of the excitation forces and hence also of the excitation frequency. However their interpretation is greatly simplified by considering them as limits of the forced response as the excitation frequency tends to either a *low frequency limit*, defined as zero ($\omega = 0$), or a *high frequency limit*, defined as a frequency sufficiently greater than the natural frequencies of the modes of interest so that it can be effectively considered as an infinitely high frequency ($\omega \rightarrow +\infty$).

In this section, a physical interpretation of the relationships presented in Equations (3.24)-(3.27) will be presented, based on the relationships between the response, spatial and modal models. The forthcoming analyses are based on the general case of systems with complex property matrices. For systems with real spatial property matrices the same arguments apply, but Equations (3.20)-(3.23) should be used instead of Equations (3.24)-(3.27).

- **Equation (3.24) relates the spatial and modal representations of the receptance matrix when the excitation frequency is equal to the *low frequency limit*.**

Proof:

The spatial representation of the receptance matrix as the excitation approaches the *low frequency limit* may be determined from Equation (3.15):

$$\lim_{\omega \rightarrow 0} [\alpha(\omega)] = \lim_{\omega \rightarrow 0} [[K] - \omega^2[M] + i\omega[C]]^{-1} = [K]^{-1} \quad (3.32)$$

On the other hand, the modal representation of the receptance matrix as the excitation approaches the same frequency limit may be determined from Equation (3.28):

$$\begin{aligned} \lim_{\omega \rightarrow 0} [\alpha(\omega)] &= \lim_{\omega \rightarrow 0} \begin{bmatrix} [\Phi_{R1}] & [\Phi_{R2}] \end{bmatrix} \begin{bmatrix} [i\omega I - \lambda_1] & [0] \\ [0] & [i\omega I - \lambda_2] \end{bmatrix} \begin{bmatrix} [\Phi_{L1}]^T \\ [\Phi_{L2}]^T \end{bmatrix} \\ &\quad \begin{matrix} N \times N & N \times 2N & 2N \times 2N & 2N \times N \end{matrix} \end{aligned} \quad (3.33)$$

$$= \begin{bmatrix} [\Phi_{R1}] & [\Phi_{R2}] \end{bmatrix} \begin{bmatrix} [-\lambda_1] & [0] \\ [0] & [-\lambda_2] \end{bmatrix} \begin{bmatrix} [\Phi_{L1}]^T \\ [\Phi_{L2}]^T \end{bmatrix}$$

Equation (3.24) follows directly from Equations (3.32) and (3.33).

- **Equation (3.25) relates the spatial and modal representations of the mobility matrix, $(i\omega)[\alpha(\omega)]$, when the excitation frequency is equal to either the *low or high frequency limits*.**

Proof:

The spatial representation of the mobility matrix as the excitation approaches the *low frequency limit* may be determined using Equation (3.15):

$$\lim_{\omega \rightarrow 0} [i\omega \cdot \alpha(\omega)] = \lim_{\omega \rightarrow 0} (i\omega) \cdot [[K] - \omega^2[M] + i\omega[C]]^{-1} = 0 \quad (3.34)$$

The modal representation of the mobility matrix as the excitation approaches the same frequency limit may be determined from Equation (3.29):

$$\begin{aligned} & \lim_{\omega \rightarrow 0} (i\omega \cdot [\alpha(\omega)]) \\ &= \lim_{\omega \rightarrow 0} \begin{bmatrix} [\Phi_{R1}] & [\Phi_{R2}] \end{bmatrix} \begin{bmatrix} [\lambda_1][i\omega I - \lambda_1]^{-1} & [0] \\ [0] & [\lambda_2][i\omega I - \lambda_2]^{-1} \end{bmatrix} \begin{bmatrix} [\Phi_{L1}]^T \\ [\Phi_{L2}]^T \end{bmatrix} \\ &= \begin{bmatrix} [\Phi_{R1}] & [\Phi_{R2}] \end{bmatrix} \begin{bmatrix} [\Phi_{L1}]^T \\ [\Phi_{L2}]^T \end{bmatrix} \end{aligned} \quad (3.35)$$

Equation (3.25) follows directly from Equations (3.34) and (3.35). For the *high frequency limit*, the spatial representation of the mobility matrix can be determined using Equation (3.15):

$$\begin{aligned} \lim_{\omega \rightarrow \infty} [i\omega \cdot \alpha(\omega)] &= \lim_{\omega \rightarrow \infty} (i\omega) \cdot [[K] - \omega^2[M] + i\omega[C]]^{-1} \\ &= \lim_{\omega \rightarrow \infty} \left[\frac{[K]}{i\omega} - i\omega[M] + [C] \right]^{-1} = 0 \end{aligned} \quad (3.36)$$

In terms of the modal parameters, this mobility is computed using Equation (3.28):

$$\begin{aligned} & \lim_{\omega \rightarrow 0} (i\omega \cdot [\alpha(\omega)]) \\ &= \lim_{\omega \rightarrow \infty} (i\omega) \cdot \begin{bmatrix} [\Phi_{R1}] & [\Phi_{R2}] \end{bmatrix} \begin{bmatrix} [i\omega I - \lambda_1]^{-1} & [0] \\ [0] & [i\omega I - \lambda_2]^{-1} \end{bmatrix} \begin{bmatrix} [\Phi_{L1}]^T \\ [\Phi_{L2}]^T \end{bmatrix} \\ &= \lim_{\omega \rightarrow \infty} \begin{bmatrix} [\Phi_{R1}] & [\Phi_{R2}] \end{bmatrix} \begin{bmatrix} \left[I - \frac{\lambda_1}{i\omega} \right]^{-1} & [0] \\ [0] & \left[I - \frac{\lambda_2}{i\omega} \right]^{-1} \end{bmatrix} \begin{bmatrix} [\Phi_{L1}]^T \\ [\Phi_{L2}]^T \end{bmatrix} \\ &= \begin{bmatrix} [\Phi_{R1}] & [\Phi_{R2}] \end{bmatrix} \begin{bmatrix} [\Phi_{L1}]^T \\ [\Phi_{L2}]^T \end{bmatrix} \end{aligned} \quad (3.37)$$

Equation (3.25) can be deduced directly from the results of Equations (3.36) and (3.37).

- **Equation (3.26) relates the spatial and modal representations of the inertance matrix, $(i\omega)^2 [\alpha(\omega)]$, when the excitation frequency is equal to the *high frequency limit*.**

Proof:

The spatial representation of the inertance matrix as the excitation approaches the *high frequency limit* may be determined using Equation (3.15):

$$\begin{aligned} \lim_{\omega \rightarrow \infty} [(i\omega)^2 \cdot \alpha(\omega)] &= \lim_{\omega \rightarrow \infty} (i\omega)^2 \cdot [[K] - \omega^2 [M] + i\omega [C]]^{-1} \\ &= \lim_{\omega \rightarrow \infty} \left[\frac{[K]}{(i\omega)^2} + [M] + \frac{[C]}{(i\omega)} \right]^{-1} = [M]^{-1} \end{aligned} \quad (3.38)$$

The modal representation of the inertance matrix as the excitation approaches the same frequency limit may be determined using Equation (3.29):

$$\begin{aligned} \lim_{\omega \rightarrow \infty} [(i\omega)^2 \cdot [\alpha(\omega)]] &= \lim_{\omega \rightarrow \infty} (i\omega) \cdot [i\omega \cdot [\alpha(\omega)]] \\ &= \lim_{\omega \rightarrow \infty} (i\omega) \cdot \begin{bmatrix} [\Phi_{R1}] & [\Phi_{R2}] \end{bmatrix} \begin{bmatrix} \lambda_1 [i\omega I - \lambda_1]^{-1} & [0] \\ [0] & \lambda_2 [i\omega I - \lambda_2]^{-1} \end{bmatrix} \begin{bmatrix} [\Phi_{L1}]^T \\ [\Phi_{L2}]^T \end{bmatrix} \\ &= \begin{bmatrix} [\Phi_{R1}] & [\Phi_{R2}] \end{bmatrix} \begin{bmatrix} \lambda_1 & [0] \\ [0] & \lambda_2 \end{bmatrix} \begin{bmatrix} [\Phi_{L1}]^T \\ [\Phi_{L2}]^T \end{bmatrix} \end{aligned} \quad (3.39)$$

Equation (3.26) follows from Equations (3.38) and (3.39).

- **Equation (3.27) represents the effect of damping on the rate of change of acceleration, or jerk, matrix when the excitation frequency is equal to the *high frequency limit*.**

We will focus only on the physical interpretation of the right hand side of the equation.

The left hand side can be obtained by the method used in Section 3.4.

The jerk matrix, $[\mathcal{J}(\omega)]$, is defined as:

$$[\mathcal{J}(\omega)] = (i\omega)^3 \cdot [\alpha(\omega)] = (i\omega)^3 [[K] - [M]\omega^2 + i\omega[C]]^{-1} \quad (3.40)$$

If damping were not present in the system, then the jerk matrix would be defined as:

$$[\mathcal{J}_0(\omega)] = (i\omega)^3 [[K] - [M]\omega^2]^{-1} \quad (3.41)$$

The effect of damping on the jerk matrix is then:

$$[\mathcal{J}(\omega)] - [\mathcal{J}_0(\omega)] = (i\omega)^3 \left[[[K] - [M]\omega^2 + i\omega[C]]^{-1} - [[K] - [M]\omega^2]^{-1} \right] \quad (3.42)$$

Using the identity $[[A]^{-1} - [B]^{-1}] = [A]^{-1}[[B] - [A]][B]^{-1}$, the limit of the effect of damping on the jerk matrix as the excitation frequency tends to infinity is:

$$\begin{aligned} & \lim_{\omega \rightarrow \infty} \left[[\mathcal{J}(\omega)] - [\mathcal{J}_0(\omega)] \right] \\ &= \lim_{\omega \rightarrow \infty} (i\omega)^3 \left[[[K] - [M]\omega^2 + i\omega[C]]^{-1} [-i\omega[C]] [[K] - [M]\omega^2]^{-1} \right] \\ &= \lim_{\omega \rightarrow \infty} \left[\left[\frac{[K]}{(i\omega)^2} + [M] + \frac{[C]}{i\omega} \right]^{-1} [-[C]] \left[\frac{[K]}{(i\omega)^2} + [M] \right]^{-1} \right] \\ &= -[M]^{-1}[C][M]^{-1} \end{aligned} \quad (3.43)$$

3.7 Summary

In this Chapter, the modal and response models of rotating machinery structures have been described. The equations that define the relationships between the spatial and modal models have been derived analytically.

A physical interpretation of these equations has been given, in terms of the theoretical limit values of the receptance, mobility, accelerance and jerk matrices of the studied systems, as the excitation frequency tends to zero or to infinity.

The relationships between the three types of model that have been presented in this Chapter will be the basis for the derivation of the modal characterisation method presented in the next Chapter.

CHAPTER 4

Estimation of the modal properties of rotating machinery structures from measured vibration data

4.1 Introduction

In Chapter 1, the ‘column-row’ method for determining the modal parameters of rotating machinery structures was described. It was argued that its main practical limitation lies on the need to measure a complete row of the FRF matrix, which is difficult to carry out in practice but nevertheless necessary in order to determine the left eigenvectors.

The present Chapter introduces a method for determining the left eigenvectors of rotating machinery structures based on measurements of its FRFs. The goal of the method is to reduce the time and effort expended on the modal characterisation of these systems, by reducing the number of locations at which the excitation forces must be applied during modal tests.

The approach taken is to compute the left eigenvectors using the eigenvalues and the right eigenvectors, complete sets of which can be determined from one column of the FRF matrix. The computation procedure is based on the relationships between the different models that were derived in the previous Chapter.

4.2 Evaluation of the ‘column-row’ method

Complete characterisation of the behaviour of rotating machinery structures, unlike that of non-rotating structures, requires knowledge of their left eigenvectors as well as of their eigenvalues and right eigenvectors. For certain classes of system, such as undamped gyroscopic systems, the left eigenvectors are simply the complex conjugates of their right counterparts. However, in most cases, the two sets of eigenvectors do not obey such simple relationship and need to be determined directly from measured data. Traditionally, this is achieved through the ‘column-row’ method introduced by Nordmann [35], which was described in Chapter 1.

Although other characterisation methods exist for systems with specific types of spatial properties, such as skew-symmetric damping matrices, etc., the column-row method has the advantage that it is applicable to a broad variety of systems because it does not rely on assumptions about the symmetry of the spatial property matrices, or on any special relationships among the modal parameters.

On the other hand, one of its limitations is that it is impossible to simplify the testing scheme which is used to obtain the necessary response data, even if some characteristics of the system being studied are known before the tests. For example, in most cases the spatial properties are represented by real mass, damping and stiffness matrices. One of the direct consequences of this is that the eigenvalues and eigenvectors occur in complex conjugate pairs. This feature considerably simplifies the relationships that exist between the right- and left-eigenvectors, and although they may still not be as simple as for the case of undamped gyroscopic systems, they can nevertheless be used to determine some or all the necessary elements of the left-eigenvectors once the right eigenvectors are known.

In spite of the simplifications that are possible for systems with real property matrices, the measurement procedure prescribed in the ‘column-row’ method is the same regardless of whether the spatial property matrices are real or complex. One of the disadvantages of this inflexibility is that, instead of deriving some modal parameters from others, we are forced to determine all of them afresh from measured data. This requires more data to be gathered than are strictly necessary, as will be seen in the present Chapter, and imposes an unnecessarily complicated measurement scheme.

Another situation in which the measurement scheme results unnecessarily complicated is when the non-symmetry of the spatial property matrices is associated with only a few of the total DOFs. This is because the number of independent quantities that comprise the property matrices is larger when the matrix has large asymmetric regions than when it is predominantly symmetric. In most rotating machines, the asymmetry of the property matrices is limited only to the DOFs that lie on the rotating components or the components that support them directly, since it is there that the circulatory forces originate.

Hence, it is reasonable to expect that fewer data are required to model machines in which only a few of the DOFs lie on rotating components than are required for machines in which most of them do. However, the measurement scheme of the ‘column-row’ method is the same regardless of the amount of data required, as a full column and a row must be measured in every case.

To summarise, the ‘column-row’ method requires no knowledge of the properties of the system, but this generality comes at the cost of imposing a difficult measurement procedure in cases where it can be simplified. Prior knowledge of the system being tested should allow for a reduction in the number of measurements required for its

modal characterisation, since some of its modal parameters may be predicted from information about the system that is already possessed before the tests.

The characterisation method described in this Chapter is aimed at using this prior knowledge of the system in order to reduce the number of row elements of the FRF matrix that are required to build the modal models of rotating machines. The proposed method is based on the following assumptions: (a) that the spatial property matrices are real, (b) that the number of DOFs that are associated with the asymmetry of the spatial property matrices is known, (c) that the system at hand can be represented by a discrete model within the frequency range of interest, and (d) that the mass matrix is symmetric.

The fact that the asymmetry of the spatial property matrices originates only at the DOFs of its rotating components is important for the successful application of the method. This will be explained in more detail in the following section.

4.3 Rotating machines as structural assemblies

For modelling purposes, a rotating machine can be regarded as an assembly of two substructures: one formed by the non-rotating components and another formed by the rotating ones. When isolated, each of these substructures can be represented by a dynamic stiffness matrix. For the non-rotating substructure this matrix is symmetric, whereas for that containing the rotating components it is generally asymmetric. When the two substructures are coupled these matrices combine into a single dynamic stiffness matrix for the whole assembly. Although this resulting matrix is not symmetric, its asymmetry is limited to those DOFs which are associated with the rotating components, as shown in Figure 4.1.

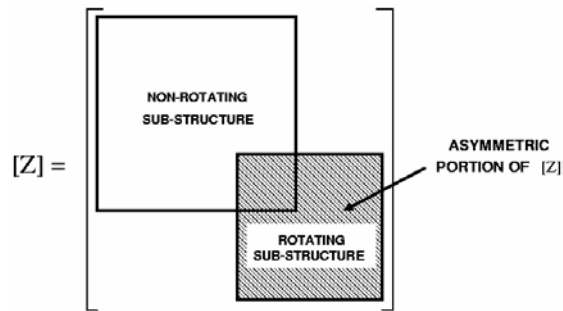


Figure 4.1 – Dynamic stiffness matrix, $[Z]$, of a rotating machine

Similarly, the asymmetric portions of the damping and stiffness matrices of the assembly only involve DOFs of the rotating components.

It is important to note that the asymmetric portion of the damping matrix is not necessarily related to the same DOFs as that of the stiffness matrix. This is because the circulatory forces represented in the two matrices do not necessarily originate at the same parts of the machine. For instance, a rotating rigid disk can give rise to gyroscopic moments that contribute to the asymmetry of the damping matrix but not to that of the stiffness matrix. On the other hand, elements like a hydrodynamic bearing may contribute to the asymmetry of both matrices. As a consequence of this, the number of DOFs related to the asymmetric portions is different for the damping and stiffness matrices.

4.4 Overview of the proposed characterisation method

As with the column-row method, the characterisation method proposed here starts with the measurement of a complete column of the FRF matrix, from which the right-eigenvectors and eigenvalues are extracted.

The approach then is to compute elements of the left eigenvectors using the fewest possible row elements of the FRF matrix. This is done using the relationships that exist between the spatial and modal models which were derived in the previous Chapter.

For machines in which all of the DOFs lie on rotating components, it is not possible to establish any equations to aid in the computation of the left-eigenvectors, so these parameters must be determined purely from measured data. For such systems the proposed method is equivalent to the ‘column-row’ method, since a complete row of the FRF matrix needs to be measured, in addition to one column.

In contrast, for machines in which only a few of the DOFs lie on rotating components it is often possible to establish a large number of equations to complement the measured data for the computation of the left-eigenvectors. For these systems, the required number of measurements will vary according to the size of the asymmetric portions of the spatial property matrices. With large sizes of these asymmetric portions, fewer relationships can be established, so more measurements are required to compute the left-eigenvectors.

The number of FRF row elements that need to be measured is that required to establish enough equations to determine the complete left-eigenvectors.

4.5 Equations for the computation of the left eigenvectors

The left eigenvectors may be computed using the relationships between the spatial and modal models that were presented in the previous Chapter. However, the computation cannot be carried out directly since the equations that express such relationships involve the unknown spatial property matrices, in addition to the sought left eigenvectors. This

means that the total number of unknown parameters will exceed the number of equations that can be obtained from matrix Equations (3.20)-(3.23).

In order to overcome this limitation, advantage can be taken of the fact that the mass matrix, and perhaps some portions of the damping and stiffness matrices, are symmetric. Additional equations may be established between elements of the mass, damping and/or stiffness matrices one side of their main diagonals and the corresponding symmetric elements on the opposite side.

The number of equations will be limited by the sizes of the asymmetric regions of the damping and stiffness matrices, as well as by the total number of DOFs of the system. This is treated in more detail in Section 4.6.4.1.

The following discussions are based on Equations (3.20)-(3.23), which were derived in Chapter 3 for systems with real spatial property matrices, and are restated here as Equations (4.1)-(4.4):

$$\operatorname{Re}([\Phi_R][\lambda]^{-1}[\Phi_L]^T) = -\frac{1}{2}[K]^{-1} \quad (4.1)$$

$$\operatorname{Re}([\Phi_R][\Phi_L]^T) = [0] \quad (4.2)$$

$$\operatorname{Re}([\Phi_R][\lambda][\Phi_L]^T) = \frac{1}{2}[M]^{-1} \quad (4.3)$$

$$\operatorname{Re}([\Phi_R][\lambda]^2[\Phi_L]^T) = -\frac{1}{2}[M]^{-1}[C][M]^{-1} \quad (4.4)$$

The computation procedure requires that the right eigenvectors and the eigenvalues be determined beforehand through the measurement and analysis of the FRFs associated with one column of the FRF matrix.

4.5.1 Effects of matrix symmetry on the relationships between the spatial and modal models

4.5.1.1 Matrix symmetry and partial symmetry

As discussed in Section 4.3, the asymmetry of the spatial property matrices of rotating machinery is associated only with the DOFs of its rotating components or their supports. We will now express this condition in the form of a matrix equation, so that it can later be used to derive expressions for the computation of the left eigenvectors.

Let us assume that a rotating machine has 10 DOFs, only 4 of which lie on its rotating components. It is possible that its damping and stiffness matrices are asymmetric. For this discussion we will assume that any asymmetry has its origins in the 4 DOFs of the rotating components, but the conclusions may be extended to cases where it also affects the support DOFs.

If we consider one of the spatial property matrices, say the stiffness matrix, and arrange its rows and columns so that the 4 DOFs of the rotating components occupy the 4 rightmost columns and the 4 lowest rows, then the stiffness matrix will have the layout presented in Figure 4.2.

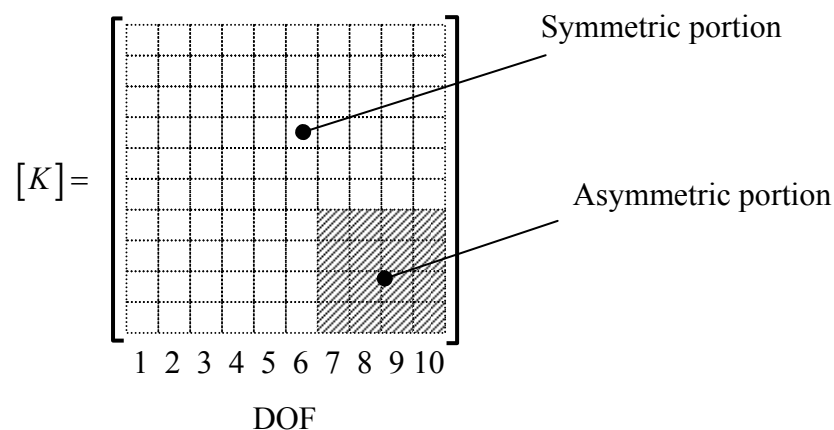


Figure 4.2 – Structure of the stiffness matrix

where the shaded region corresponds to the DOFs of the rotating components. The symmetric portion of $[K]$ spans the six leftmost columns, which form a 10×6 submatrix that is equal to the transpose of that formed by the 6 uppermost rows. Thus, we have:

$$[K][I_K] = [K]^T [I_K] \quad (4.5)$$

where:

$$[I_K] = \begin{bmatrix} [I]_{6 \times 6} \\ [0]_{4 \times 6} \end{bmatrix} \quad (4.6)$$

with $[I]_{6 \times 6}$ representing a 6×6 identity matrix and $[0]_{4 \times 6}$ a 4×6 matrix of zeros.

In a more general case, the DOFs corresponding to the rotating components will not be grouped in the last rows and columns, so $[I_K]$ may adopt more complicated forms than that defined in Equation (4.6). In any case, the matrix $[I_K]$ will have as many rows as the system has DOFs and as many columns as there are DOFs associated with the symmetric portion of the stiffness matrix. One element per column is unity and the remaining ones are zeros. The position of the unit element is different for every column, and corresponds to the position of a column of the property matrix within its symmetric portion. For example, for a 4-DOF system with a symmetric portion comprising DOFs 1 and 3, the matrix $[I_K]$ will be:

$$[I_K] = \begin{bmatrix} 1 & 0 \\ 0 & 0 \\ 0 & 1 \\ 0 & 0 \end{bmatrix} \quad (4.7)$$

We will refer to the matrix $[I_K]$ as the symmetry selection matrix for $[K]$. A similar matrix, $[I_C]$, can be derived to select the symmetric portions of $[C]$.

4.5.1.2 Relationships between the modal parameters

Apart from the matrix of left eigenvectors, Equations (4.1)-(4.4) involve the matrix of their complex conjugates. However, this latter matrix can be eliminated if Equation (4.2) is expressed as:

$$[\Phi_R][\Phi_L]^T + [\Phi_R^*][\Phi_L^*]^T = [0] \quad (4.8)$$

so that $[\Phi_L^*]$ can be substituted in Equations (4.1), (4.3) and (4.4), yielding:

$$\left([\Phi_R][\lambda]^{-1}[\Phi_R]^{-1} - [\Phi_R^*][\lambda^*]^{-1}[\Phi_R^*]^{-1}\right)[\Phi_R][\Phi_L]^T = -[K]^{-1} \quad (4.9)$$

$$\left([\Phi_R][\lambda][\Phi_R]^{-1} - [\Phi_R^*][\lambda^*][\Phi_R^*]^{-1}\right)[\Phi_R][\Phi_L]^T = [M]^{-1} \quad (4.10)$$

$$\begin{aligned} \left([\Phi_R][\lambda]^2[\Phi_R]^{-1} - [\Phi_R^*][\lambda^*]^2[\Phi_R^*]^{-1}\right)[\Phi_R][\Phi_L]^T = \dots \\ - [M]^{-1}[C][M]^{-1} \end{aligned} \quad (4.11)$$

whence the unknown matrices are those of the left eigenvectors and of the spatial properties.

To simplify Equations (4.9)-(4.11), we may define a matrix $[G]$ as:

$$[G] = [\Phi_L]^{-T}, \quad (4.12)$$

with which the right- and left-hand sides of Equations (4.9)-(4.11) may be inverted and equated to arrive at the following expressions:

$$[G][U_K(\Phi_R, \lambda)] = [K] \quad (4.13)$$

$$[G][U_M(\Phi_R, \lambda)] = [M] \quad (4.14)$$

$$[G][U_C(\Phi_R, \lambda)] = [C] \quad (4.15)$$

where:

$$[U_K(\Phi_R, \lambda)] = -[\Phi_R]^{-1} \left([\Phi_R][\lambda]^{-1}[\Phi_R]^{-1} - [\Phi_R^*][\lambda^*]^{-1}[\Phi_R^*]^{-1} \right)^{-1} \quad (4.16)$$

$$[U_M(\Phi_R, \lambda)] = [\Phi_R]^{-1} \left([\Phi_R][\lambda][\Phi_R]^{-1} - [\Phi_R^*][\lambda^*][\Phi_R^*]^{-1} \right)^{-1} \quad (4.17)$$

$$\begin{aligned} [U_C(\Phi_R, \lambda)] = & -[U_M(\Phi_R, \lambda)] \cdot [[\Phi_R][\lambda]^2[\Phi_R]^{-1} \dots \\ & - [\Phi_R^*][\lambda^*]^2[\Phi_R^*]^{-1}] \cdot [\Phi_R][U_M(\Phi_R, \lambda)] \end{aligned} \quad (4.18)$$

The unknowns in Equations (4.13)-(4.15) are the spatial property matrices and the matrix $[G]$. The matrices $[U_K(\Phi_R, \lambda)]$, $[U_M(\Phi_R, \lambda)]$ and $[U_C(\Phi_R, \lambda)]$ are functions of the known eigenvalues and right eigenvectors only.

The left eigenvectors may be computed directly from $[G]$ using Equation (4.12). For this reason, the next steps of the computation procedure will focus on determining the elements of $[G]$.

In order to determine the elements of $[G]$, it is first necessary to eliminate the spatial property matrices from Equations (4.13)-(4.15). This will be achieved using the symmetry of the mass matrix and/or the partial symmetry of the damping and stiffness matrices.

Taking account of the fact that the mass matrix is symmetric, Equation (4.14) can be used to establish the following expression:

$$[G][U_M(\Phi_R, \lambda)] = [U_M(\Phi_R, \lambda)]^T [G]^T \quad (4.19)$$

Similar expressions can be obtained for the stiffness and damping matrices by implementing the symmetry selection matrices, $[I_K]$ and $[I_C]$, in Equations (4.13) and (4.15), respectively:

$$[G][U_K(\Phi_R, \lambda)][I_K] = [U_K(\Phi_R, \lambda)]^T [G]^T [I_K] \quad (4.20)$$

$$[G][U_C(\Phi_R, \lambda)][I_C] = [U_C(\Phi_R, \lambda)]^T [G]^T [I_C] \quad (4.21)$$

Equations (4.19)-(4.21) do not involve the spatial property matrices, and hence they express relationships exclusively between the modal parameters. These equations may be used together with the known eigenvalues and right eigenvectors to determine the elements of $[G]$. However, it must be noted that the solution to the system formed by the three matrix equations is not unique, since any solution matrix may be multiplied by an arbitrary constant to yield another solution.

To obtain a complete system of equations with a unique solution, a normalisation equation based on the measured column of the FRF matrix may be implemented. The way in which this is done will be discussed in the following Sections.

4.5.2 Normalisation equation

Every element of the FRF matrix is related to the normalised right and left eigenvectors in accordance with Equation (3.31). It has been mentioned that after one column of the FRF matrix has been measured, it is possible to determine one element of each

normalised left eigenvector, in addition to the right eigenvectors and eigenvalues. This means that not only $[\lambda]$, $[\Phi_R]$, but also one row of $[\Phi_L]$ may be determined from one column of the FRF matrix.

4.5.2.1 Modal parameter estimation

Standard modal analysis algorithms may be used to express an FRF as a superposition of several response components, each of which is associated with an individual mode. Each component requires two parameters to be determined: a modal constant, ${}_r A_{jk}$, and an eigenvalue, λ_r , for the mode associated with it. Conventional modal analysis methods are based on the following representation of the FRF:

$$\alpha_{jk}(\omega) = \sum_{r=1}^N \left(\frac{{}_r A_{jk}}{i\omega - \lambda_r} + \frac{{}_r A_{jk}^*}{i\omega - \lambda_r^*} \right) \quad (4.22)$$

A modal constant is associated with a particular mode, identified by the subscript r , and to specific response measurement and excitation locations, denoted by the subscripts j and k , respectively. The relationship between a modal constant and the corresponding elements of the normalised eigenvectors is:

$${}_r A_{jk} = (\Phi_R)_{jr} (\Phi_L)_{kr} \quad (4.23)$$

After one column of the FRF matrix is measured, say the k_0 th column, it is possible to determine the modal constants corresponding to that column. This means that the modal constants given by:

$${}_r A_{jk_0} = (\Phi_R)_{jr} (\Phi_L)_{k_0 r} \quad (4.24)$$

are known for all r and j .

Identification of a modal constant does not enable the individual determination of the right and left eigenvector elements. However, since an identified modal constant fixes the value of the product of two of these elements, one of them can be arbitrarily chosen and the other one determined through Equation (4.24).

A relatively easy way to normalise the eigenvectors is to give a unit value to the k_0 th element of each left eigenvector:

$$(\Phi_L)_{k_0 r} = 1 \quad \forall \quad r \quad (4.25)$$

In this way, Equation (4.24) may be used to relate the right eigenvectors with the identified modal constants, as:

$$(\Phi_R)_{j r} = {}_r A_{j k_0} \quad \forall \quad r \quad (4.26)$$

Since the modal constants are determined directly from the measured data, then the normalised right eigenvectors are automatically identified.

It is important to note that only one element of each left eigenvector may be assigned an arbitrary unit value. In this case, these were the k_0 th elements of each of the vectors. If more columns of the FRF matrix are measured, additional elements of the left eigenvectors should be determined using Equation (4.24) together with the already known right eigenvectors.

4.5.2.2 Derivation of the normalisation equation

The normalisation procedure described in the preceding section yields one complete row of the left eigenvector matrix which may be used in the computation of the matrix $[G]$ defined in section 4.5.1.2.

If Equation (4.12) is rearranged in the following way:

$$[G][\Phi_L]^T = [I]_{N \times N} \quad (4.27)$$

then the elements of a known row of $[\Phi_L]$, say the k_0 th row, which are numerically identical to the k_0 th column-vector of the matrix $[\Phi_L]^T$, $\{[\Phi_L]^T\}_{k_0}$, can be used to establish the following equation in the unknown matrix $[G]$:

$$[G]\{[\Phi_L]^T\}_{k_0} = \{i_G\} \quad (4.28)$$

where the k_0 th element of the vector $\{i_G\}$ has unit value and the remaining elements are zeros.

Equation (4.28) will be referred to as the *normalisation equation*. This equation can be expanded if more rows of the left eigenvectors are known. For example, if rows k_0 , k_1 , k_2 , ... , etc. of the normalised left eigenvectors matrix are determined, then their transposes may be arranged to form the columns of a matrix, $[\Phi_G]$, defined as:

$$[\Phi_G] = \left[\{[\Phi_L]^T\}_{k_0}, \{[\Phi_L]^T\}_{k_1}, \{[\Phi_L]^T\}_{k_2}, \dots \right] \quad (4.29)$$

Similarly, a matrix, $[I_G]$, may be formed with columns k_0 , k_1 , k_2 , ... , etc. of an $N \times N$ identity matrix, $[I]_{N \times N}$, so that Equation (4.28) may be rewritten as:

$$[G][\Phi_G] = [I_G] \quad (4.30)$$

If q is the number of known rows of the left eigenvector matrix and N is the number of DOFs of the system, then $[G]$ has dimensions $N \times N$, while $[I_G]$ and $[\Phi_G]$ have dimensions $N \times q$.

4.6 Computation of the left eigenvectors

In the previous Section, the symmetry or partial symmetry of the spatial property matrices, as well as the measured FRF data, were incorporated into the relationships between the spatial and the modal models derived in Chapter 3. As a result of this, Equations (4.19)-(4.21) and (4.30) were obtained. Using these equations, it is possible to compute the unknown matrix $[G]$, from which the left eigenvectors may be directly determined, as was discussed in Section 4.5.1.2. In this Section, a procedure for the computation is presented.

Equations (4.19)-(4.21) and (4.30) may all be expressed in the following general form:

$$[G][U] + [V][G]^T [W] = [B] \quad (4.31)$$

However, in order to determine the unknown elements of the matrix $[G]$ from these equations it is first necessary to transform them into a simpler form, so that they can be treated using a conventional method of solution. We will refer to this simpler form as the ‘canonical form’ of the equations [4], which is defined as:

$$[A]\{y\} = \{b\} \quad (4.32)$$

where the dimensions of the coefficients matrix, $[A]$, and the vectors $\{y\}$ and $\{b\}$ are, respectively, $m \times n$, $n \times 1$ and $m \times 1$. In order to transform Equations (4.19)-(4.21) and (4.30) from the general form given in Equation (4.31) to their canonical forms

expressed by Equation (4.32), we will make use of the Kronecker product, which is defined in the next Subsection.

4.6.1 The Kronecker product

Definition:

Let $[A]$ and $[B]$ be two rectangular matrices with dimensions $m \times n$ and $p \times q$, respectively. The Kronecker product of these two matrices is then [4]:

$$[A] \otimes [B] = \begin{bmatrix} a_{11}[B] & a_{12}[B] & \cdots & a_{1n}[B] \\ a_{21}[B] & a_{22}[B] & \cdots & a_{2n}[B] \\ \vdots & \vdots & & \vdots \\ a_{m1}[B] & a_{m2}[B] & \cdots & a_{mn}[B] \end{bmatrix} \quad (4.33)$$

The resulting product matrix has dimensions $mp \times nq$.

4.6.2 Transformation of matrix equations into canonical form

To derive the canonical form of the general form equation (4.31) it is first necessary to express both $[G]$ and $[B]$ in vectorised form. This is achieved by creating a column vector consisting of the columns of the original matrix placed successively one below the other. For example, if we define $[G]$ in terms of its column vectors as:

$$[G] = [\{g_1\}, \{g_2\}, \{g_3\}, \dots] \quad (4.34)$$

then its vectorised form will be:

$$\{g\} = \begin{Bmatrix} \{g_1\} \\ \{g_2\} \\ \{g_3\} \\ \vdots \end{Bmatrix} \quad (4.35)$$

A similar expression may be defined for the vectorised form of matrix $[B]$.

If the dimensions of $[G]$ and $[V]$ in Equation (4.31) are $N \times N$, and those of $[U]$, $[W]$ and $[B]$ are $N \times p$, then use of the Kronecker product allows the transformation of Equation (4.31) into its canonical form, given by:

$$\left[\left(U^T \otimes I_{N \times N} \right) + \left(W^T \otimes V \right) \cdot [P]_{N^2 \times N^2} \right] \{g\} = \{b\} \quad (4.36)$$

in which $\{g\}$ and $\{b\}$ are the vectorised forms of matrices $[G]$ and $[B]$, respectively, and the matrix $[P]_{N^2 \times N^2}$ is a permutation matrix that transforms the vectorised form of an $N \times N$ matrix into the vectorised form of its transpose; i.e. if $\{g\}$ represents the vectorised form of matrix $[G]$ and $\{g_T\}$ represents the vectorised form of $[G]^T$, then the following relationship holds:

$$[P]_{N^2 \times N^2} \cdot \{g\} = \{g_T\} \quad (4.37)$$

The permutation matrix is used to express the unknown elements of the matrices $[G]$ and $[G]^T$ using a single vectorised form. Finding the solution of Equation (4.36) then requires determining the elements of a single vector, $\{g\}$.

4.6.3 Canonical form of the equations for the computation of the left eigenvectors

Using the template of Equation (4.36), with the following conditions:

$$[U] = [U_M(\Phi_R, \lambda)] = [U_M]; [V] = -[U_M]^T; [W] = [I]_{N \times N}; [B] = [0] \quad (4.38)$$

then Equation (4.19) may be rewritten in its canonical form as:

$$\left[([U_M]^T \otimes [I]_{N \times N}) - ([I]_{N \times N} \otimes [U_M]^T) \cdot [P]_{N^2 \times N^2} \right] \{g\} = \{0\} \quad (4.39)$$

where the $N \times N$ matrix $[U_M]$ is a function of the right eigenvectors and the eigenvalues, the $N^2 \times 1$ vector $\{g\}$ is the vectorised form of matrix $[G]$, and $\{0\}$ is a column vector of zeros of dimensions $N^2 \times 1$.

The canonical forms of Equations (4.20) and (4.21) are, respectively:

$$\left[([U_K \cdot I_K]^T \otimes [I]_{N \times N}) - ([I_K]^T \otimes [U_K]^T) \cdot [P]_{N^2 \times N^2} \right] \{g\} = \{0\} \quad (4.40)$$

$$\left[([U_C \cdot I_C]^T \otimes [I]_{N \times N}) - ([I_C]^T \otimes [U_C]^T) \cdot [P]_{N^2 \times N^2} \right] \{g\} = \{0\} \quad (4.41)$$

where the $N \times N$ matrices $[U_K]$ and $[U_C]$ are functions of the eigenvalues and right eigenvectors, and $\{g\}$ and $\{0\}$ are as defined for Equation (4.39).

Finally, the canonical form of Equation (4.30) is:

$$([\Phi_G]^T \otimes [I]_{N \times N}) \{g\} = \{i_G\} \quad (4.42)$$

where $\{i_G\}$ is the vectorised form of the $N \times q$ matrix $[I_G]$ defined in Section 4.5.2.2.

Equations (4.39)-(4.42) can be merged into a single canonical-form equation, so that conventional solution methods may be applied to determine the elements of $\{g\}$. This vector would then be used to reconstruct $[G]$, so that the matrix of left eigenvectors can be determined.

The merger of Equations (4.39)-(4.42) leads to the following expression:

$$[A_G] \cdot \{g\} = \begin{Bmatrix} \{0\} \\ \{0\} \\ \{0\} \\ \{i_G\} \end{Bmatrix} \quad (4.43)$$

where:

$$[A_G] = \begin{bmatrix} ([U_M]^T \otimes [I]_{N \times N}) - ([I]_{N \times N} \otimes [U_M]^T) \cdot [P]_{N^2 \times N^2} \\ \dots \dots \dots \\ ([U_K \cdot I_K]^T \otimes [I]_{N \times N}) - ([I_K]^T \otimes [U_K]^T) \cdot [P]_{N^2 \times N^2} \\ \dots \dots \dots \\ ([U_C \cdot I_C]^T \otimes [I]_{N \times N}) - ([I_C]^T \otimes [U_C]^T) \cdot [P]_{N^2 \times N^2} \\ \dots \dots \dots \\ [\Phi_G]^T \otimes [I]_{N \times N} \end{bmatrix} \quad (4.44)$$

In this equation, the matrix of coefficients, $[A_G]$, is formed by: (a) functions of the eigenvalues and right eigenvectors, (b) independently defined matrices, such as the permutation and identity matrices, and (c) known elements of the left eigenvectors, obtained from the measured row element(s) of the FRF matrix. On the other hand, the right hand side of the equation consists of zeros or known columns of the identity matrix.

In its canonical form, the system of equations (4.43) can be solved for the unknown elements of $\{g\}$ through a variety of methods. For example, if the matrix of coefficients is represented as $[A_G]$ and the vector on the right-hand side of the same equation is represented as $\{b\}$, then a solution of the following form may be obtained for the vector $\{g\}$ using the Moore-Penrose pseudo-inverse method [3]:

$$\{g\} = [[A_G]^T [A_G]]^{-1} [A_G]^T \{b\} \quad (4.45)$$

The conditions for the solution to be unique are discussed in the next Section.

4.6.4 Conditions for the existence of a unique solution

For a physical system with N DOFs, Equation (4.43) involves N^2 unknowns, which are the elements of $\{g\}$. For the solution to this linear system of equations to be unique, at least N^2 of the individual equations that constitute it must be linearly independent. To determine in which cases this condition is satisfied, we shall first consider the total number of equations that can be obtained. This number depends on the following parameters:

- a) the number of DOFs of the system,
- b) the number of DOFs associated with the asymmetric regions of the damping and stiffness matrices, and
- c) the number of measured columns of the FRF matrix.

4.6.4.1 Total number of equations

The individual equations that constitute the system defined in (4.43), and which correspond to the first three blocks of the matrix $[A_G]$, are obtained using the symmetry or partial symmetry of the mass, stiffness and damping matrices, respectively. Those corresponding to the fourth block are associated with the relationship between the matrix $[G]$ and the left eigenvector elements determined through measurements of FRFs on different columns of the FRF matrix. The case of the symmetry relationships will be analysed first.

A symmetric matrix of dimensions $N \times N$ has N^2 elements, out of which only $N(N + 1)/2$ need to be specified to completely define the matrix. These can be, for example, the elements along and above the main diagonal. The remaining $N(N - 1)/2$ elements may be determined by an equal number of symmetry relationships between them and the already defined ones. These relationships equate an element on one side of the main diagonal to its symmetric counterpart on the opposite side. For example, let $[A]$ be a symmetric matrix. Then the symmetry relationships between its elements are defined by the equations:

$$a_{jk} = a_{kj} , \quad 1 \leq j \leq N, \quad 1 \leq k \leq j - 1 \quad (4.46)$$

where a_{jk} represents the element on the j th row and the k th column of $[A]$.

Following this symmetry approach, the number of equations, p_m , that can be obtained from the mass matrix of a system with N DOFs is then:

$$p_m = \frac{N(N - 1)}{2} \quad (4.47)$$

These equations correspond to the first block of $[A_G]$. The number of equations associated with this block is larger for systems with a large number of DOFs than for smaller order systems.

Additional equations may be obtained by treating the stiffness and damping matrices in a similar fashion. However, attention must be paid to the fact that these matrices may have asymmetric portions, the elements within which cannot be used to derive symmetric relationships like those defined above.

The number of equations that can be established for the stiffness and damping matrices depends on the order of the system, as well as on the extent of their asymmetric portions. If these portions are associated with n_k and n_c DOFs, respectively, then the number of equations that can be obtained through symmetry relationships are:

$$p_k = \frac{N(N-1)}{2} - \frac{n_k(n_k-1)}{2} \quad (4.48)$$

for the stiffness matrix, and:

$$p_c = \frac{N(N-1)}{2} - \frac{n_c(n_c-1)}{2} \quad (4.49)$$

for the damping matrix. These equations are associated with the second and third blocks of $[A_G]$, respectively. The number of equations that constitute these blocks is large for large order systems in which only a few of the DOFs are associated with the asymmetric portions of their stiffness and damping matrices.

The fourth block of $[A_G]$ corresponds to the relationships that exist between elements of matrix $[G]$ and the elements of the left eigenvectors obtained from measured row elements of the FRF matrix. If q different columns of the FRF matrix are measured,

then an equal number of elements of each left eigenvector can be directly determined and the number of equations of (4.43) associated with the fourth block of $[A_G]$ is:

$$p_g = q \cdot N \quad (4.50)$$

As more columns of the FRF matrix are measured, the number of equations in this block grows.

The total number of equations involved in matrix Equation (4.43) is given by the expression:

$$\begin{aligned} p_{total} &= p_m + p_k + p_c + p_g \\ &= \frac{3}{2}N(N-1) - \frac{1}{2}n_K(n_K-1) - \frac{1}{2}n_C(n_C-1) + q \cdot N \end{aligned} \quad (4.51)$$

As was mentioned earlier, the existence of a unique solution to (4.43) requires that the number of unknowns, N^2 , be equal to, or less than, the number of linearly independent equations, $p_{l.i.}$, which, in general, is smaller than the total number of equations, p_{total} .

Hence, the following necessary, but not sufficient, condition for the existence of a unique solution to (4.43) may be established:

$$p_{total} \geq p_{l.i.} = N^2 \quad (4.52)$$

This expression may be used to detect whether the number of measured row elements of the FRF matrix is insufficient to obtain a unique solution to (4.43), but it should not be used to determine whether it is sufficient. For this, it should be considered that enough measurements would lead to a sufficient number of linearly independent equations in (4.43). Thus, the criteria used to determine whether enough measurements have been carried out should not be based on the total number of equations produced, but on the

number of those that are linearly independent. In the following Section, the derivation of such criteria is presented.

4.6.4.2 Required number of measurements

The number of linearly independent equations that may be obtained from matrix Equation (4.43) can be determined by calculating the rank of its coefficients matrix, $[A_G]$. Although the complexity of such a matrix complicates the analytical derivation of its rank, an inductive derivation based on various numerical examples was obtained.

4.6.4.2.1 Description of the trial system models

Trial systems were used to determine the number of row elements, q , of the FRF matrix that need to be measured in order to allow obtaining a unique solution to Equation (4.43). This number is affected by three parameters: the number of DOFs associated with the asymmetric portions of the stiffness and damping matrices, n_k and n_c , respectively, and the total number of DOFs of the physical system, N .

The trial models consisted of the three spatial property matrices, formulated so that their dimensions and those of their asymmetric portions corresponded the desired values of N , n_k and n_c .

The elements of the property matrices were computed systematically for the following parameter ranges:

$$2 \leq N \leq 25 \tag{4.53}$$

$$0 \leq n_k \leq N \tag{4.54}$$

$$0 \leq n_c \leq N \tag{4.55}$$

4.6.4.2.2 Use of the trial system models

After calculating the spatial matrices, all the modal parameters of the system were determined using a commercial eigensolver (MATLAB function 'EIG').

The eigenvectors were normalised afterwards, following the criteria given in Section 4.5.2.1. With information from the right eigenvectors and the eigenvalues, and also different numbers of elements of the left eigenvector, according to the parameter q , the matrix of coefficients of Equation (4.43) was computed. Afterwards, its rank was determined using the MATLAB function 'RANK' and the condition estimator 'RCOND'. For every example, the minimum value of q required for the rank of the coefficients matrix, $[A_G]$, to be equal to N^2 was determined.

In Appendix A, the results obtained for systems with 15 DOFs are presented and discussed.

The following requirements for the computation of the left eigenvectors were determined by correlating the parameters N , n_k and n_c with the number of required FRF row elements, q , from the examples that were solved:

$$q \geq 1 \quad (4.56)$$

$$q \geq \sqrt{n_c^2 + n_k^2} - N + 1 \quad (4.57)$$

$$q \geq \max(n_c, n_k) - 2[N - \min(n_c, n_k)] \quad (4.58)$$

In Equation (4.58), $\max(n_c, n_k)$ and $\min(n_c, n_k)$ denote the largest and the smallest, respectively, of the two parameters n_c and n_k . The sought value of the parameter q was that which simultaneously satisfied the three inequalities given above, and thus ensured that enough linearly independent equations were available to compute the left eigenvectors through Equation (4.43).

4.7 Two special cases

Equations (4.56)-(4.58) may be used to derive the number of elements from a row of the FRF that must be measured to determine the left eigenvectors for two cases of practical importance:

Case 1. If either the damping or the stiffness matrices are symmetric ($n_c = 0$ or $n_k = 0$), only one column of the FRF matrix is required to determine all the left eigenvectors. Included in this category are, for example, damped gyroscopic systems, in which only the damping matrix is asymmetric due to the effects of gyroscopic moments. These systems will be studied in more detail in the next Section.

Case 2. If the asymmetric components of the damping and stiffness matrices have the same order ($n_c = n_k = n$) then the required number of elements of the FRF matrix is:

$$q = 3n - 2N \quad (4.59)$$

Using this equation, it can be deduced that if:

$$n \leq \frac{2N + 1}{3} \quad (4.60)$$

then only one column of the FRF matrix needs to be measured in order to compute the left eigenvectors.

This case is especially important in situations where it may be possible to predict the DOFs at which circulatory forces originate, although no information may be possessed about the type of these forces, i.e. whether they are proportional to the velocities or to the displacements of the system. In these situations, Equation (4.59) may lead to an overestimation of the number of required measurements, but this overestimation

compensates for the lack of knowledge about the characteristics of the circulatory forces that affect the system.

Using Equation (4.59) it is also possible to deduce that if the asymmetric regions of both the damping and stiffness matrices are associated with all the DOFs of the system under consideration, then computation of the left eigenvectors requires FRF measurements from a complete row of the FRF matrix. That is, if $n = N$ in Equation (4.59) then:

$$q = 3n - 2N = N \quad (4.61)$$

4.8 Damped gyroscopic systems

Gyroscopic moments arise when a body rotates around an axis that does not maintain a constant spatial orientation, but on the contrary undergoes transversal angular motions. This type of motion is especially common in rotating machinery, since most of the rotating components are mounted onto shafts that are not rigidly fixed in space, but quite contrarily undergo translational and angular displacements when the machine vibrates. Specifically, the angular displacements of the shaft cause the axes of rotation of the other elements to tilt, thus originating the gyroscopic moments.

Several attempts have been made to characterise the dynamics of damped and undamped gyroscopic systems, and specifically to develop methods for determining the left eigenvectors. However, to the best knowledge of the author, analytical tools for the prediction of these modal parameters only exist for the undamped case.

In this Section, an analytical technique is presented by means of which the left eigenvectors of damped gyroscopic systems may be determined using the right

eigenvectors and the eigenvalues of the physical systems. The technique is based on Equations (4.19)-(4.21) and (4.30).

For the class of damped gyroscopic systems that will be analysed here, the mass and stiffness matrices are considered to be symmetric and the damping matrix is considered to be asymmetric due to the combination of true damping and gyroscopic forces. The extreme case in which the asymmetry of this matrix is associated with all the DOFs of the system will be considered.

If the stiffness matrix is symmetric, then $[I_K]$ in Equation (4.20) is an identity matrix, so the equation may be rewritten as:

$$[G][U_K] = [U_K]^T [G]^T \quad (4.62)$$

where $[U_K]$ is a function of the right eigenvectors and eigenvalues of the system. If the matrix $[G]^T$ is eliminated using Equations (4.19) and (4.62), then the following expression can be obtained:

$$[U_M][U_K]^{-1} = [G]^{-1}([U_K]^{-1}[U_M])^T [G] \quad (4.63)$$

This expression may be used to derive the elements of the matrix $[G]$, although for this the products $([U_M][U_K]^{-1})$ and $([U_K]^{-1}[U_M])^T$ may be more conveniently expressed in terms of their eigenvalues and right eigenvectors as:

$$[U_M][U_K]^{-1} = [\Psi_{MK}] [\lambda_{MK}] [\Psi_{MK}]^{-1} \quad (4.64)$$

$$([U_K]^{-1}[U_M])^T = [\Psi_{KM}] [\lambda_{KM}] [\Psi_{KM}]^{-1} \quad (4.65)$$

Through algebraic manipulation of these two equations, it may be shown that the diagonal matrix $[\lambda_{KM}]$ is the matrix of eigenvalues of the diagonal matrix $[\lambda_{MK}]$, i.e.:

$$[\lambda_{MK}] \cdot [[\Psi_{MK}]^{-1} [U_K] [\Psi_{KM}]^{-T}] = [[\Psi_{MK}]^{-1} [U_K] [\Psi_{KM}]^{-T}] \cdot [\lambda_{KM}] \quad (4.66)$$

This means that both matrices are identical:

$$[\lambda_{MK}] \equiv [\lambda_{KM}] \quad (4.67)$$

With this consideration, it can be deduced that the product $[\Psi_{KM}]^{-1} [G] [\Psi_{MK}]$ results in a diagonal matrix, and hence the following expression can be established:

$$[G] = [\Psi_{KM}] [D] [\Psi_{MK}]^{-1} \quad (4.68)$$

where $[D]$ is a diagonal matrix to be determined from one measured column of the FRF matrix. This column may be the same from which the right eigenvectors and eigenvalues of the system were derived. Assuming that the k_0 th column of the FRF matrix was measured, then Equation (4.28) may be used together with Equation (4.68) to derive the following expression:

$$[D] [\Psi_{MK}]^{-1} \{ \Phi_G \}_{k_0} = [\Psi_{KM}]^{-1} \{ i_G \}_{k_0} \quad (4.69)$$

where $\{ i_G \}_{k_0}$ is the k_0 th column of an $N \times N$ identity matrix and $\{ \Phi_G \}_{k_0}$ is a vector formed by the k_0 th elements of each left eigenvector of the physical system, which can be determined from the measured FRFs.

Using Equation (4.69), the non-zero elements of the diagonal matrix $[D]$ can be computed from:

$$d_{kk} = \frac{\left\{ [\Psi_{KM}]^{-1} \cdot \{ i_G \}_{k_0} \right\}_k}{\left\{ [\Psi_{MK}]^{-1} \cdot \{ \Phi_G \}_{k_0} \right\}_k} ; \quad 1 \leq k \leq N \quad (4.70)$$

Using this equation together with Equation (4.68), the matrix $[G]$ can be determined. Alternatively, the same two equations may be used to derive the following expression for the direct computation of the left eigenvectors:

$$[\Phi_L] = [\Psi_{KM}]^{-T} [D]^{-1} [\Psi_{MK}]^T \quad (4.71)$$

where $[\Psi_{MK}]$, $[\Psi_{KM}]$ and $[D]$ are defined in (4.64), (4.65) and (4.70), respectively.

The procedure that has just been described allows the determination of the left eigenvectors of a system with symmetric mass and stiffness matrices and asymmetric damping matrix. A similar procedure may be followed when the mass and damping matrices are symmetric but the stiffness matrix is asymmetric. However, this would require using $[U_C]$ instead of $[U_K]$ in Equation (4.62).

4.9 Use of the characterisation method

The basic steps for the use of the characterisation method that has been presented in this Chapter are given below. These steps serve only as a guideline, as it may be necessary to consider other practical issues for specific applications:

- (a) If dealing with a continuous system, establish the frequency range of interest and the DOFs for the measurement of the response. This may be based on the results of exploratory measurements or on computer models of the system being studied.
- (b) Determine the number of DOFs that are related to the asymmetric portions of the damping and stiffness matrices, according to the mechanical elements with which they are associated and to the type of circulatory force, i.e. displacement- or velocity-dependent, that may originate on them. For example, it would be

reasonable to consider that the asymmetric portion of the damping matrix would contain those DOFs that lie on rotating components with high rotational moments of inertia, as they are likely to give rise to gyroscopic forces, which are velocity-dependent.

- (c) Compute the number of row elements of the FRFs required. This may be achieved through the inequalities given in Section 4.6.4.2.2.
- (d) Measure the FRFs associated with one column plus the required number of row elements of the FRF matrix of the rotating machine structure.
- (e) Determine the eigenvalues and normalised right eigenvectors from the measured data, as well as the element(s) of the normalised left eigenvectors associated with the measured row elements of the FRF matrix.
- (f) Establish a linear system of equations for the computation of the remaining elements of the left eigenvectors and solve the system.

In the next Chapter, the application of the methods described here is illustrated using one numerical model and an industrial test-rig.

CHAPTER 5

Case studies

5.1 Introduction

The case studies used in this Chapter illustrate the application of the characterisation method presented in Chapter 4. For brevity, this method will be referred to as the “predictive method”, since it is used to predict the left eigenvectors of a system, instead of deriving them directly from measurements.

The first case study was carried out on a numerical model of a 4-DOF rigid rotor. The starting point for the characterisation of the rotor was a set of numerically-simulated FRF ‘measurements’. In order to evaluate the performance of the predictive characterisation method under idealised conditions, these simulated measurements were considered to be free of noise. It is shown that the method performs well with noise-free data, but also that small errors in the modal analysis of ‘measured’ FRFs affect the accuracy with which the left eigenvectors can be predicted.

This case study demonstrates that it is possible to fully characterise a dynamic system without the need to measure a full row of its FRF matrix.

The second case study was performed on an industrial test structure, called the “windmill test-rig”. Its dynamic characterisation was carried out using the same method as in the previous case, with the exception that the data used in this second case study was obtained by experiments. On this occasion, the objective was to evaluate the performance of the predictive method in a case where (a) the system under consideration is continuous and hence possesses an infinite number of DOFs, and (b)

the measured response data are considerably affected by noise. The effect of having close modes on the accuracy of the method, and the selection of an optimal set of DOFs to perform the characterisation, are also explored in this second case study.

The accuracy of the characterisation via the predictive method depends on the quality of the measured FRF data. The presence of measurement noise usually has adverse effects on the outcome of modal analysis. These effects are accentuated in cases where the system under consideration has two or more close modes. In this case study the performance of the predictive method under this condition was evaluated.

It is shown that the predicted left eigenvectors can be used to make accurate estimations of the response of the system to excitation forces applied at locations different to those used for the measurements. One of the practical applications of this feature is that it allows us to determine the response that would ensue due to an excitation applied onto a rotating component, without the need to perform the measurement in practice.

5.2 Case study 1: numerical model of a 4-DOF rigid rotor

The rotor used in this first case study is illustrated in Figure 5.1. It consists of a rigid shaft with rigid disks firmly attached at its two ends. The disks are mounted on flexible and damped supports, as shown in the Figure. The density of the rotor is considered to be that of steel, and its speed of rotation is 3000 rev/min in a clockwise (CW) sense, as viewed from its right end.

The left support is anisotropic, but its cross-stiffness characteristic is symmetric with respect to the orthogonal coordinate system defined by the x_1 and x_2 axes. The stiffness matrix associated with this support is:

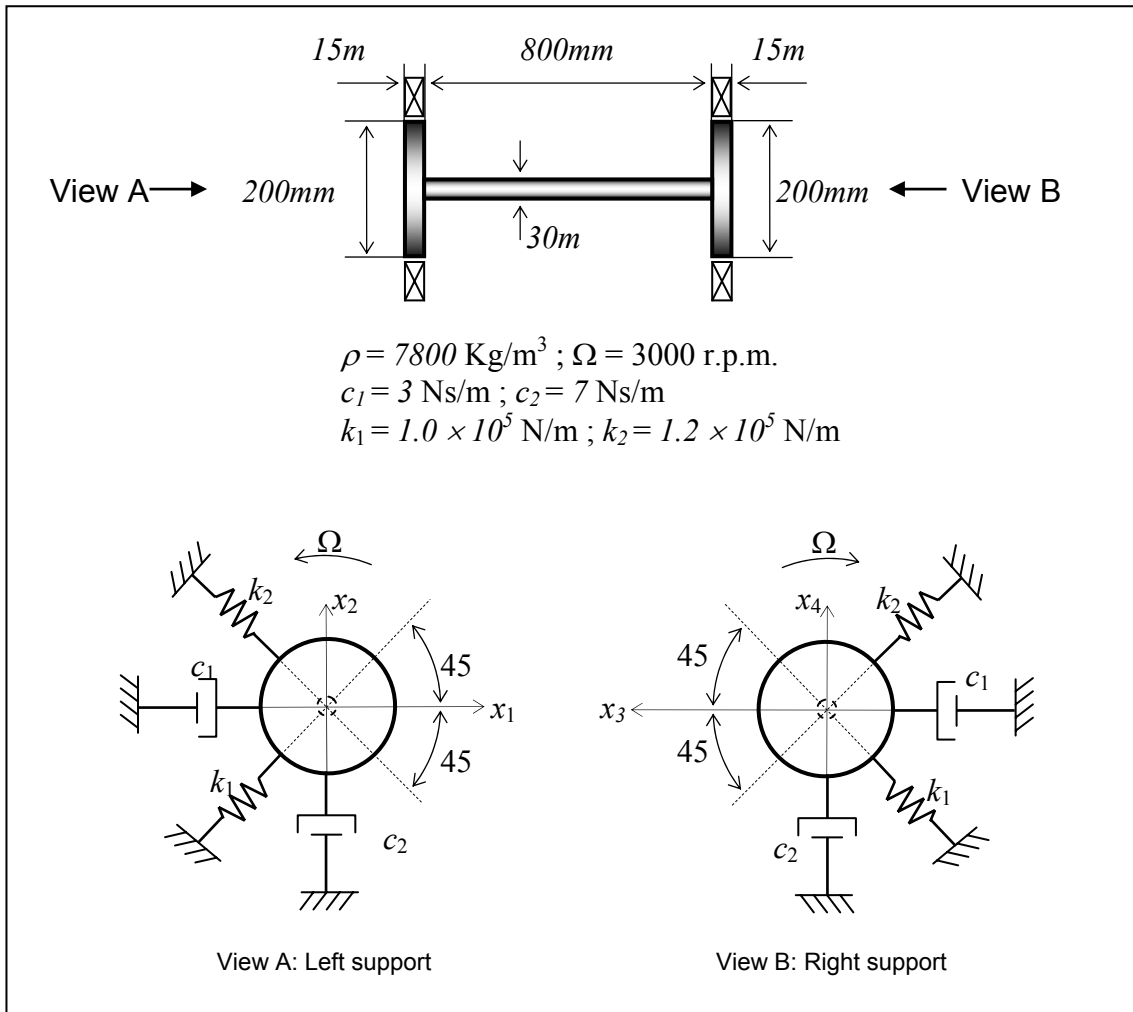


Figure 5.1 - 4-DOF rigid rotor

$$[K_A] = \begin{bmatrix} 1.100 & 0.100 \\ 0.100 & 1.100 \end{bmatrix} \times 10^5 \quad \frac{N}{m} \quad (5.1)$$

The right support has an asymmetric cross-stiffness characteristic, which emulates that of a hydrodynamic bearing. Its stiffness matrix with respect to the orthogonal coordinate system defined by the x_3 and x_4 axes is:

$$[K_B] = \begin{bmatrix} 1.100 & 0.124 \\ 0.076 & 1.100 \end{bmatrix} \times 10^5 \quad \frac{N}{m} \quad (5.2)$$

When the rotor spins, gyroscopic forces arise due to the combined effects of the large angular momentum of the disks about their spin axis and the angular precession of this

axis. These effects introduce a skew-symmetric component into the damping matrix of the system.

The DOFs used for the analysis will be those associated with the motion of the rotor along the axes x_1 , x_2 , x_3 and x_4 defined in Figure 5.1. The mass, damping and stiffness matrices corresponding to these DOFs are, respectively:

$$[M] = \begin{bmatrix} 5.161 & 0 & 0.720 & 0 \\ 0 & 5.161 & 0 & 0.720 \\ 0.720 & 0 & 5.161 & 0 \\ 0 & 0.720 & 0 & 5.161 \end{bmatrix} \text{ Kg} \quad (5.3)$$

$$[C] = \begin{bmatrix} 3.000 & 17.620 & 0 & -17.620 \\ -17.620 & 7.000 & 17.620 & 0 \\ 0 & -17.620 & 3.000 & 17.620 \\ 17.620 & 0 & -17.620 & 7.000 \end{bmatrix} \frac{N}{m/s} \quad (5.4)$$

$$[K] = \begin{bmatrix} 1.100 & 0.100 & 0 & 0 \\ 0.100 & 1.100 & 0 & 0 \\ 0 & 0 & 1.100 & 0.124 \\ 0 & 0 & 0.076 & 1.100 \end{bmatrix} \times 10^5 \frac{N}{m} \quad (5.5)$$

The dimension of the system is $N = 4$. From Equations (5.4) and (5.5) it can be seen that the number of DOFs involved in the asymmetric portions of the damping and stiffness matrices, which appear enclosed in dashed-line rectangles, are, respectively, $n_c = 4$ and $n_k = 2$. The mass matrix is symmetric, consistent with the assumptions of the predictive characterisation method.

The procedure to determine the left eigenvectors of the system using simulated FRF measurements will now be demonstrated.

5.2.1 Required FRFs

In accordance with Equations (4.56)-(4.58), which are restated here as (5.6)-(5.8) with the values of the parameters n_c and n_k given in the previous Subsection, the full characterisation of the system requires measuring a full column of the FRF matrix and a minimum of two elements from one of its rows. The fulfilment of this requirement makes it possible to satisfy the following three inequalities simultaneously:

$$q \geq 1 \quad (5.6)$$

$$q \geq \sqrt{n_c^2 + n_k^2} - N + 1 = 1.4721 \quad (5.7)$$

$$q \geq \max(n_c, n_k) - 2[N - \min(n_c, n_k)] = 0 \quad (5.8)$$

The accelerance FRFs corresponding to the first column of the FRF matrix, plus an additional FRF from the first row are presented in Figure 5.2. We will refer to these as the ‘measured’ FRFs, since they will play exactly the same role as true measured FRFs would in the characterisation of a real system.

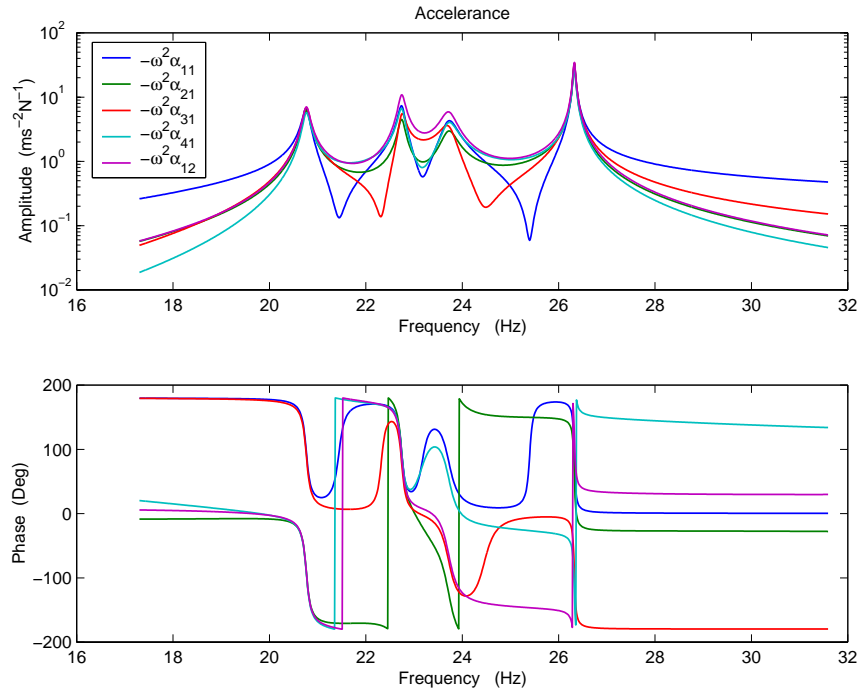


Figure 5.2 – FRFs of a 4-DOF rigid rotor

5.2.2 Modal analysis of the FRF data

A set of natural frequencies, damping factors and modal constants for the system may be determined through modal analysis of the ‘measured’ FRFs. For this case study, the ICATS¹ modal analysis software was used. Table 5.1 presents the values of the natural frequencies and damping factors obtained using a least-squares line-fit method on the ‘measured’ data. The estimated modal constants for the complete set of ‘measured’ FRFs are given in Table 5.2.

Table 5.1 – Estimated natural frequencies and hysteretic damping factors

MODE, r	ω_r (Hz)	η_r
1	20.7650	0.0065
2	22.7429	0.0059
3	23.7181	0.0133
4	26.3260	0.0017

Table 5.2 – Estimated modal constants for a hysteretic damping model

FRF	MODE 1	MODE 2	MODE 3	MODE 4
$-\omega^2 \alpha_{11}$	0.0063 - 0.1638i	0.0043 - 0.1478i	-0.0079 - 0.1851i	-0.0005 - 0.1736i
$-\omega^2 \alpha_{21}$	-0.0019 + 0.1546i	0.0075 - 0.0965i	0.0714 + 0.1175i	-0.0792 - 0.1433i
$-\omega^2 \alpha_{31}$	0.0044 - 0.1725i	-0.0014 - 0.1102i	-0.0088 + 0.1519i	0.0045 + 0.1786i
$-\omega^2 \alpha_{41}$	0.0000 + 0.1448i	0.0020 - 0.1320i	-0.0797 - 0.1514i	0.0798 + 0.1357i
$-\omega^2 \alpha_{12}$	-0.0460 - 0.0005i	0.0631 + 0.0021i	-0.0689 - 0.0304i	0.0516 + 0.0320i

In order to predict the left eigenvectors it is important to note that the estimated modal constants correspond to a hysteretically-damped system model, whereas the predictive method was developed for viscously damped systems. Hence, it is necessary to determine a set of modal parameters that are consistent with a viscously-damped system model, before an the estimation of the left eigenvectors through this method can be carried out.

¹ Imperial College Analysis and Testing Software

If the hysteretical and viscous damping factors are considered constant and equal to their values at the resonance, then the damped natural frequencies, $\bar{\omega}_r$, critical damping ratios, ζ_r , and complex eigenvalues, λ_r , corresponding to a viscously-damped system model are related to the natural frequencies, ω_r , and damping factors, η_r , of its hysteretically-damped equivalent through the following expressions:

$$\bar{\omega}_r = \omega_r \sqrt{1 - \frac{\eta_r^2}{4}} \quad (5.9)$$

$$\zeta_r = \frac{\eta_r}{2} \quad (5.10)$$

$$\lambda_r = -\zeta_r \omega_r + i\bar{\omega}_r = -\frac{\eta_r \omega_r}{2} + i\omega_r \sqrt{1 - \frac{\eta_r^2}{4}} \quad (5.11)$$

The natural frequencies, critical damping ratios and complex eigenvalues for a viscously damped system model that are equivalent to those presented in Table 5.1 are given in Table 5.3.

Table 5.3 – Estimated natural frequencies and critical viscous damping ratios

MODE, r	$\bar{\omega}_r$ (Hz)	ζ_r	λ_r (rad/s)
1	20.7649	0.0033	-0.4255 + 130.47i
2	22.7428	0.0029	-0.4185 + 142.90i
3	23.7176	0.0066	-0.9889 + 149.02i
4	26.3260	0.0008	-0.1406 + 165.41i

The manner in which the modal constants for a viscously damped system model are determined from a hysteretically-damped equivalent is described in Appendix B. In order to provide a reference to assess the accuracy with which these parameters were estimated, the exact values of the modal constants were computed directly from the spatial property matrices given in Equations (5.3)-(5.5). The estimated modal constants

for the viscously damping system model are then compared with their exact values in Table 5.4. The ‘ERROR’ column expresses the differences between the magnitudes of the exact and the estimated modal constants as a percentage of the magnitudes of their exact values.

Table 5.4 – Comparison of modal constants $\times 10^3$, for a viscous damping model

MODE	FRF	EXACT	ESTIMATED	ERROR %
1	$-\omega^2\alpha_{11}$	0.0060 - 0.1649i	0.0063 - 0.1638i	0.6910
	$-\omega^2\alpha_{21}$	-0.0015 + 0.1544i	-0.0019 + 0.1546i	0.2896
	$-\omega^2\alpha_{31}$	0.0041 - 0.1724i	0.0044 - 0.1725i	0.1834
	$-\omega^2\alpha_{41}$	0.0002 + 0.1441i	0.0000 + 0.1448i	0.5052
	$-\omega^2\alpha_{12}$	-0.0019 + 0.1763i	-0.0019 + 0.1763i	0.0000
2	$-\omega^2\alpha_{11}$	0.0031 - 0.1471i	0.0043 - 0.1478i	0.9442
	$-\omega^2\alpha_{21}$	0.0081 - 0.0973i	0.0075 - 0.0965i	1.0242
	$-\omega^2\alpha_{31}$	-0.0018 - 0.1110i	-0.0014 - 0.1102i	0.8057
	$-\omega^2\alpha_{41}$	0.0003 - 0.1311i	0.0020 - 0.1320i	1.4672
	$-\omega^2\alpha_{12}$	0.0047 - 0.2218i	0.0073 - 0.2208i	1.2557
3	$-\omega^2\alpha_{11}$	-0.0087 - 0.1851i	-0.0079 - 0.1851i	0.4317
	$-\omega^2\alpha_{21}$	0.0724 + 0.1166i	0.0714 + 0.1175i	0.9802
	$-\omega^2\alpha_{31}$	-0.0067 + 0.1518i	-0.0088 + 0.1519i	1.3836
	$-\omega^2\alpha_{41}$	-0.0802 - 0.1505i	-0.0797 - 0.1514i	0.6037
	$-\omega^2\alpha_{12}$	-0.0997 + 0.2319i	-0.1020 + 0.2312i	0.9524
4	$-\omega^2\alpha_{11}$	-0.0004 - 0.1734i	-0.0005 - 0.1736i	0.1290
	$-\omega^2\alpha_{21}$	-0.0790 - 0.1432i	-0.0792 - 0.1433i	0.1367
	$-\omega^2\alpha_{31}$	0.0044 + 0.1785i	0.0045 + 0.1786i	0.0792
	$-\omega^2\alpha_{41}$	0.0797 + 0.1357i	0.0798 + 0.1357i	0.0635
	$-\omega^2\alpha_{12}$	0.0969 - 0.1558i	0.0967 - 0.1560i	0.1542

5.2.3 Eigenvector normalisation

The estimated modal constants may be used to derive a set of normalised right eigenvectors as well as two elements of the normalised left eigenvectors. Normalisation allows for one element of either the right or the left eigenvector of each mode to be

defined arbitrarily. However, for every FRF, the modal constants are related to the corresponding elements of the normalised right and left eigenvectors through the following expression:

$${}_r \mathbf{A}_{ij} = (\Phi_R)_{ri} (\Phi_L)_{rj} \quad (5.12)$$

where r indicates the mode number, and i and j indicate the row and column of the FRF matrix to which the measured FRF corresponds.

In this case study, the elements corresponding to the ‘measured’ point FRF, $\alpha_{11}(\omega)$, were considered to be equal to each other:

$$(\Phi_R)_{r1} = (\Phi_L)_{r1} = \sqrt{{}_r \mathbf{A}_{11}} \quad (5.13)$$

for all modes. The remaining elements of the normalised right eigenvectors were then determined from the following expression, using the appropriate index, i :

$$(\Phi_R)_{ri} = \frac{{}_r \mathbf{A}_{i1}}{{}_r \mathbf{A}_{11}} \cdot (\Phi_R)_{r1} \quad (5.14)$$

and those of the normalised left eigenvectors were obtained through the following expression, using the appropriate index, j :

$$(\Phi_L)_{rj} = \frac{{}_r \mathbf{A}_{1j}}{{}_r \mathbf{A}_{11}} \cdot (\Phi_L)_{r1} \quad (5.15)$$

Using Equations (5.14) and (5.15), together with the estimated modal constants given in Table 5.4, the normalised right eigenvectors and two elements of each normalised left eigenvector were determined. These are presented in Table 5.5.

Table 5.5 – Estimated elements of the normalised right and left eigenvectors

	MODE 1	MODE 2	MODE 3	MODE 4
$\{\Phi_R\}_r$	0.0092 - 0.0089i	0.0087 - 0.0085i	0.0094 - 0.0098i	0.0093 - 0.0093i
	-0.0085 + 0.0086i	0.0060 - 0.0053i	-0.0026 + 0.0098i	0.0035 - 0.0119i
	0.0096 - 0.0095i	0.0062 - 0.0066i	-0.0085 + 0.0073i	-0.0094 + 0.0098i
	-0.0078 + 0.0081i	0.0077 - 0.0077i	0.0040 - 0.0119i	-0.0030 + 0.0116i
$\{\Phi_L\}_r$	0.0092 - 0.0089i	0.0087 - 0.0085i	0.0094 - 0.0098i	0.0093 - 0.0093i
	-0.0097 + 0.0098i	0.0131 - 0.0126i	-0.0175 + 0.0064i	0.0136 - 0.0032i

5.2.4 Results

For brevity, in the rest of this case study the normalised right and left eigenvectors will be referred to simply as the right and left eigenvectors.

Once the eigenvalues, the right eigenvectors and two elements of each left eigenvector were identified from the ‘measured’ FRF data, it was possible to establish a system of equations in the form of Equation (4.43) to compute the remaining left eigenvector elements.

In order to provide a reference to assess the accuracy with which these elements were computed, the exact values of the modal constants were determined directly from the spatial property matrices given in Equations (5.3)-(5.5). The estimated left eigenvectors are compared with their exact counterparts in Table 5.6. The ‘ERROR’ column expresses the magnitude of the difference between the estimated and the exact values of each left eigenvector element as a percentage of that of the exact value.

5.2.5 Discussion

In this case study, the left eigenvectors of the rotor depicted in Figure 5.1 were determined from ‘measurements’ of one column of the FRF matrix plus one additional element from one row.

Table 5.6 – Comparison of left eigenvector elements

MODE	EXACT	ESTIMATED	ERROR %
1	0.0092 - 0.0089i	0.0092 - 0.0089i	0.0000
	-0.0096 + 0.0098i	-0.0097 + 0.0098i	0.7289
	0.0086 - 0.0084i	0.0086 - 0.0085i	0.8318
	-0.0100 + 0.0103i	-0.0100 + 0.0104i	0.6966
2	0.0087 - 0.0085i	0.0088 - 0.0084i	1.1627
	0.0131 - 0.0128i	0.0131 - 0.0126i	1.0920
	0.0109 - 0.0121i	0.0109 - 0.0118i	1.8421
	0.0096 - 0.0099i	0.0098 - 0.0098i	1.6215
3	0.0094 - 0.0098i	0.0094 - 0.0099i	0.7364
	-0.0174 + 0.0065i	-0.0175 + 0.0064i	0.7614
	-0.0124 + 0.0117i	-0.0124 + 0.0115i	1.1731
	0.0145 - 0.0041i	0.0147 - 0.0043i	1.8770
4	0.0093 - 0.0093i	0.0093 - 0.0093i	0.0000
	0.0136 - 0.0031i	0.0136 - 0.0032i	0.7169
	-0.0087 + 0.0092i	-0.0087 + 0.0094i	1.5795
	-0.0139 + 0.0036i	-0.0139 + 0.0037i	0.6964

With this it was shown that it is possible to obtain the complete set of modal parameters of a rotating machine structure without the need to measure a complete row of its FRF matrix in addition to one column. Moreover, from the results presented in Table 5.6, it can be seen that the prediction of the left eigenvectors can be carried out with accuracy within 2% of the correct values, which is superior to that which is usually attainable in the analysis of genuine measured data.

These results suggest that the predictive method may be used to produce accurate estimations of the left eigenvectors. However, it does not provide an indication of the degree in which some experimental factors, such as measurement noise, affect the accuracy of the estimated modal parameters.

The errors reported in Table 5.6 may be traced back to three main sources. The first of these is the numerical truncation of the quantities involved in the calculation to 4 significant figures. Although truncation at this level may not have an important effect at

most stages of the calculation, this may be the case when relatively small quantities are involved.

The second possible source of error is the process of identification of the eigenvalues and modal constants from ‘measured’ FRF data. The accuracy with which these parameters are identified depends on several choices made during the modal analysis of the data, such as the selection of the curve-fitting algorithm used and the choice of data points on which to perform the curve-fits. The choices made for the analysis depend on the skills of the analyst and this human factor may be a cause of errors in the parameter estimations.

The third possible source of error is the use algorithms designed for hysteretically-damped systems, and may be the main factor affecting the accuracy of the estimated parameters, since the measured FRFs correspond to a viscously-damped system. Although within limited frequency intervals, for example around the resonance regions, the behaviour of a viscously-damped system may be satisfactorily characterised using a hysteretically-damped system model, the characterisation errors due to the discrepancy between the assumed and the actual models cannot be completely eliminated.

Apart from numerical errors, the estimation of modal parameters may also be influenced by experimental factors such as measurement noise and the selection of DOFs for the excitation of the test-piece and for the measurement of its response. The way in which these issues are taken into consideration is illustrated in the second case study.

5.3 Case study 2: the “windmill test-rig”

The objective of this case study was to evaluate the performance of the predictive characterisation method when applied to real machinery structures.

This study was aimed at the characterisation of the “windmill test-rig”, which is shown in Figure 5.3. The rig was originally used in industry for the investigation of dynamic phenomena that originate due to rotor-stator interactions in aero engines. Its design can be seen to purposefully endow it with some of the distinctive characteristics of an airplane wing assembly. Its main flexible component, (1), which may be considered to play the part of the wing structure, has markedly anisotropic transverse stiffness characteristics with high flexibility in both the vertical and the horizontal directions. It also has a large mass mounted firmly onto it. The mass consists of a stationary drum, (2), resembling an engine casing, inside which the main rotor is mounted. The rotor consists of a slender steel shaft, which is only supported at one of its ends by two roller bearings closely spaced together, forming a cantilever configuration. The opposite end of the shaft has a heavy steel bulkhead mounted onto it. With the rig in operation, the rotation of the bulkhead, combined with the vibration of the shaft, generates large gyroscopic forces even at low rotation speeds.

The system is driven by a stepper motor, (3), which is connected to the main rotor through a hollow steel shaft, (4). An Oldham coupling is used to connect this shaft to the motor and a bellows coupling to connect it to the main rotor. This combination of couplings compensates for parallel and angular misalignments and isolates the vibration of the motor from that of the main rotor. A solid-state controller is used to set the running speed of the rig.

5.3.1 Test plan

In order to achieve the objective of this case study, it was necessary to characterise the behaviour of the test rig by two different methods, one based on the predictive method described in Chapter 4 and another one based on the identification of the left eigenvectors directly from measured data.

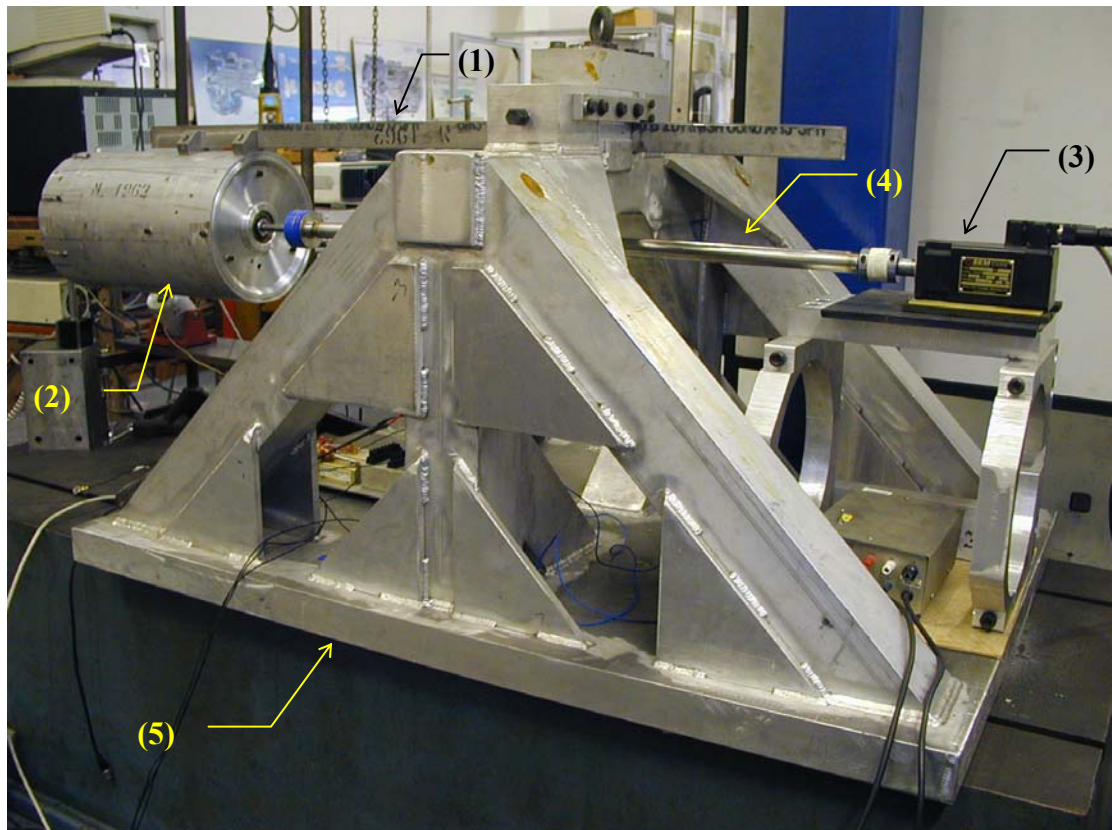


Figure 5.3 – The “windmill test-rig; (1) elastic beam, (2) drum, (3) stepper motor, (4) hollow drive shaft, (5) support structure.

This double characterisation provides a means to crosscheck the results obtained with the predictive method, so that its performance may be evaluated.

5.3.1.1 Predictive method approach

With this approach, the FRFs associated with one column of the FRF matrix are measured. If required, some additional elements of one of the rows of the same matrix are measured as well. A set of right eigenvectors and eigenvalues of the system is obtained through the modal analysis of the measured FRFs. These modal parameters are then used to compute the left eigenvectors using the procedure described in Chapter 4.

5.3.1.2 Direct identification of the left eigenvectors from measurements

There exist at least two possible methods to determine the modal parameters of the rig directly from measurements. The first of these is based on the procedure described by

Nordmann [35], which consists of measuring the elements in one column and one row of the FRF matrix while the rotor is spinning. This approach, as was discussed in Chapter 1, has some practical limitations, especially when the excitation is to be applied onto the rotating shaft. Additionally, it has the inconvenience that attaching the excitation equipment to different points of the structure during the measurement of the FRF matrix row may produce small variations of the modal parameters between measurements of the individual FRFs. The extent of this effect was investigated by measuring the response of the structure to an excitation force applied successively at two different locations, and measuring the point FRF on each occasion. The two DOFs considered were numbers² 20 and 25 on the test structure.

The FRF curves corresponding to the frequency range from 0 to 30 Hz for both excitation locations are compared in Figure 5.4. It can be seen in the Figure that the resonant frequencies of some of the modes are perceptibly affected by the change in the location of the exciter. This creates an inconsistency amongst the modal parameters extracted from the different FRFs, which has an adverse effect on the accuracy with which the modal parameters of the test structure can be estimated.

In order to circumvent this problem, an alternative measurement method was developed, based on two considerations: (a) that due to the absence of oil film bearings and the low internal damping of the shaft, it is unlikely that circulatory forces will arise that could destroy the symmetry of the stiffness matrix of the rig, and (b) that, given the high rotational inertia of the shaft and bulkhead, the circulatory forces affecting the behaviour of the rig are mainly gyroscopic. These two considerations support the case that only the damping matrix will exhibit a significant degree of asymmetry.

² A description of the numbering system used for the DOFs is given in Section 5.3.5, Figure 5.15.

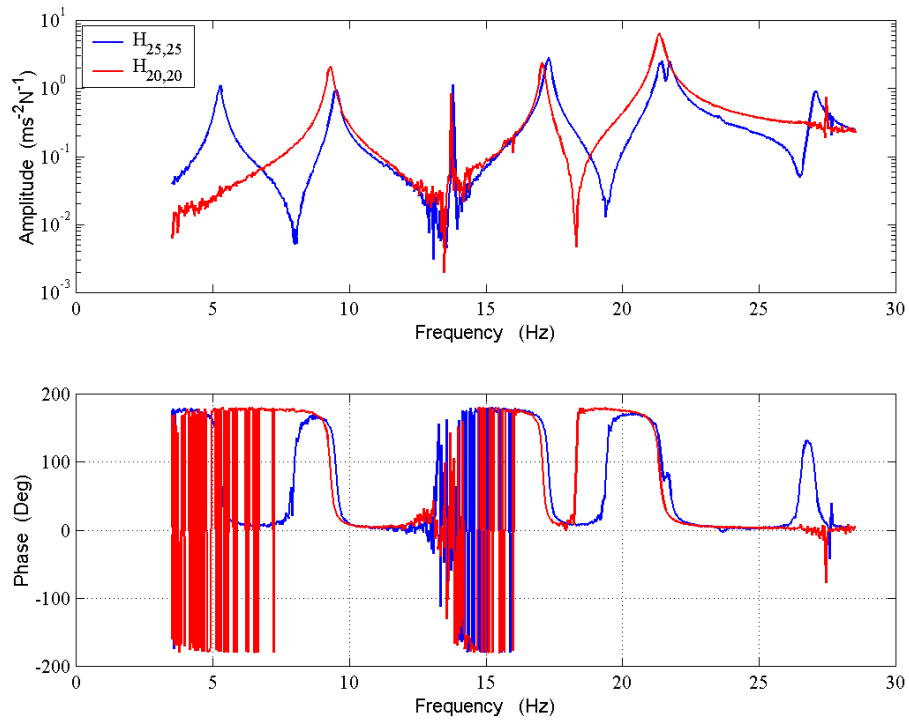


Figure 5.4 – Point FRFs at two different locations

Taking this into account, it may then be possible to replace the difficult measurement of one row of the FRF matrix with the measurement of its corresponding column but with the rotor spinning in a direction opposite to that in which it originally spun. The rationale behind this approach is that, by inverting the sense of rotation, the sense of the gyroscopic moments is also inverted. Consequently, the damping, dynamic stiffness and FRF matrices of the test structure associated with this new sense of rotation become the transposes of the corresponding matrices for the original sense of rotation. This implies that measuring a row of the FRF matrix with the rotor spinning in one direction is equivalent to measuring the corresponding column with the rotor spinning in the opposite direction.

Two direct implications of this assumption are: (a) that the point FRFs should not be affected by the change in the sense of rotation of the shaft, and (b) that the effect of changing the sense of rotation should be reversed by exchanging the excitation and response measurement locations.

The first of these implications was verified in this case study by measuring the point FRFs corresponding to DOF 25 for the two senses of rotation. The measured FRFs are compared in Figure 5.5. As can be seen, the two FRFs are nearly identical, except for the phase variations in the vicinity of 13 Hz, which was close to the running speed of the rotor. In fact, the spike that appears at that frequency does not correspond to a structural resonance, but to the component of vibration that is synchronous with the speed of rotation.

To test the second implication, a transfer FRF was measured with the rotor spinning clockwise (CW) at 831 rev/min and measuring the FRF corresponding to an excitation applied at DOF 25 and a response measured at DOF 20. A second measurement consisted on running the test structure with the rotor spinning counter-clockwise (CCW) at 831 rev/min and measuring the FRF corresponding to an excitation applied at DOF 20 and a response measured at DOF 25.

The measurements of these two FRFs are compared in Figure 5.6. It can be seen that, apart from the frequency shifts that have been attributed to the change in exciter location, the measured FRFs are similar to each other throughout the whole frequency range.

A small discrepancy is visible in the vicinity of 21Hz, which is close to the natural frequencies of two double modes. This discrepancy may be caused by the high sensitivity of this type of modes to small perturbations, such as the change in exciter location. However, in spite of this discrepancy near the close modes, the amplitudes and phases of the FRFs agree well with each other.

The two results discussed above provide evidence that, for the case of the test structure under consideration, it is possible to emulate the exchange of the excitation and the response measurement locations by inverting the sense of rotation of the main shaft.

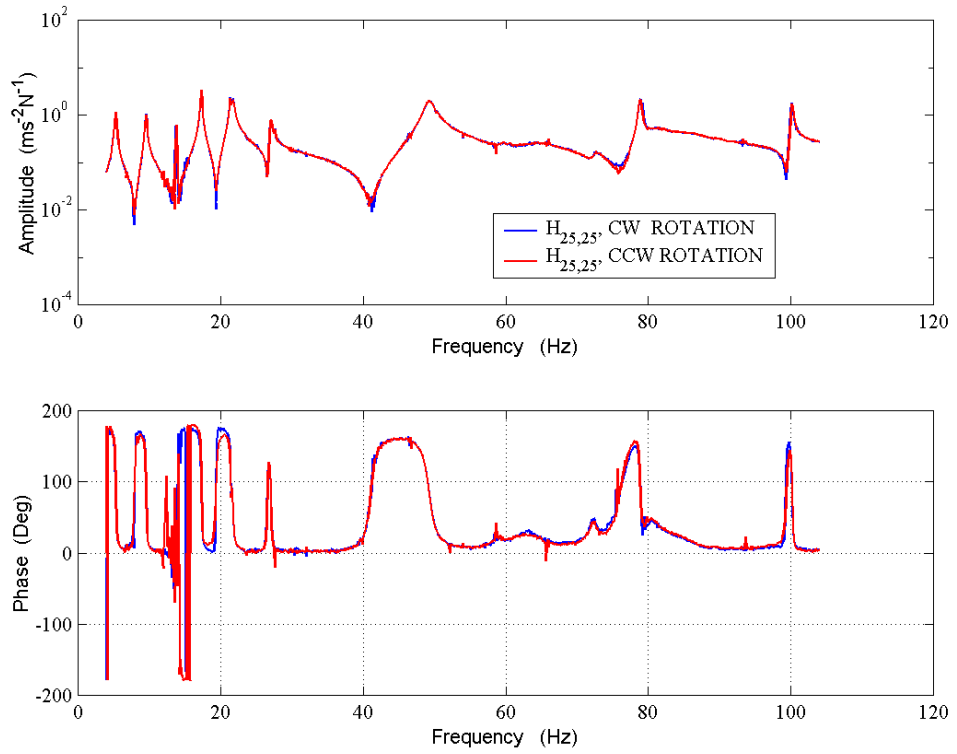


Figure 5.5 – Point FRFs for two senses of rotation

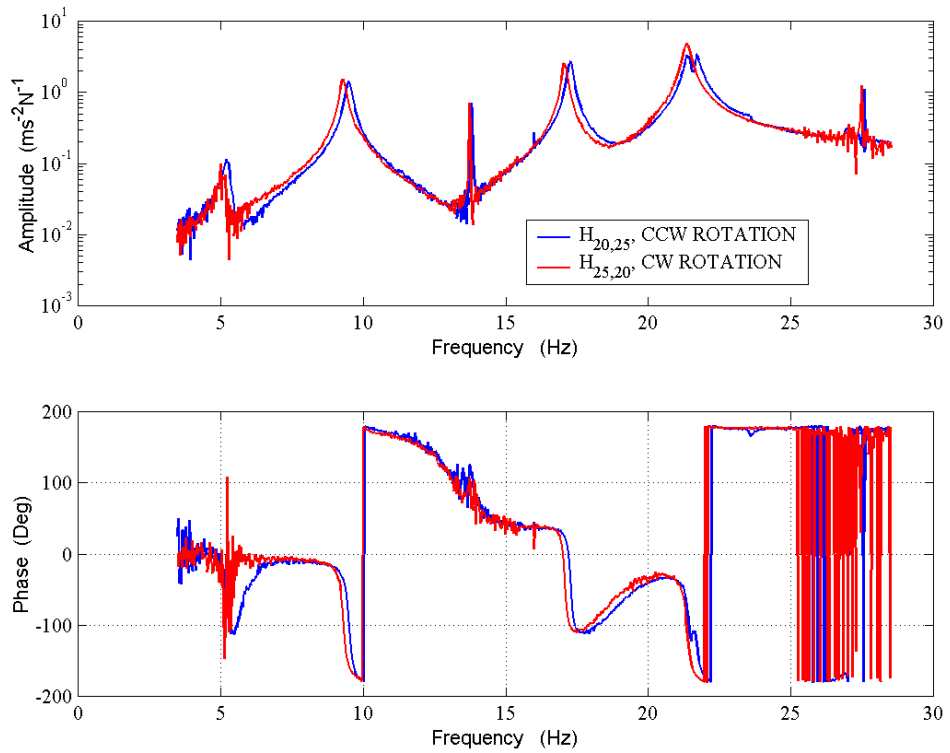


Figure 5.6 – Equivalence of inverting the sense of rotation and exchanging the excitation and measurement locations for transfer FRFs

5.3.2 Scope of the characterisation

The predictive characterisation method is based on the assumption that the dynamic behaviour of the system under consideration may be suitably described using a finite number of modes. Since the test structure used for the present case study is a continuous system, and hence possesses an infinite number of modes, it is necessary to establish a finite frequency range within which it abides by the assumptions of the predictive method.

In order to determine this frequency interval, point FRFs corresponding to three different exciter locations were measured. This made it possible to determine the natural frequencies of the test structure while reducing the possibility of neglecting a mode due to its not being excited at this stage of the tests. The point FRFs corresponding to DOFs 11, 20 and 25 are presented in Figure 5.7.

From the FRFs presented in this Figure, it can be seen that there is a large frequency interval between 30 and 45 Hz within which the test structure has no natural frequencies. This fact was taken advantage of for establishing the frequency range to be used for the characterisation of the test structure. Since the effect of all modes with natural frequencies above 30 Hz is relatively small within the interval from 0 to 30 Hz, then it was considered that the behaviour of the system could be adequately described in terms of the modes with natural frequencies below 30 Hz. Thus, the frequency range for the characterisation was set from 0 to 30 Hz. The natural frequencies of the system identified for this range are given in the Table 5.7.

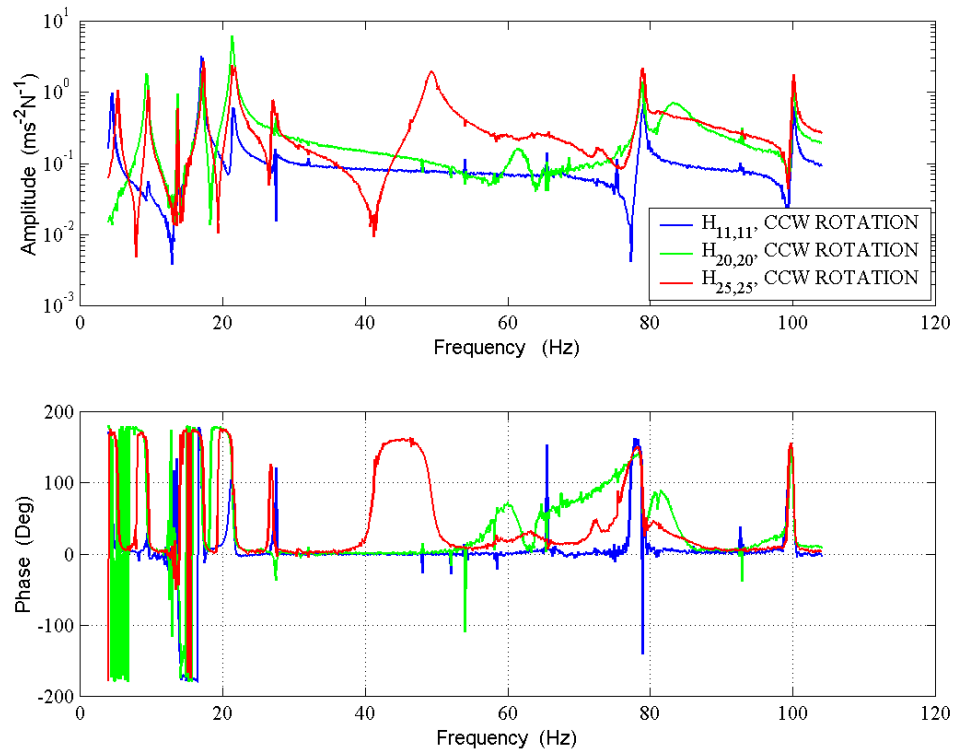


Figure 5.7 – Point FRFs used for frequency range selection

Table 5.7 – Natural frequencies at 831 rev/min, CCW

MODE	NATURAL FREQUENCY (Hz)
1	5.25
2	9.50
3	17.25
4	21.40
5	21.71
6	27.11

In Figure 5.8, an enlarged view of the portion of Figure 5.7 corresponding to the selected frequency range is shown. The amplitudes of the different modal components of the response vary with the DOF at which the point FRF is measured. The blue line, corresponding to the point FRF at DOF 11, shows that from this location the second and sixth modes are not effectively excited, whereas the green line, corresponding to DOF 20, indicates that neither the first nor the sixth modes can be excited effectively from

this location. The red line corresponds to a point FRF measured at DOF 25. All the modes appear to be well excited from this location. However, the peak corresponding to the first mode is seen to correspond to a different frequency as does that of the FRF for DOF 11. Investigation of this discrepancy led to the conclusion that it was caused by the effect of exciter location, and not by the existence of a different mode in the 3 – 5 Hz frequency range. The way in which this was verified was by comparing the transfer FRFs corresponding to (a) an excitation applied at DOF 11 and response measured at DOF 25 with CW rotation of the shaft, and (b) an excitation applied at DOF25 and a response measured at DOF 11 with CCW rotation of the shaft. The two FRFs are plotted in Figure 5.9.

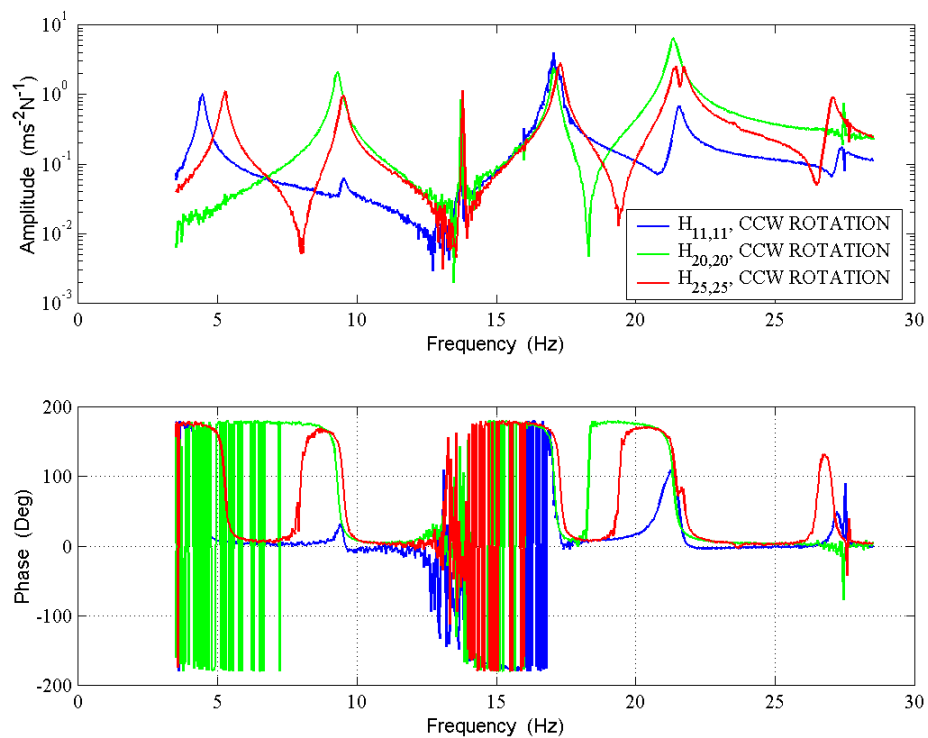


Figure 5.8 – Enlarged view of the selected frequency range

As was discussed in the previous Section, the two measurements should yield the same FRFs, since the effect of a change in the sense of rotation reverses the exchange of the excitation and the response measurement locations.

If the exciter location had no effect on the natural frequencies of the mode(s) associated with the leftmost peaks in the blue and red curves in Figure 5.8, then the corresponding like-coloured curves in Figures 5.8 and 5.9 should be identical in the range from 3 to 7 Hz, since the inversion of rotation cancels-out the exchange of locations for the excitation and the response measurement. The fact that they are not identical within this range suggests that there exists only one mode in this region, and that the shift of the natural frequencies is due to the effects of exciter attachment, which is the only condition that is common for the curves of the same colour in Figures 5.8 and 5.9.

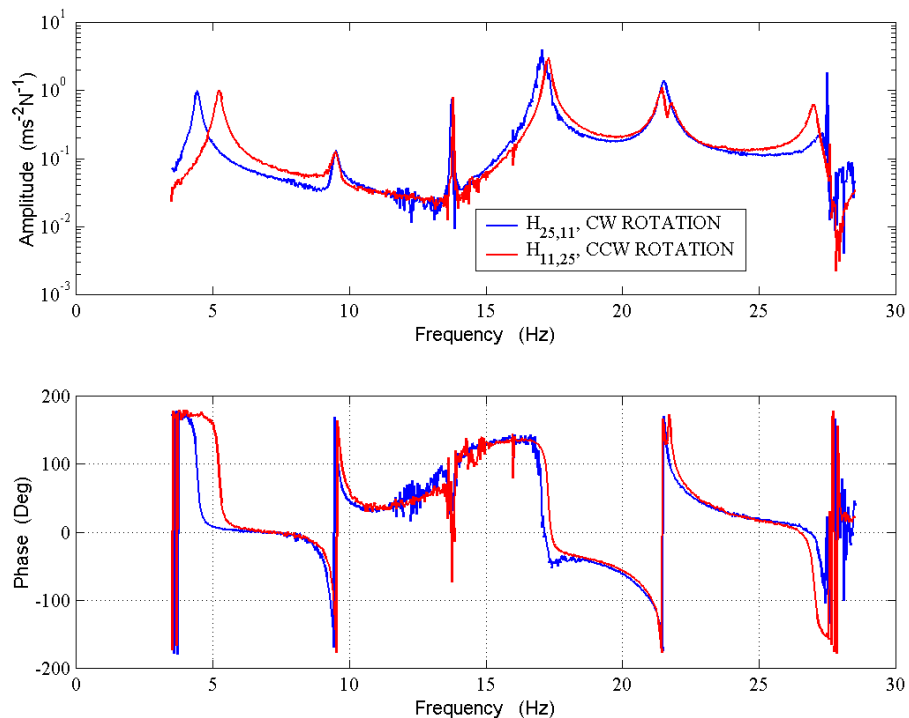


Figure 5.9 – Variation of the first natural frequency due to exciter attachment

It should be noted that sixth mode in the selected frequency range is not as effectively excited by a force applied at DOF 25 as are the other modes. This, together with the fact that its natural frequency is similar to the second harmonic of the rotational frequency, may affect the accuracy with which its modal parameters are determined.

However, based on the FRF data presented in Figure 5.8, it was concluded that out of the three candidate excitation locations, i.e. DOFs 11, 20 and 25, the latter is the best

choice to excite the modes whose natural frequencies lie within the selected frequency range of 0 to 30 Hz.

5.3.3 Selection of the speed of rotation

5.3.3.1 Factors considered

The speed at which the shaft rotates is an important parameter for the characterisation, since the magnitudes of the gyroscopic forces generated in the rotor are directly related to this parameter. If the speed is excessively low, then the gyroscopic effects may be so weak that the test structure can be satisfactorily characterised using the classical methods designed for stationary structures. On the other hand, an excessively high speed can trigger the unstable vibration of the main rotor.

Thus, it was necessary to choose a rotation speed that allowed considerable gyroscopic forces to develop, but that at the same time was low enough to prevent the test structure from becoming unstable.

One additional factor related to the choice of speed of rotation was the need to minimise the interference between the response of the test structure at its resonances and the components of vibration with a frequency equal to that of rotation or its harmonics.

A rotation speed of 831 rev/min, or, equivalently, 13.85 cycles/sec was used. This rotation speed was chosen so that it was well below the first critical speed of the shaft, of approximately 21 cycles/sec.

5.3.3.2 Effects of rotation on the behaviour of the test structure

In Figure 5.10, the point FRFs associated with DOF 25 for the rotor (a) at rest and (b) rotating at 831 rev/min in a CCW sense, are compared. As can be seen, the natural frequencies of the lowest two modes are only very slightly affected by the gyroscopic

forces. However, the natural frequencies of at least three of the remaining modes are significantly affected. In Table 5.8, the natural frequencies for of the test structure with the rotor at rest are compared with those obtained with the rotor spinning at 831 rev/min in the CCW direction.

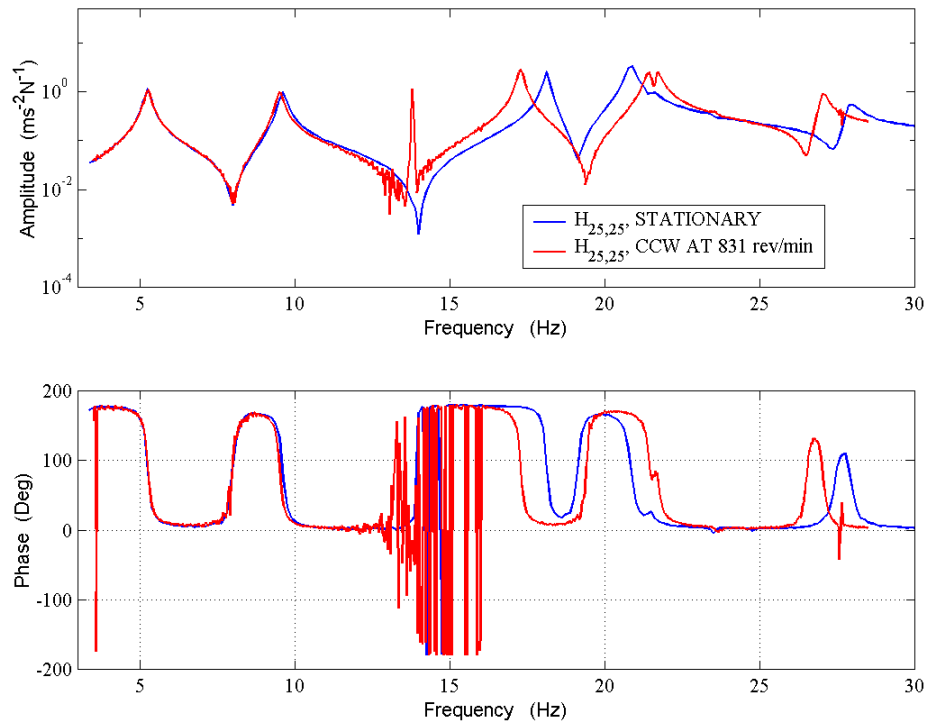


Figure 5.10 – Effect of gyroscopic forces on the behaviour of the test structure

Table 5.8 – Comparison of the natural frequencies (Hz) of the test structure in stationary and rotating conditions

MODE	STATIONARY	CCW ROTATION
1	5.23	5.25
2	9.60	9.50
3	18.12	17.25
4	20.87	21.40
5	21.64	21.71
6	27.92	27.11

5.3.4 Execution of the tests

5.3.4.1 Speed control

The first step in the tests was to set up the speed of the rotor. This was done using a solid-state speed controller. The speed was measured using a stroboscope aimed at the bulkhead side of the main rotor and adjusting the controller settings until the desired speed was attained. The speed was monitored at regular intervals during the tests and a variability of less than 3 rev/min was observed.

5.3.4.2 Excitation

Pseudo-random excitation forces [39] were applied to the test structure using an electromagnetic exciter attached to the outer surface of the drum by means of a pushrod, as shown in Figure 5.11. The signal fed to the exciter was generated using a Bruel & Kjaer Type 2032 FFT analyser and amplified using a Gearing and Watson PA30 power amplifier.

A Bruel & Kjaer Type 8200 force transducer was inserted between the pushrod and the test structure to measure the applied forces.

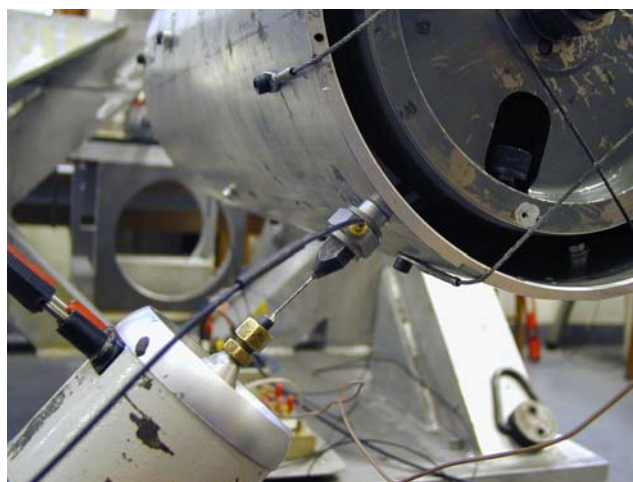


Figure 5.11 – Attachment of the electromagnetic exciter

Apart from the exploratory measurements used to define the test conditions, all the measurements were performed with the exciter attached at DOF 25, as is shown in Figure 5.11. The skewed position of the exciter, at about 50 degrees from the horizontal, allowed for the excitation of both vertical and horizontal modes of vibration.

5.3.4.3 Response measurement

The response was measured at several points along the drum of the test structure and along its supporting beam using a Bruel & Kjaer Type 4383 accelerometer. The mounting of the accelerometer is illustrated in Figure 5.12(a). The response was also measured at the bulkhead side of the main shaft using a Bently Nevada model 50029-01 displacement transducer system, positioned either horizontally or vertically near the bulkhead mounting nut. Its mounting in the horizontal position is shown in Figure 5.12(b).

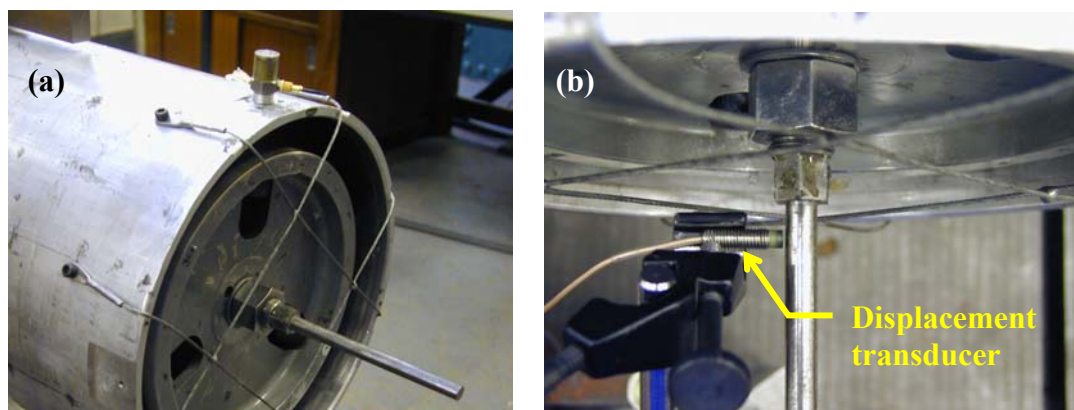


Figure 5.12 – Transducers used for measurements on (a) stationary, and (b) rotating components of the test structure (top view).

The accelerometer was attached to the test structure using either bees wax or an aluminium nut glued onto the outer surface of the drum with high-strength adhesive. The displacement transducer was fixed using a magnetic base.

5.3.4.4 Signal conditioning

The force and acceleration signals were conditioned and amplified using two separate Bruel and Kjaer Type 2626 conditioning units. The filters in both units were set to eliminate the signal components below 0.3 Hz and above 300 Hz. These settings allowed maintaining the distortion of the signals to a minimum level at each of the resonances within the frequency range of interest.

The signals from the displacement transducers were conditioned using the oscillator / demodulator unit that forms part of the transducer system.

5.3.4.5 Signal processing

The signals from the force transducer and from one of either the accelerometer or the displacement transducer were fed into the FFT analyser for each FRF measurement. No windows were applied to the signals, as a pseudo-random excitation force was used [39].

The signal processing was based on a frequency interval comprising 800 equally-spaced frequency values in the range from 3.75 Hz to 28.5 Hz. This allowed determining the FRFs with a frequency resolution of 31.25 mHz. Although these frequency settings shortened the selected frequency interval, they had no effect on the resonant responses, from which the modal parameters were estimated at a later stage.

The signal analyser was used to obtain the FRFs for one combination of excitation and response measurement locations at a time. The tests were repeated until all of the required FRFs were measured. The FRF data were stored in a personal computer for their further modal analysis.

5.3.4.6 Transducer calibration

The acceleration, force and displacement transducers were calibrated using, respectively, a Polytec model OFV050 laser Doppler vibrometer (LDV), a calibration mass and a micrometer as calibration references.

Calibration of the accelerometer was achieved by comparing its readings to those obtained from the LDV within the range from 3 to 100 Hz. The calibration setup is shown in Figures 5.13(a) and 5.13(b). The accelerometer was bolted onto the head of an electromagnetic exciter and a piece of reflective tape was attached to its upper surface, on which the LDV was focused. A sinusoidal signal was applied to the exciter in order to produce a harmonic vibration of the accelerometer. The signal voltages from the accelerometer and the LDV were recorded for 30 frequency values in the range from 3 to 100Hz. After converting the velocity readings of the LDV into equivalent accelerations, the voltages obtained from the accelerometer were used to determine the following mean calibration factor for the accelerometer with its signal conditioner:

$$\gamma_A = 0.9375 @ 0.839^\circ \frac{\text{ms}^{-2}}{\text{V}} \quad (5.16)$$

This factor was applied to the voltage signals obtained from the accelerometer in order to determine their corresponding acceleration values.

The force transducer was calibrated following a standard procedure that required the use of a reference mass of 10 kg together with the already calibrated accelerometer. The calibration setup is shown in Figures 5.14(a) and 5.14(b). The force transducer was bolted onto the reference mass using an aluminium nut. An electromagnetic exciter was connected to the force transducer by means of a slim pushrod, as seen in Figure 5.14(a). The calibrated accelerometer was bolted to the opposite side of the reference mass, as shown in Figure 5.14(b), also using an aluminium nut.

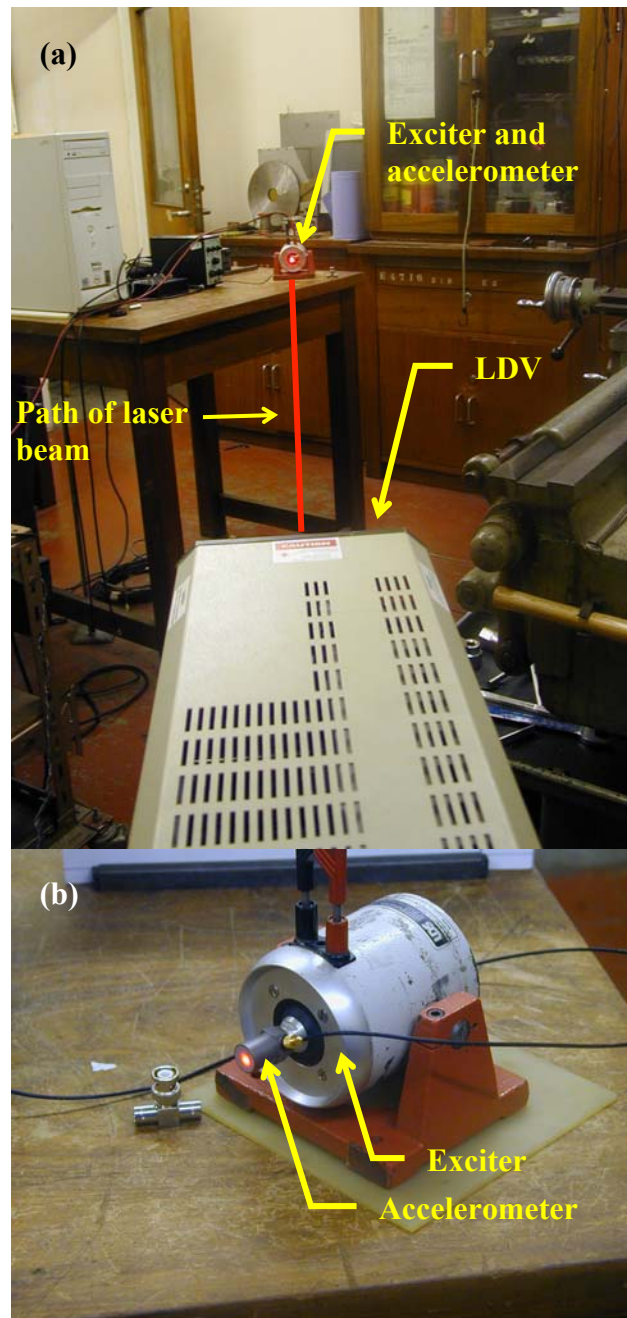


Figure 5.13 – (a) Use of a LDV as a calibration reference, (b) mounting of an accelerometer for calibration.

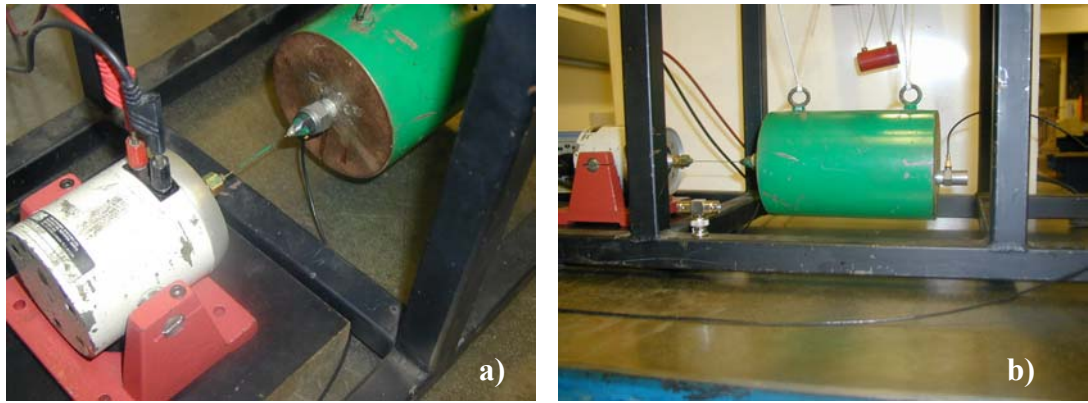


Figure 5.14 – (a) Attachment of the exciter to the force transducer, (b) mounting of the calibrated accelerometer.

The electromagnetic exciter was operated in the same way as it was for the calibration of the accelerometer.

To obtain the calibration factor for the force transducer with its signal conditioner, a reference force was computed first as the product of the reference mass and the acceleration measured by the calibrated accelerometer. This reference force was used together with the voltage signal from the force transducer to determine the following mean calibration factor:

$$\gamma_F = 0.9829 @ 0.035^\circ \frac{\text{N}}{\text{V}} \quad (5.17)$$

The displacement transducer was calibrated statically using a micrometer. 22 readings were taken for gaps within ± 0.635 mm of the midpoint of the linear range of the transducer. The mean calibration factor determined for this transducer together with its oscillator / demodulator unit was:

$$\gamma_x = 1.27 \times 10^{-4} \frac{\text{m}}{\text{V}} \quad (5.18)$$

5.3.5 FRF measurements

The DOFs with respect to which the measurements on the test structure were carried out are defined in Figures 5.15(a) and 5.15(b).

Two sets of FRF measurements were performed, both with an excitation force applied at DOF 25. The first set, which will be referred to as the ‘trial’ set, was obtained with the rotor of the test structure spinning at 831 rev/min in a CCW sense, as viewed from the bulkhead side. The response was measured at each of the 26 DOFs. These FRFs corresponded to a column of the FRF matrix. They are presented in Figure 5.16 to provide the reader with an idea of the noise present in the measurements, the variation ranges of the vibration levels and the overall consistency of the FRF set.

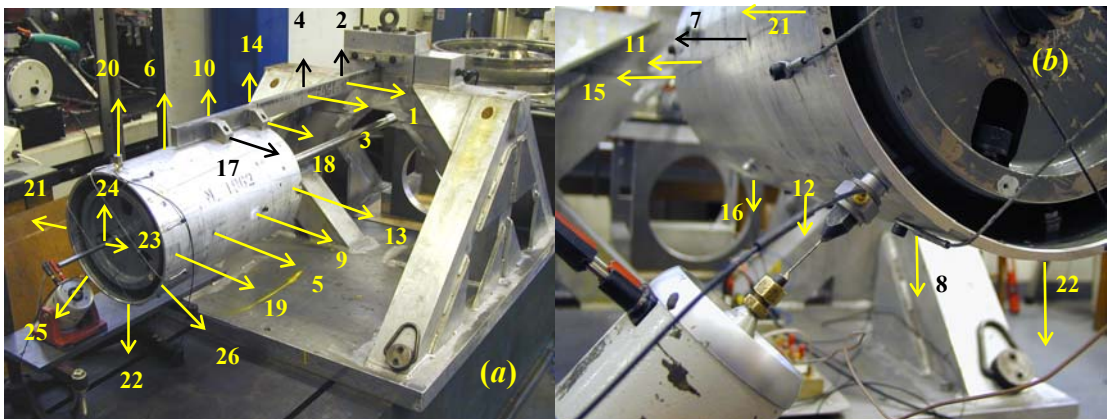


Figure 5.15 – Test DOFs on the (a) front side and (b) back side of the test structure

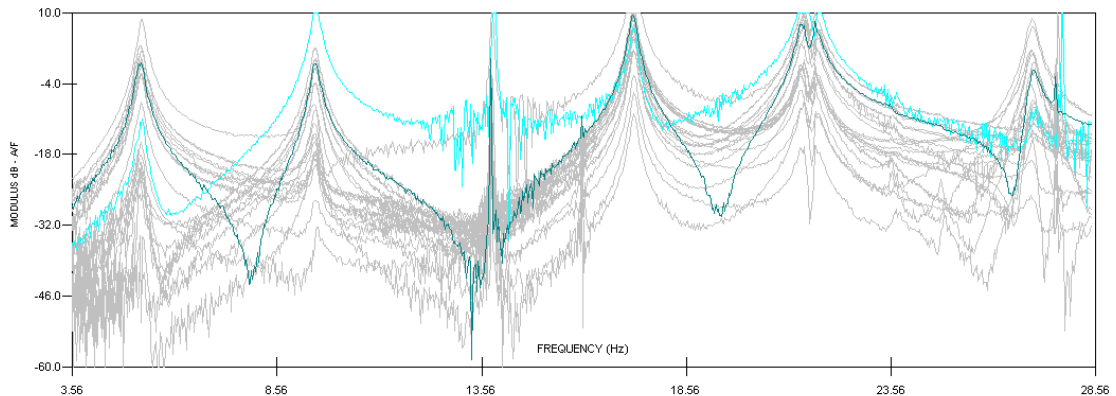


Figure 5.16 – FRFs from one column of the FRF matrix

The second set of data, which we will refer to as the ‘reference’ set, was taken with a similar setup as was used for the first set, but with the rotor spinning in the opposite sense, i.e. CW, at 831 rev/min. As was discussed in Section 5.3.1.2, for this particular case study, measuring a column of the FRF matrix in these conditions is equivalent to measuring a row of the same matrix with the rotor spinning in a CCW sense. Thus, right eigenvectors obtained through conventional modal analysis of this ‘reference’ set of data are equal to the left eigenvectors of the test structure in a CCW rotating condition. These eigenvectors were used to assess the accuracy of the left eigenvectors obtained by applying the predictive characterisation method to the ‘trial’ set of FRFs.

5.3.6 Modal analysis of the measured FRFs

Each of the measured FRFs was analysed independently in order to ensure the highest degree of accuracy of the identified right eigenvectors and eigenvalues, thus minimising the errors in the estimated left eigenvectors.

The modal analysis was carried out using the line-fit method of the ICATS modal analysis package. For each FRF, a set of natural frequencies, hysteretic damping loss factors and modal constants for each mode were obtained. The results from all the FRFs were collated into a single set of data containing the natural frequencies, damping factors and mode shape vectors corresponding to a hysteretically-damped system model.

The natural frequency and damping factor for each mode were computed as a weighted average of their individual values from each FRF. The weighting factors were taken as the magnitudes of the modal constants corresponding to that mode on each particular FRF.

The next step consisted of converting the modal parameters into equivalent parameters for a viscously-damped system model. This was done in the way described in Section 5.2.2. The eigenvalues and normalised right eigenvectors are presented in Appendix C.

It is important to note that since the characterisation was based on the consideration that both the mass and the stiffness matrices were symmetric, as was discussed earlier, then only one column of the FRF matrix was required to compute the left eigenvectors, as the test structure was then considered to approximate to a damped gyroscopic system, the measurement requirements for which have been stated in Section 4.8.

Once the right eigenvectors and complex eigenvalues corresponding to the viscously damped system model of the test structure were obtained, a reduction of the number of DOFs was required for the computation of the left eigenvectors. This stage of the analysis is described in the following Section.

5.3.7 Data reduction and computation of the left eigenvectors

Up to this point in the analysis, the eigenvalues and right eigenvectors corresponding to the 6 modes of interest were determined. The eigenvectors were defined with respect to all 26 DOFs. However, the use of the predictive method to determine the left eigenvectors requires only as many DOFs as there are modes. Thus, an appropriate data reduction procedure was required before the left eigenvectors could be computed.

Two factors were taken into consideration to perform the data reduction: firstly, as was discussed in Chapter 2, the one-to-one relationship between the asymmetry of the spatial property matrices and the presence of circulatory forces in the system can only be established if the DOFs that are used to describe the system are mutually orthogonal. Thus, the assumption that the mass and stiffness matrices are symmetric because there

exist no circulatory forces that are proportional to the accelerations or the displacements of the test structure is only valid if the orthogonality of the DOFs is ensured.

This kind of orthogonality can be achieved, for example, if the 6 chosen DOFs consist of 3 pairs of DOFs, each pair corresponding to two orthogonal coordinate axes with a common origin. However, other combinations of selected DOFs may also produce the same result.

The second factor that was considered is that at some stages of the predictive method it is required to invert the matrix of right eigenvectors, see for example Equations (4.16)-(4.18). Thus, it is desirable that the right eigenvectors, as observed from the chosen DOFs, be orthogonal, so that the eigenvector matrix is non-singular in order to minimise errors in the inversion of this matrix.

Orthogonalisation of the right eigenvectors constitutes a well-known problem in structural dynamics, which may be satisfactorily addressed using elimination techniques based, for example, on the effective independence (EI) [23] or QR decomposition [42] algorithms.

For the case study being presented here, the effective independence algorithm was chosen. However, it was first noted that none of the mode shapes included flexural motion of the drum. Hence, from each pair of diametrically opposed DOFs on its surface, only the one pointing upwards or rightwards, when viewed from the bulkhead end of the test structure, was kept.

DOF 25 was specified as a necessary selection, since this was the DOF at which the excitation was applied, and the point FRF corresponding to this DOF was necessary in order to normalise the eigenvectors.

The effective independence algorithm was applied to the matrix of right eigenvectors that corresponded to the remaining DOFs. The selected DOFs are ordered in the following Table, according to their suitability to yield an orthogonal set of right eigenvectors.

Table 5.9 – Evaluation of DOFs based on the effective independence algorithm

DOF
25
6
13
23
24
26
17
5
10
18
9
14
3
4
1
2



BETTER



WORSE

Based the results obtained through the use of the effective independence method, the order of the right eigenvector matrix was reduced to six, keeping only the elements of the right eigenvectors corresponding to DOFs 6, 13, 23, 24, 25 and 26. The computation of the left eigenvectors was then carried out using the six eigenvalues and the corresponding reduced right eigenvector sub-matrix based on hose DOFs.

5.3.8 Results

The computed left eigenvectors, $[\Phi_L]$, correspond to the test structure spinning in a CCW sense. They may be compared with the right eigenvectors, $[\Phi_R]$, of the test structure spinning in the CW sense. The two sets of eigenvectors are expected to be equivalent for the reasons stated in Section 5.3.1.2. They are presented in polar

coordinate format in Table 5.10, to facilitate their comparison. The ‘ERROR’ column expresses the magnitude of the difference between the computed and the measured eigenvector elements, as a percentage of the magnitude of the measured ones.

Table 5.10 – Comparison between two theoretically equivalent sets of eigenvectors

MODE r	DOF	COMPUTED $\{\Phi_L\}_r$, CCW		MEASURED $\{\Phi_R\}_r$, CW		ERROR %
		MAG	ANGLE	MAG	ANGLE	
1	6	0.0019	133.96	0.0027	136.82	28.51
	13	0.0183	135.07	0.0173	134.60	5.65
	23	0.0539	135.23	0.0510	129.43	11.82
	24	0.0050	99.61	0.0027	68.90	109.08
	25	0.0249	-45.02	0.0239	-43.15	5.36
	26	0.0264	135.16	0.0216	137.04	22.36
2	6	0.0164	141.35	0.0163	137.76	6.34
	13	0.0018	16.62	0.0020	31.82	7.18
	23	0.0062	-35.52	0.0033	-60.88	104.59
	24	0.0483	140.79	0.0510	139.96	5.53
	25	0.0131	-45.68	0.0134	-44.93	2.52
	26	0.0148	-31.28	0.0146	-31.14	1.37
3	6	0.0088	85.74	0.0079	92.82	17.12
	13	0.0116	174.21	0.0106	-179.42	14.99
	23	0.0304	-1.27	0.0285	-2.24	6.75
	24	0.0064	-46.28	0.0070	-92.48	75.31
	25	0.0119	-44.49	0.0119	-46.23	3.07
	26	0.0128	-151.63	0.0118	-147.82	11.15
4	6	0.0107	136.80	0.0137	137.81	21.73
	13	0.0013	121.89	0.0053	46.28	96.87
	23	0.0110	-84.07	0.0129	-133.17	78.08
	24	0.0150	32.25	0.0221	-34.50	96.18
	25	0.0096	-49.31	0.0128	-33.91	34.14
	26	0.0092	-47.84	0.0120	-23.32	43.85
5	6	0.0117	161.05	NOT DETECTED		-----
	13	0.0072	50.95			
	23	0.0125	-146.91			
	24	0.0315	-84.98			
	25	0.0086	-36.67			
	26	0.0148	11.27			
6	6	0.0011	-110.47	0.0012	152.74	146.42
	13	0.0091	-24.96	0.0097	-55.25	50.90
	23	0.0056	-26.80	0.0057	-59.15	55.36
	24	0.0025	-8.95	0.0004	58.25	533.90
	25	0.0049	-44.52	0.0047	-40.09	8.62
	26	0.0071	119.12	0.0056	117.18	28.09

5.3.9 Discussion

5.3.9.1 Errors in the prediction of the left eigenvectors

The errors in the prediction of the left eigenvectors are considerably larger in this experimental case study than they were in the numerical one presented in the first part of this Chapter. This can be seen by comparing the error columns of Tables 5.6 and 5.10.

In this second case study, the accuracy of the predictions is affected by two factors that were not present in the first one: (a) the existence of noise in the measurements, and (b) the presence of two close modes of vibration in the vicinity of 21.5 Hz, as seen from the natural frequencies presented in Table 5.7.

In the test structure, measurement noise was known to originate especially at the bearings that supported the main rotor. Measurement noise affects the accuracy with which the modal constants are estimated from the measured FRFs. The errors in the estimation of these parameters are in turn translated into errors in the estimations of the right eigenvectors and damping values, and ultimately on the predicted left eigenvectors.

The effects of noise on the parameters corresponding to a mode depend on the amplitude of the vibration component of that mode for the specific DOF in question. These effects are more prominent if the amplitude is small. This may occur if the element of the right eigenvector associated with that DOF having a small magnitude, or if the mode not effectively excited.

The effects of noise may explain why the largest errors in the prediction of the left eigenvectors, as seen in Table 5.10, occur for the DOFs at which the measured

eigenvectors have the smallest amplitudes. The elements corresponding to these DOFs have been marked in blue in the Table.

It may be noted that the errors associated with the sixth mode are large for every DOF. However, it should be taken into account that a force applied at DOF 25 is not as effective at exciting this mode as it is at exciting the others. This can be seen from the small magnitudes of the elements corresponding to this mode in the 'Measured' column of Table 5.10, as well as from the smaller amplitudes of the peaks corresponding to this mode in all the FRFs that have been presented for this case study.

One observation from Table 5.10 that cannot be explained with the argument that the vibration amplitude is small is that the errors associated with the fourth mode are also large for every DOF, in spite of this mode being well excited by the force applied at DOF 25.

With respect to the fourth mode, the errors in the identification of its modal constants may be due to its closeness to another mode in the vicinity of 21.5 Hz. This consideration will now be discussed in more detail.

The accurate identification of the modal components of an FRF curve that correspond to two close modes is a difficult task, especially in cases where the FRF data are affected by noise. This is because of the small differences that exist between the curves that define the two modal components of vibration as functions of frequency. The form of these curves is given in Equation (4.22). Successful identification of the modal components of an FRF relies on the detection of the differences between the two curves. However, the differences may be so small that they may be confused with the measurement noise. Thus, the effects of noise combined with the closeness of the two modes around the 21.5 Hz region may explain the large errors encountered in the identification of the left eigenvectors of the fourth mode.

As seen in Table 5.10, the fifth mode could not be identified in the FRFs corresponding to the second set of measured FRFs. This may also be due to the closeness of the fourth and fifth modes, and possibly to slight variations in the speed of rotation that occurred during the measurement of the two sets of FRFs.

5.3.9.2 Prediction of FRFs corresponding to unmeasured columns of the FRF matrix

Although some of the elements of the left eigenvectors were inaccurately predicted, their estimation is good enough to allow us to make reasonable predictions of the FRFs corresponding to various locations of the excitation force, using only data measured with one exciter location.

The practical value of this type of capability is that it relaxes the need to install an exciter at several DOFs to determine how a machine structure will respond to forces applied onto them. This predictive capability is especially useful when it is desired to determine the response caused by a force applied at a rotating component, since without this alternative it would be necessary to actually attach an exciter to the rotating component in order to measure the ensuing response, which is a task that poses many practical problems [22].

In the present case study, the FRFs corresponding to an excitation applied at DOF 25 were measured at each of the 26 DOFs defined for the tests, which were defined in Section 5.3.5. The modal analysis of these data led to the identification of six eigenvalues and a set of six right eigenvectors, consisting of six elements each. These modal parameters were then used to compute the left eigenvectors of the test structure corresponding to the same modes and the same DOFs.

The combined use of the parameters to predict the response of the test structure to an excitation applied at DOFs other than DOF 25 will now be illustrated. The prediction of the response is based on the modal expansion of the FRF functions that was presented in Equation (4.22).

As a first example, the predicted response at DOF 25 due to an excitation applied at DOF 26 with the rotor of the test structure spinning at 831 rev/min in a CCW sense is plotted in Figure 5.17. It is compared with its corresponding measurement from the ‘reference’ FRF set, which, as was discussed in Section 5.3.1.2, consists of the response at DOF 26 due to an excitation applied at DOF 25 with the rotor spinning in CW sense.

As can be seen in Figure 5.17, good agreement between the measurement and the prediction is achieved in both the amplitude and the phase plots. However, it is worth mentioning that some discrepancy exists for the frequency region around 21.5 Hz, which may be due to the errors in the identified left eigenvectors for the fourth and fifth modes. As discussed previously, these errors may be caused by the closeness of the two modes and the difficulty to estimate their right eigenvectors and eigenvalues. Both the amplitude and phase plots show discrepancies between the predicted and the measured values around this region of the plot.

The sharp spike that appears at about 13 Hz is the 1X component of vibration, which is possibly due to the residual unbalance of the rotor.

The predicted response at DOF 25 due to an excitation applied at DOF 23 with the rotor of the test structure spinning at 831 rev/min in a CCW sense is plotted in Figure 5.18. It is compared with its corresponding measurement, which is that of the response at DOF 23 due to an excitation applied at DOF 25 with the rotor spinning in CW sense. Similarly, the predicted response at DOF 25 due to an excitation applied at DOF 24 is compared in Figure 5.19 and with its corresponding measurement.

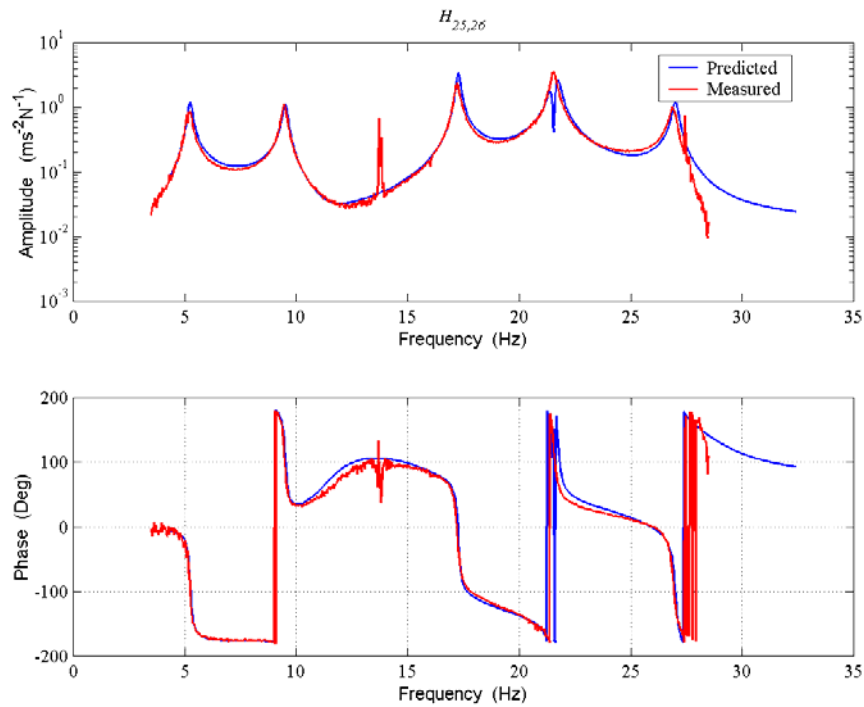


Figure 5.17 – Prediction of the accelerance at DOF 25 due to an excitation at DOF 26

DOFs 23 and 24 lie on the rotating shaft. Hence the practical value of predicting the response due to excitation forces applied at these DOFs is that it allows us to dispense with the complicated alternative of attaching an exciter onto this component in order to measure the response that would ensue under those conditions.

As can be seen in Figures 5.18 and 5.19, although the effects of measurement noise are clearly visible from the plots, the response is predicted with reasonable accuracy. The prediction of the response in the vicinity of 21.5 Hz is in error due to the closeness of the fourth and fifth modes. The peaks around 13 and 26 Hz correspond to the 1X and 2X components of vibration.

It can be seen in Figure 5.18 that the prediction of the response to an excitation applied at DOF 23 is slightly in error for the resonance region of the second mode. This may be due to the fact that DOF 23 is in the horizontal direction and the second mode of vibration consists of a vertical vibration of the test structure. Conversely, in Figure 5.19 it can be seen that the prediction of the response to an excitation at DOF 24 is slightly in

error for the first resonance region. This may be due to the fact that the first mode of vibration of the test structure consists of a horizontal motion, but DOF 24 corresponds to a vertical movement of the shaft.

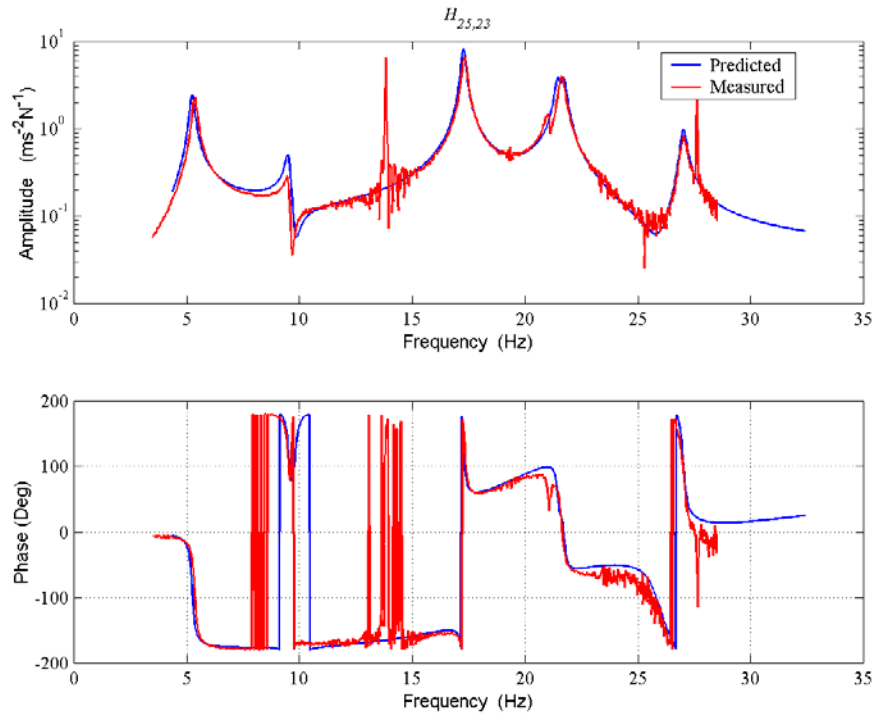


Figure 5.18 – Prediction of the accelerance at DOF 25 due to an excitation at DOF 23

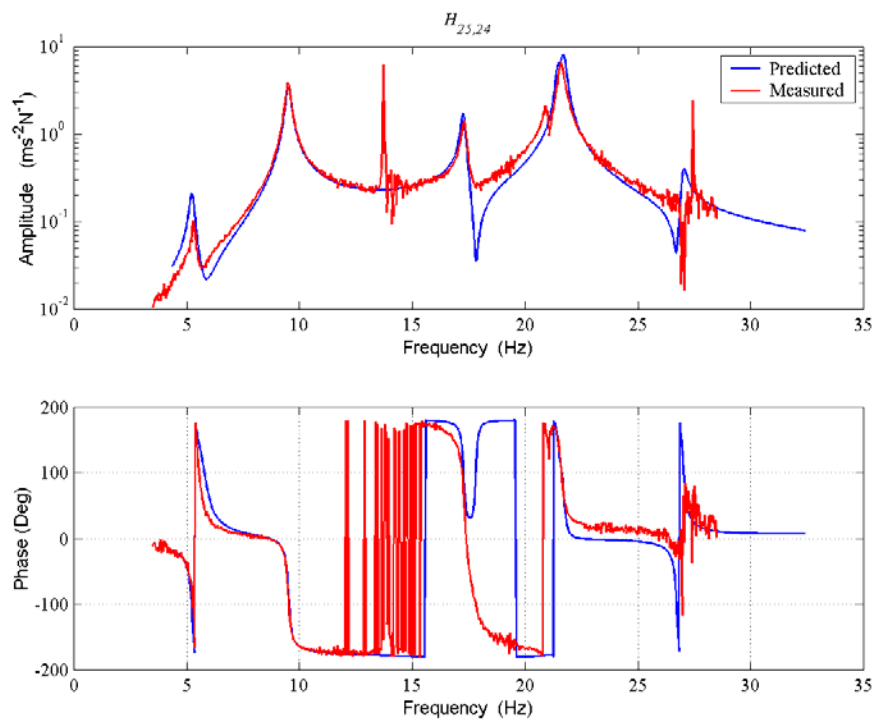


Figure 5.19 – Prediction of the response at DOF 25 due to an excitation at DOF 24

The predicted response at DOF 25 due to excitation forces applied at DOFs 6 and 13, respectively, with the rotor of the test structure spinning at 831 rev/min in a CCW sense are presented in Figures 5.20 and 5.21. Again, there is good agreement between the predicted and the measured responses, both in amplitude and in phase characteristics.

In the first of these Figures, a noticeable prediction error around the resonance region of the sixth mode can be seen. This error is probably caused by that mode not being effectively excited by a force applied at DOF 6.

5.3.9.3 Simplified prediction of the left eigenvectors

In some types of system, such as stationary structures or undamped gyroscopic systems, the left eigenvectors may be directly determined from their right counterparts without the need of any special computation method. For this reason, it is worth exploring the benefits and drawbacks of this approach in the present case study.

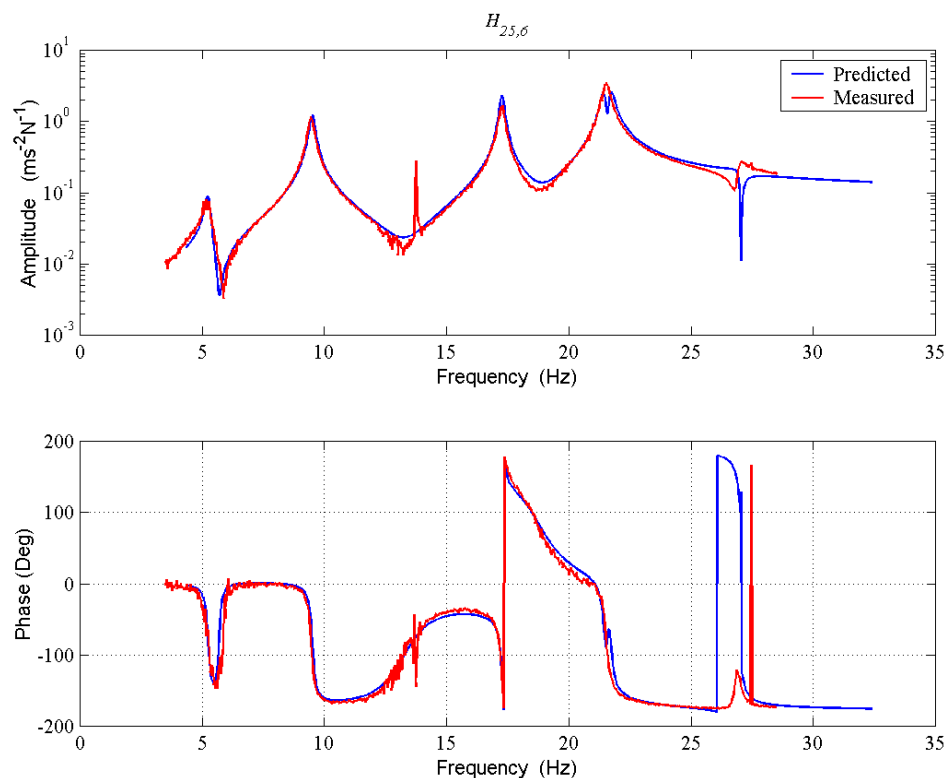


Figure 5.20 – Prediction of the response at DOF 25 due to an excitation at DOF 6

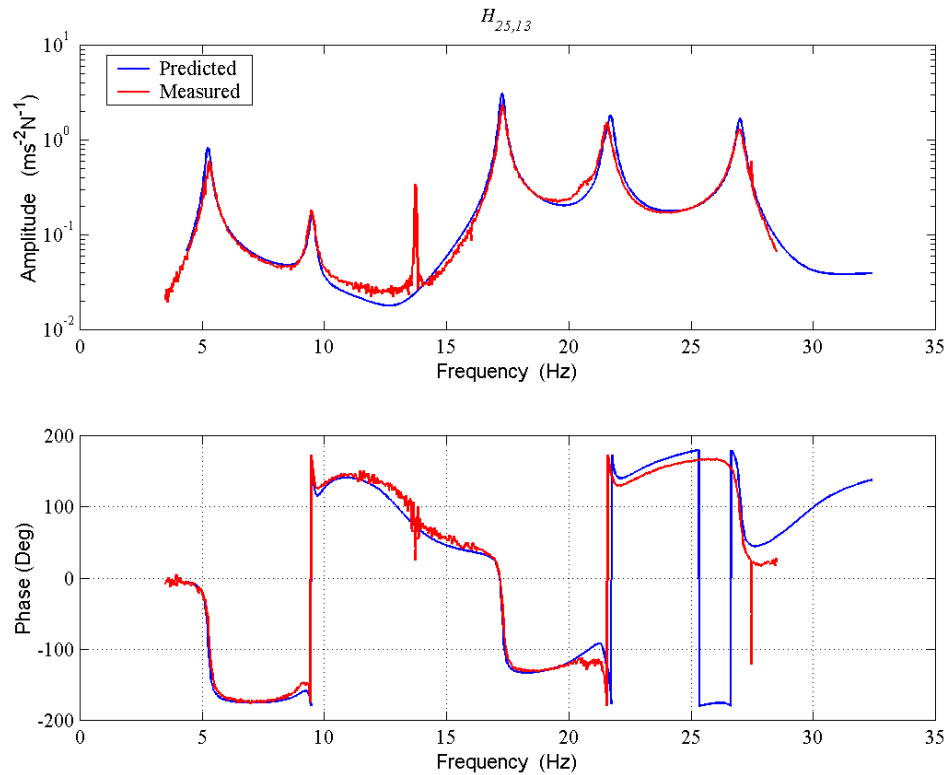


Figure 5.21 – Prediction of the response at DOF 25 due to an excitation at DOF 13

Figure 5.22 shows a prediction of the FRF associated with the response at DOF 25 caused by an excitation applied at DOF 26 with the rotor spinning in a CCW sense. As for the case of Figure 5.17, this prediction is compared with its corresponding measurement, which consists of the response at DOF 26 due to an excitation applied at DOF 25 with the rotor spinning in CW sense. However, in contrast to that case, here the prediction is carried out under the assumption that the left eigenvectors are identical to their right counterparts, as happens with conventional stationary structures.

It can be seen that the amplitude of the FRF is fairly well predicted. However, significant errors are manifested in the phase of the predicted response. Thus, applications which rely on phase measurements, such as the detection of rotor unbalance, should not make use of this simplified predictive approach.

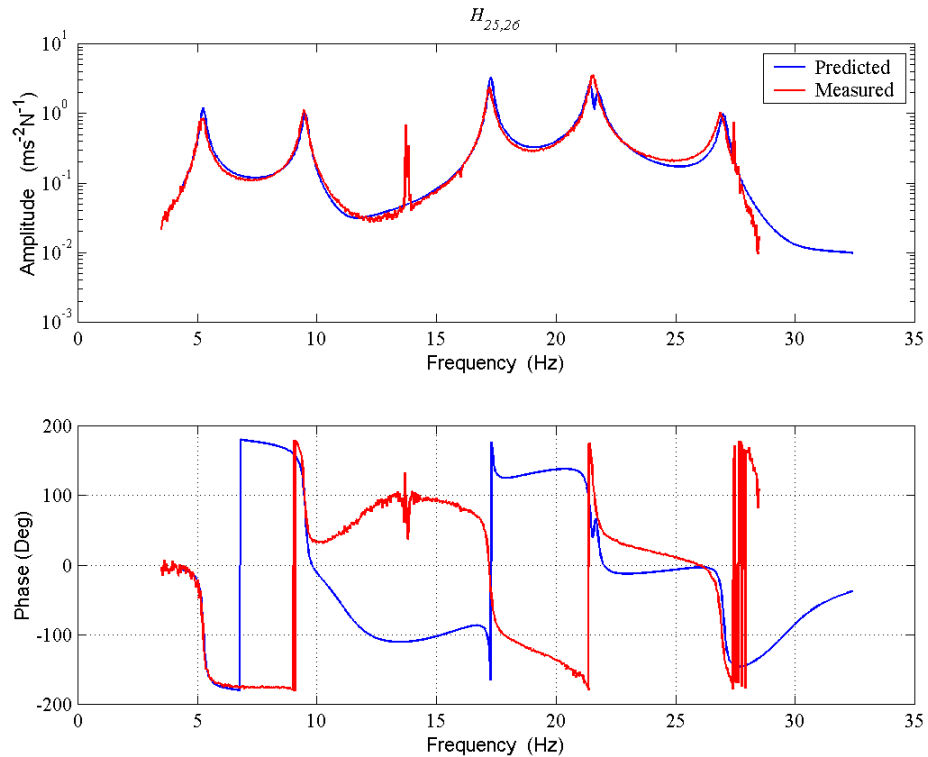


Figure 5.22 – Prediction of the response at DOF 25 due to an excitation at DOF 26 using the right eigenvectors only

A prediction of the same response can be carried out assuming that the left eigenvectors are identical to the complex conjugates of their right counterparts, as occurs in undamped gyroscopic systems. The predicted response at DOF 25 caused by an excitation applied at DOF 26 with the rotor spinning in a CCW is compared with its corresponding measurement in Figure 5.23. The prediction of the FRF amplitude may be seen to be slightly worse in this example than in the former one, and its phase characteristics can be seen to be considerably in error.

It may be concluded that, in the present case study, simplified predictions like the ones just carried allow determining the amplitude of an FRF with reasonable accuracy, but that the prediction of its phase characteristics is considerably in error. In comparison to these simplified approaches, the predictive characterisation method allows us to make more accurate predictions of the response that would be produced by excitation forces applied to different DOFs of a test-piece.

5.3.9.4 Use of non-optimal DOFs

On occasions, it may be necessary to determine the FRFs at DOFs other than those deemed optimal using the effective independence algorithm. It may then be necessary to sacrifice, to some extent, the accuracy of the predicted modal parameters or FRFs, so that the required information can be obtained.

The effect of selecting non-optimal DOFs on the accuracy of the predictions will vary depending on the DOFs selected. When only a few of the DOFs that constitute the optimal set are replaced by others, the accuracy of the predictions may only be affected slightly. For example, if the prediction of the FRF presented in Figure 5.17 is carried out using the replacing DOFs 6 and 13 in the optimal set with DOFs 3 and 4, then the result will be that shown in Figure 5.24.

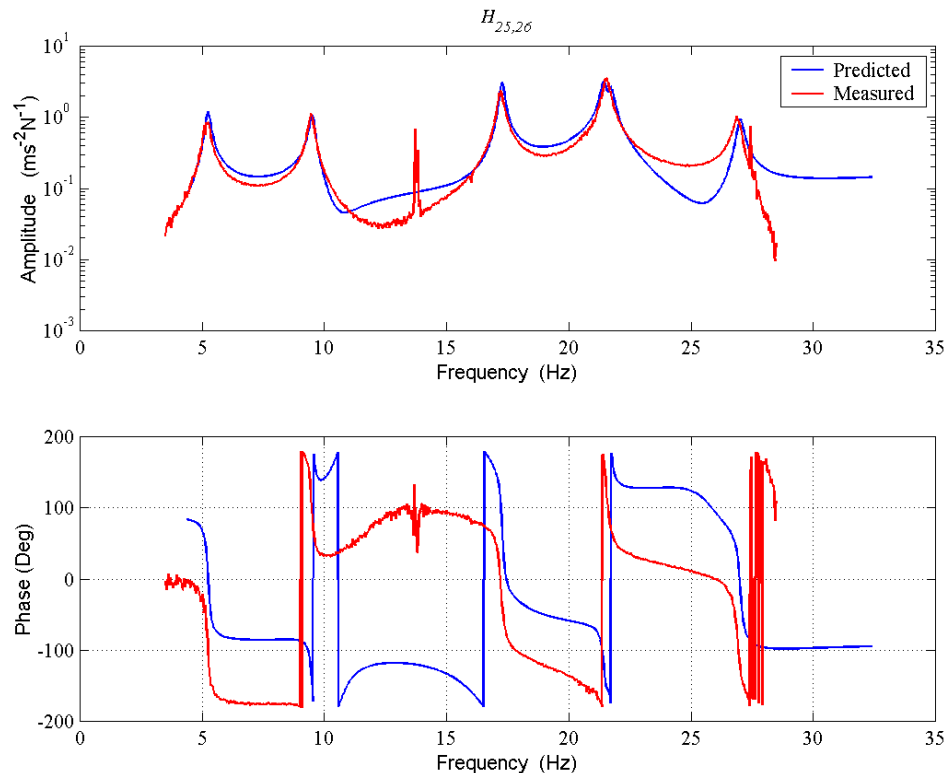


Figure 5.23 – Prediction of the response at DOF 25 due to an excitation at DOF 26 using the right eigenvectors and their complex conjugates

As can be seen in Figure 5.24, the predicted FRF matches the measured one closely. The discrepancies are mainly noticeable near the resonance region of the sixth mode, both in the amplitude and phase plots.

If the non-optimal set is further degenerated by replacing even more DOFs of the optimal set by other DOFs, then the response could be similar to that presented in Figure 5.25, where the DOFs chosen for the prediction were 3, 4, 9, 12, 25 and 26. As can be seen, in this case both the amplitude and phase of the predicted FRF are considerably in error.

From these examples, it may be concluded that an adequate selection of the DOFs is necessary to obtain an accurate prediction of unmeasured row elements of the FRF matrix.

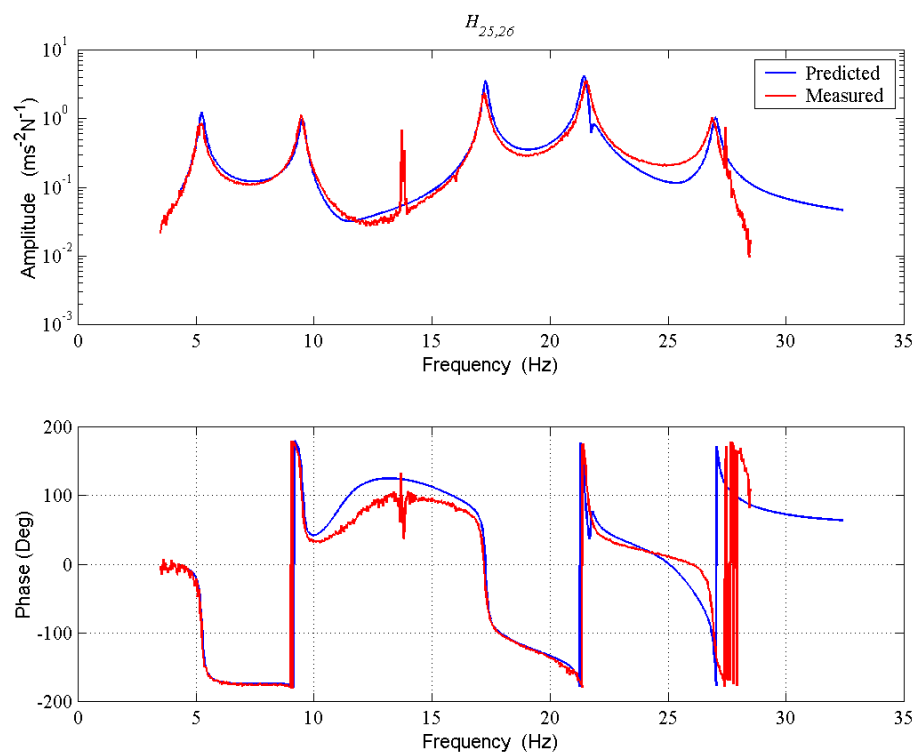


Figure 5.24 – Prediction of the response at DOF 25 due to an excitation at DOF 26 computed with DOFs 3, 4, 23, 24, 25 and 26

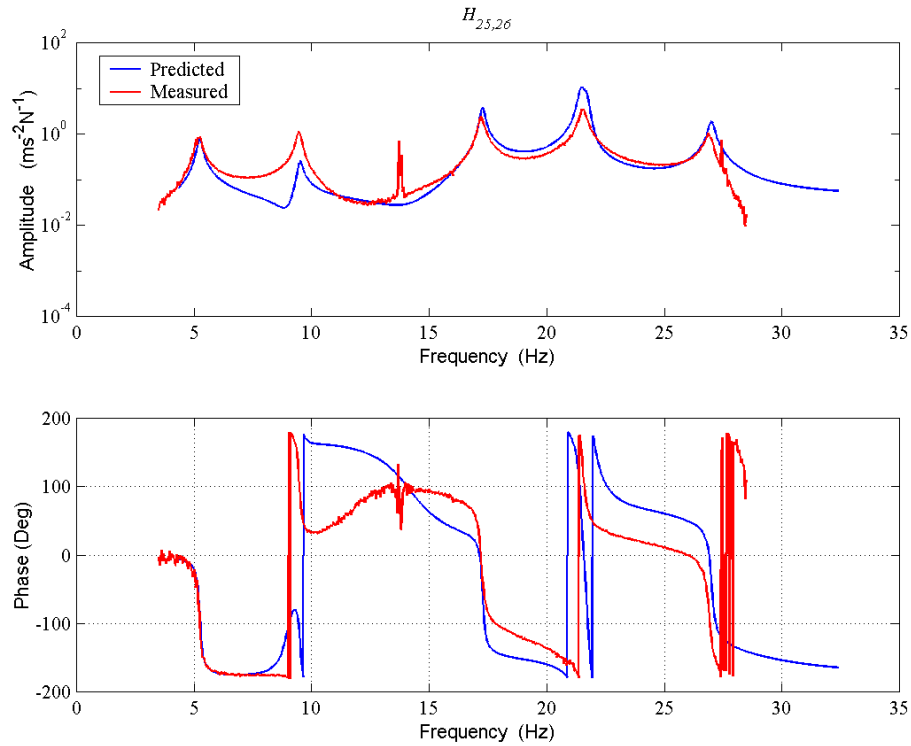


Figure 5.25 – Prediction of the response at DOF 25 due to an excitation at DOF 26 computed with DOFs 3, 4, 9, 12, 25 and 26

5.4 Summary

In this Chapter, the application of the modal characterisation method presented in Chapter 4 has been illustrated using two case studies. The first of these was carried out on the computer model of a 4-DOF rotor and was used to demonstrate the feasibility of obtaining the complete model of a system without the need to measure a complete row, in addition to a column, of its matrix of FRFs.

The second case study was performed on an industrial test structure. The purpose of this case study was to demonstrate the applicability of the abovementioned characterisation method to real systems. This task required taking into consideration two factors that did not appear in the first case study: (a) the fact that the test structure is a continuous system and hence its characterisation required establishing a way to describe it as a discrete system, and (b) the presence of noise in the measurements.

It was shown that, if a continuous system can be represented by a truncated model within a limited frequency interval, then it is possible to predict its modal parameters using the characterisation method described in Chapter 4.

It was also shown that the accuracy with which the left eigenvectors could be determined is affected by the accuracy with which the modal constants of the relevant modes can be determined from the measured data. This, in turn, is affected by the presence of noise in the measurements.

The effects of measurement noise were seen to be more prominent for the DOFs at which the response amplitudes were small, or for frequency regions in the vicinity of close modes.

It was shown that in spite of the effects of noise, the predicted left eigenvectors are suitable for the prediction of a complete row of the FRF matrix using only measurements of one of its columns.

It was demonstrated in Section 5.3.9.3 that neglecting the presence of damping or circulatory forces in a system, in order to simplify the prediction of the left eigenvectors, may lead to considerable errors in their determined values. This was demonstrated here the prediction of FRFs corresponding to excitation at locations other than that used to perform the measurements.

With respect to DOF selection, it was demonstrated that the effective independence algorithm can be used to determine DOFs that allow an optimal estimation of the left eigenvectors and the FRFs. It was shown that, although the use of a non-optimal set of DOFs degrades the quality of the predicted parameters, this practice may be resorted to in cases where it is important to consider a specific DOF that was not ranked within the optimal set through the effective independence algorithm.

CHAPTER 6

Summary, conclusions and recommendations for future work

6.1 Summary

This thesis deals with the modal characterisation of rotating machinery using a structural dynamics approach. The work that is reported here is aimed at simplifying the modal characterisation of this class of systems, by minimising the number of frequency response function (FRF) measurements that are required to determine their modal parameters.

Within the scope of this work, rotating machines are considered as structural assemblies of rotating and non-rotating components. The term ‘rotating machinery structures’ is used to refer to such assemblies. The use of a structural approach allows us to carry out their dynamic characterisation exclusively in terms of their response to controlled excitation forces, without focusing on the interactions between their individual components.

It is argued that one of the main differences between rotating machinery structures and conventional, non-rotating, structures is that the former do not abide by the principles of reciprocity. This is reflected in: (a) their spatial models, by the asymmetry of the damping and stiffness matrices; (b) their modal models, by the need to define a left eigenvector for each mode of vibration, in addition to the corresponding eigenvalue and right eigenvector, and (c) their response models, by the asymmetry of their frequency response function (FRF) matrices.

It is shown that the use of a structural dynamics approach allows us to discriminate between the degrees of freedom (DOFs) that are associated with the rotating and the non-rotating components of a machine structure, so that the asymmetric portions of its spatial property matrices can be clearly delimited. This is proved to be advantageous, as it forms the basis for the derivation of the relationships that exist between the parameters that constitute their modal models.

These relationships are implemented in the design of a modal characterisation method, which is presented in the thesis. The goal of the method is to simplify the execution of modal tests by using these relationships to supplement measured FRF data. It is shown that in most cases a complete modal characterisation can be achieved without measuring a complete row of the FRF matrix. The number of elements of this row that are required is established as a function of the number of DOFs associated with the asymmetric regions of the damping and stiffness matrices.

The application of the characterisation method presented here is illustrated using two case studies. The first of these is carried out on the computer model of a 4-DOF rigid rotor. With this case study, the theoretical feasibility of the method is demonstrated and its accuracy in the absence of measurement noise is evaluated.

The second case study deals with the characterisation of an industrial test-rig. With this case study, some of the problems related to the practical application of the proposed characterisation method are highlighted. The discussions regarding the use of the method in this case study are focused on: (a) the effects of measurement noise and of the existence of close modes of vibration on the accuracy of the identified modal parameters; (b) the process of selecting the DOFs used to derive the model of the test-rig; (c) the use of the method for the prediction of the response caused by excitation

forces applied at different DOFs, and (d) the advantages and disadvantages of using simplifying assumptions about the relationships between the right and left eigenvectors.

6.2 Conclusions

The conclusions stated in this Section are based on the objectives of the thesis, which were established in Chapter 1. The conclusions associated with the intermediate objectives (i) to (vi) will be presented first, followed by those corresponding to the main objective of the thesis.

- Conclusions with respect to objective (i): *To develop a strategy for the modelling of rotating machinery that facilitates their study through a structural dynamics approach.*

It is possible to model rotating machinery as structural assemblies of rotating and non-rotating components. This modelling strategy allows us to identify the points, or more generally the DOFs, at which the forces that may contribute to the skew-symmetric components of the damping and stiffness matrices can originate. With this information, it is possible to delimit the asymmetric portions of these matrices.

These asymmetric portions consist of those entries of the matrices that are associated with the DOFs of the machine components that either rotate or support rotating components directly.

This modelling strategy facilitates the study of rotating machinery structures, since it enables the use of the symmetric portions of the damping and stiffness matrices to simplify the relationships that exist between the spatial and modal parameters of these systems.

- Conclusions with respect to objective (ii): *To derive the mathematical relationships that exist between the spatial and the modal parameters of rotating machinery structures.*

The derivation of exact relationships between the spatial and modal parameters of rotating machinery structures requires an elimination of any arbitrary scaling factor used in the description of the right and left eigenvectors. This can be achieved through the use of the normalised versions of the eigenvectors.

The relationships between the spatial and the modal parameters can be expressed in terms of the spatial and modal representations of the receptance, mobility, accelerance and jerk matrices corresponding to (a) a *low frequency limit* for the excitation forces, which was defined as zero in the thesis, and (b) a *high frequency limit*, which was defined as a frequency well above the highest resonant frequency of interest, so that the response corresponding to this value of the excitation frequency could be considered equivalent to that corresponding to an infinitely-high excitation frequency. The derived relationships between the spatial and modal parameters are based on the spatial and modal representations of:

- (a) the receptance matrix associated with an excitation frequency equal to the *low frequency limit*;
- (b) the mobility matrix associated with an excitation frequency equal to either the *low or high frequency limits*;
- (c) the inertance matrix associated with an excitation frequency equal to the *high frequency limit* , and

(d) the matrix that expresses the effect of damping on the rate of change of acceleration, called the jerk matrix, for an excitation frequency equal to the *high frequency limit* .

- Conclusions with respect to objective (iii): *To develop a method for the computation of the left eigenvectors of rotating machinery structures.*

The computation of the left eigenvectors of rotating machinery structures can be based on:

- (a) the relationships that exist between the spatial and modal parameters;
- (b) knowledge of the number of DOFs associated with the symmetric regions of the damping and stiffness matrices, and
- (c) the measurement of one complete column of the FRF matrix, plus a number of elements from one of its rows.

The combination of (a) and (b) allows us to establish relationships between the modal parameters of rotating machinery structures. These relationships were given in Section 4.5.1.2.

The computation of the left eigenvectors can be based on supplementing the measurements of the FRFs with these relationships, so that the number of FRF measurements that are needed to determine those parameters can be minimised.

The combined use of (a), (b) and (c) enables us to derive a linear system of equations in which the unknowns are the elements of the left eigenvectors, and the coefficients that define each of the equations can be determined directly from the measured FRFs.

The solution to the system of equations can be carried out with conventional procedures. The generalised pseudo-inverse matrix method [3] was used in the examples presented in the thesis.

- Conclusions with respect to objective (iv): *To determine the conditions in which simpler measurement schemes than the ones currently used for the modal testing of rotating machinery structures can be devised.*

In most cases, the complete modal characterisation of rotating machinery structures can be carried out without the need to measure a complete row of their FRF matrices, provided that not every DOF of the system is associated with the asymmetric portions of the damping and stiffness matrices.

In general, the number of elements of the FRF matrix that need to be measured depends on the total number of DOFs of the system and on the number of these DOFs associated with the asymmetric portions of the damping and stiffness matrices. If these numbers are known, then it is possible to compute how many row elements of the FRF matrix are required to determine the complete modal model.

The number of left eigenvector elements that need to be determined directly from measured data grows with the size of the asymmetric regions of the spatial property matrices. For this reason, rotating machinery structures in which only a few of the DOFs lie on its rotating components can be identified with fewer FRF measurements than can systems of the same order but with a larger number of DOFs lying on their rotating components.

The modal parameters of systems in which only one spatial property matrix is asymmetric can be identified from measurements of just one column of the FRF matrix.

A closed-form solution was obtained for these cases, which include the important class of damped gyroscopic systems.

- Conclusions with respect to objective (v): *To design a method for the modal characterisation of rotating machinery structures.*

The modal characterisation of rotating machinery structures may be based on the relationships found between the modal parameters and the computational method used to determine the left eigenvectors. The method presented in the thesis consists of the steps given in Section 4.9.

- Conclusions with respect to objective (vi): *To evaluate the applicability of the method to practical systems.*

The use of the characterisation method presented in the thesis requires representing a rotating machine structure using a truncated model. Thus, it may be applied to practical, continuous systems, provided that their dynamic response within the frequency range of interest can be closely represented through the superposition of a finite number of modal components.

The accuracy with which the left eigenvectors can be determined is affected by the accuracy with which the modal constants of the relevant modes can be determined from the measured data. This accuracy is in turn affected by the presence of noise in the measurements.

The effects of measurement noise are likely to be more prominent for the DOFs at which the response amplitudes were small, or for frequency regions in the vicinity of close modes.

In spite of the effects of noise, the values of the left eigenvectors determined through the proposed method are suitable for the prediction of a complete row of the FRF matrix.

Neglecting the presence of damping or circulatory forces in a system, in order to simplify the prediction of the left eigenvectors, may lead to considerable errors in their determined values. This was demonstrated here through the prediction of FRFs corresponding to excitation at locations other than that used to perform the measurements.

The effective independence algorithm can be used to determine which DOFs should be considered in order to produce accurate estimations of the left eigenvectors based on measured FRF data.

Although the use of a non-optimal set of DOFs degrades the quality of the predicted parameters, this practice can be resorted to in cases where it is important to consider a specific DOF that was not ranked within the optimal set through the effective independence algorithm.

- Conclusions with respect to the main objective of the research work: *to simplify the modal testing procedure, with respect to existing ones, by means of which the modal parameters of rotating machinery structures are determined from measured response data.*

The modal characterisation method that was developed as part of this work enables a reduction in the number of measurements required for the identification of the modal parameters of rotating machinery structures. Moreover, the measurements that can be avoided through the use of this method are those that have been deemed the most problematic in existing measurement schemes, due mainly to limitations of the current

techniques for the application of excitation forces onto rotating components, and for the measurement of these forces.

The work that has been presented in this thesis demonstrates that it is possible to characterise the dynamic behaviour of rotating machines using a structural dynamics approach.

The developments that constitute this work enable a significant reduction of the time and effort required to perform the modal characterisation of rotating machinery structures.

6.3 Recommendations for future work

The work that has been presented in this thesis covers the theoretical formulation and validation of a modal characterisation method for rotating machinery structures. Further improvements to the method may result from research work regarding the following issues:

- (a) characterisation of systems with close modes,
- (b) use of residuals for the analysis of continuous systems using truncated models,
and
- (c) diversification of the experimental trials.

These issues will be described in more detail in the following Sections.

6.3.1 Characterisation of systems with close modes

It was discussed in Chapter 5 that the accuracy with which the left eigenvectors are estimated is affected by the existence of close structural modes. It is important to take

this effects into account, since it is likely that rotating machinery structures possess modes of this kind due to the axisymmetric construction of some of their components, especially the rotating ones.

The accuracy with which the all the left eigenvectors of a rotating machine are estimated is affected by the accuracy with which the eigenvalues and the right eigenvectors of the close modes are determined from the measured FRF data.

A possible continuation of the work presented here is to modify the procedures for the selection of DOFs to be used in the computation of the left eigenvectors, so that they allow us to identify the right eigenvectors and eigenvalues associated with the close modes with the highest possible accuracy.

6.3.2 Use of residuals for the analysis of continuous systems

In the study of non-rotating structures, the use of residual modes may greatly improve the frequency response characteristics of a model, so that it more closely matches those of the physical system that it represents.

In a similar way, residuals may be used to improve the representation of a rotating machine structure through a finite order model. Thus, it may be possible to improve estimations of the left eigenvectors in cases where there is significant influence from modes lying outside the frequency range of interest.

The inclusion of residual modes in the computation of the left eigenvectors may be particularly useful in cases where the dynamic behaviour of a rotating machine structure cannot be satisfactorily described, within the frequency range of interest, in terms of the components of vibration associated with the modes whose natural frequencies fall

within this range. This can occur, for example, when the natural frequencies of the out-of-range modes are close to one of the limits of the frequency range of interest.

The identification of residues is a standard feature in some commercial modal analysis packages¹. Hence, an immediate continuation of the work presented here consists of determining a way in which the information regarding residual modes can be incorporated into the computation of the left eigenvectors.

6.3.3 Diversification of the experimental trials

Although the characterisation method presented in this thesis was demonstrated to be theoretically sound, its development into a reliable engineering tool requires further verification through experimental trials conducted under different conditions. Specifically, the use of the method for the characterisation of different types of rotating machinery structures, in which the asymmetry of both the damping and stiffness matrices is broken by the effects of circulatory forces, would be a valuable aid in understanding not only the potential of the method, but also its practical limitations. This would also enable the development of corrective procedures for the results obtained through it and a better assessment of its overall accuracy under different scenarios.

¹ For example, the Imperial College Analysis and Testing Software (ICATS)

Appendix A

Row elements of the FRF matrix required for computation of the left eigenvectors

Table A.1 presents the number of row elements of the FRF matrix, q , required for computation of the left eigenvectors of systems with 15 DOFs ($N = 15$) for cases with different sizes of the asymmetric regions of the damping and stiffness matrices, represented by the parameters n_c and n_k , respectively.

The value of q is that required to simultaneously satisfy the three inequalities (4.56)-(4.58), which are restated here as (A.1)-(A.3):

$$q \geq 1 \quad (\text{A.1})$$

$$q \geq \sqrt{n_c^2 + n_k^2} - N + 1 \quad (\text{A.2})$$

$$q \geq \max(n_c, n_k) - 2[N - \min(n_c, n_k)] \quad (\text{A.3})$$

Table A.1 - Required row elements, q , of the FRF matrix for a 15-DOF system

$n_c \backslash n_k$	0	2	3	4	5	6	7	8	9	10	11	12	13	14	15
0	1	1	1	1	1	1	1	1	1	1	1	1	1	1	1
2	1	1	1	1	1	1	1	1	1	1	1	1	1	1	2
3	1	1	1	1	1	1	1	1	1	1	1	1	1	1	2
4	1	1	1	1	1	1	1	1	1	1	1	1	1	1	2
5	1	1	1	1	1	1	1	1	1	1	1	1	1	1	2
6	1	1	1	1	1	1	1	1	1	1	1	1	1	2	3
7	1	1	1	1	1	1	1	1	1	1	1	1	1	2	3
8	1	1	1	1	1	1	1	1	1	1	1	1	2	3	3
9	1	1	1	1	1	1	1	1	1	1	1	1	2	3	4
10	1	1	1	1	1	1	1	1	1	1	1	2	3	4	5
11	1	1	1	1	1	1	1	1	1	1	3	4	5	6	7
12	1	1	1	1	1	1	1	1	1	2	4	6	7	8	9
13	1	1	1	1	1	1	1	2	2	3	5	7	9	10	11
14	1	1	1	1	1	2	2	3	3	4	6	8	10	12	13
15	1	2	2	2	2	3	3	3	4	5	7	9	11	13	15

The coloured areas in the previous Table indicate which of the three inequalities requires more FRF row element measurements to be satisfied, and hence determines the value of q for each specific case.

The blue coloured areas correspond to the values of n_c and n_k for which inequality (A.1) imposes the highest value of q . Similarly, the yellow and pink areas correspond to the cases in which the highest value of q is that required to satisfy inequalities (A.2) and (A.3), respectively.

As can be seen from the Table, in most cases it is possible to determine the left eigenvectors with the measurement of only one row element of the FRF matrix, in addition to the measurement of one complete column. For systems in which the asymmetric regions of the damping and stiffness matrices are associated with greater numbers of DOFs, more row elements of the FRF matrix are required to determine the left eigenvectors. The extreme case is that in which these regions of the system property matrices are associated with every DOF ($n_c = n_k = N$). In this case, a complete row of the FRF matrix must be measured, apart from a complete column, in order to determine the left eigenvectors. This corresponds to the requirements of the ‘column-row’ method described in Chapter 1.

Appendix B

Relationship between the modal constants of hysteretically- and viscously-damped system models

In a hysteretically damped system model, the receptance FRFs are expressed as a sum of modal components of the form:

$$\alpha_{jk}(\omega) = \sum_{r=1}^N \frac{{}_r \tilde{A}_{jk}}{\omega_r^2 (1 + i\eta_r) - \omega^2} \quad (\text{B.1})$$

where ω is the excitation frequency, ω_r and η_r are the natural frequency and hysteretic damping constant of the r th mode, respectively, and ${}_r \tilde{A}_{jk}^*$ is its corresponding modal constant for the j th response measurement location and the k th excitation location.

Similarly, in a viscously damped system model, the receptance FRFs are expressed as a sum of modal components of the following form:

$$\alpha_{jk}(\omega) = \sum_{r=1}^N \left(\frac{{}_r A_{jk}}{i\omega - \lambda_r} + \frac{{}_r A_{jk}^*}{i\omega - \lambda_r^*} \right) \quad (\text{B.2})$$

where ω is the excitation frequency, λ_r is the natural frequency and viscous damping constant of the r th mode, respectively, and ${}_r A_{jk}^*$ is its corresponding modal constant for the j th response measurement location and the k th excitation location.

For any given system, two sets of modal constants can be determined separately, depending on whether the system is assumed to be hysteretically or viscously damped. However, for lightly damped systems, a relationship between both sets of constants that is valid near the modal resonances can be established.

If the hysteretically and viscously damped representations of a specific modal component of a receptance FRF, say that of the r th mode, are equated then the relevant modal constants should satisfy the equation:

$$\frac{{}_r \tilde{A}_{jk}}{\omega_r^2 (1 + i\eta_r) - \omega^2} = \frac{{}_r A_{jk}}{i\omega - \lambda_r} + \frac{{}_r A_{jk}^*}{i\omega - \lambda_r^*} \quad (\text{B.3})$$

For lightly damped systems, this expression may be rewritten as:

$$\frac{{}_r \tilde{A}_{jk}}{\omega_r^2 - \omega^2} \approx \frac{{}_r A_{jk}}{i(\omega - \omega_r)} + \frac{{}_r A_{jk}^*}{i(\omega + \omega_r)} \quad (\text{B.4})$$

Furthermore, near the resonance of the r th mode this expression may be further simplified:

$${}_r A_{jk} \approx \frac{{}_r \tilde{A}_{jk}}{2i\omega_r} \quad (\text{B.5})$$

Thus, given the modal constants that correspond to either a hysteretically or a viscously damped system model, those for the other type of model may be directly determined using Equation (B.5).

Appendix C

Modal parameters of the “windmill test-rig”

Modal parameters of the windmill test-rig obtained from one column of the FRF matrix corresponding to an excitation applied at DOF 25 with the main rotor spinning at 813 rev/min in a counter-clockwise (CCW) sense, as seen from the bulkhead side.

TABLE C.1 – Modal parameters of the “windmill test-rig”

MODE r	MEASURED λ_r [rad/sec]		DOF	MEASURED $\{\Phi_R\}_r$, CCW		MEASURED $\{\Phi_L\}_r$, CCW	
	REAL	IMAG		MAG	ANGLE	MAG	ANGLE
1	-0.5957	32.8607	6	0.0021	137.3000	0.0019	133.96
			13	0.0182	132.8900	0.0183	135.07
			23	0.0535	131.5200	0.0539	135.23
			24	0.0055	164.8300	0.0050	99.61
			25	0.0249	-45.0200	0.0249	-45.02
			26	0.0260	133.8200	0.0264	135.16
2	-0.6367	59.6812	6	0.0159	129.6600	0.0164	141.35
			13	0.0019	-128.7300	0.0018	16.62
			23	0.0043	-35.5200	0.0062	-35.52
			24	0.0474	125.1400	0.0483	140.79
			25	0.0131	-45.6800	0.0131	-45.68
			26	0.0137	-62.3800	0.0148	-31.28
3	-0.5212	108.4761	6	0.0083	-175.3200	0.0088	85.74
			13	0.0112	98.3400	0.0116	174.21
			23	0.0290	-79.9900	0.0304	-1.27
			24	0.0072	-14.2300	0.0064	-46.28
			25	0.0119	-44.4900	0.0119	-44.49
			26	0.0121	64.8700	0.0128	-151.63
4	-0.7350	134.7384	6	0.0136	108.1800	0.0107	136.80
			13	0.0041	-154.5500	0.0013	121.89
			23	0.0144	19.0000	0.0110	-84.07
			24	0.0224	-64.5200	0.0150	32.25
			25	0.0096	-49.3100	0.0096	-49.31
			26	0.0110	-86.3800	0.0092	-47.84
5	-0.7333	136.3928	6	0.0092	135.1900	0.0117	161.05
			13	0.0033	-145.6300	0.0072	50.95
			23	0.0083	46.4900	0.0125	-146.91
			24	0.0108	-42.9500	0.0315	-84.98
			25	0.0086	-36.6700	0.0086	-36.67
			26	0.0088	-56.7200	0.0148	11.27
6	-0.7799	169.6593	6	0.0004	74.7500	0.0011	-110.47
			13	0.0076	-40.8900	0.0091	-24.96
			23	0.0043	-32.1000	0.0056	-26.80
			24	0.0009	-98.0000	0.0025	-8.95
			25	0.0049	-44.5200	0.0049	-44.52
			26	0.0053	143.9000	0.0071	119.12

r = Mode number, λ_r = Eigenvalue, $\{\Phi_R\}_r$ = Right eigenvector, $\{\Phi_L\}_r$ = Left eigenvector

References

- [1] Adams, M.L., "Insights into linearized rotor dynamics, part 2", *Journal of Sound and Vibration*, vol. 112, no. 1, pp. 97-110, January 1987.
- [2] Argyris, J.H. and Straub, K., "Nonlinear finite element analysis of elastic systems under nonconservative loading-natural formulation - 2. Dynamic problems", *Computer Methods in Applied Mechanics and Engineering*, vol. 28, no. 2, pp. 241-258, September 1981.
- [3] Atkinson, K.E., **An introduction to numerical analysis**, Section 9.7 – Least squares solution to linear systems, John Wiley and Sons, Inc., Singapore 1988.
- [4] Barnett, S., **Matrix methods for engineers and scientists**, McGraw-Hill, London 1979.
- [5] Betti, E., *Il Nuovo Cimento*, Series 2, vols. 7 and 8, 1872.
- [6] Brown, G.V., Kielb, R.E., Meyn, E.H., Morris, R.E. and Posta, S.J., *Lewis Research Center spin rig and its use in vibration analysis of rotating systems*, NASA Technical Papers 2304, Cleveland, Ohio, May 1984.
- [7] Bucher, I., "A helical transformation for rotating shafts allowing a simplified experimental procedure", *Proceedings of the 7th International Conference on Vibrations in Rotating Machinery*, Institution of Mechanical Engineers, Nottingham, U.K., September 2000.
- [8] Bucher, I. and Braun, S.G., "Left eigenvectors: extraction from measurements and physical interpretation", *ASME Journal of Applied Mechanics*, vol. 64, no. 1, March 1997, pp. 97-105.
- [9] Bucher, I., Ewins, D.J. and Robb, D.A., "Modal testing of rotating structures: difficulties, assumptions and practical approach", *6th International Conference of Vibration in Rotating Machinery*, Proceedings of the Institution of Mechanical Engineers, Oxford, 1996.

- [10] Childs, D., **Turbomachinery rotordynamics: phenomena, modeling and analysis**, Section 3.4 – Static characteristics and stiffness and damping coefficients for plain journal bearings, John Wiley and Sons, New York 1993.
- [11] Dai, X., Jin, Z. and Zhang, X., “Dynamic behavior of the full rotor/stop rubbing: Numerical simulation and experimental verification”, *Journal of Sound and Vibration*, vol. 251, no. 5, pp 807-822, April 2002.
- [12] Ehrich, F.F., **Handbook of Rotordynamics**, Chapter 1: Vibration considerations in the design of rotating machinery, McGraw-Hill, 1992.
- [13] Earles, S. W. E. and Badi, M. N. M., “Oscillatory instabilities generated in a double-pin and disc undamped system: a mechanism of disc-brake squeal”, *Proceedings of the Institution of Mechanical Engineers, Part C: Mechanical Engineering Science*, vol. 198, no. 4, pp. 43-50, 1984.
- [14] Ewins, D.J., **Modal testing: Theory, practice and application**, Research Studies Press, Baldock, Hertfordshire, England, 2000.
- [15] Ewins, D.J., "Modal Analysis for Rotating Machinery", *Proceedings of the NATO advanced Study Institute, Sesimbra, Portugal, May 1998*.
- [16] Gutierrez-Wing, E.S. and Ewins, D.J., "Effects of non-reciprocity on the modal properties of rotating structures", *Proceedings of the 18th International Modal Analysis Conference, San Antonio, Texas, February 2000*.
- [17] Gutierrez-Wing, E.S. and Ewins, D.J., "Test planning for rotating machinery", *Proceedings of the COST Conference, Kassel, Germany, September 2001*.
- [18] Holopainen T., Tenhunen A. and Arkkio A., “Electromagnetic circulatory forces and rotordynamic instability in electric machines”, *Proceedings of the Sixth International Conference on Rotor Dynamics (IFTOMM)*, pp. 446–463, Sydney, Australia, September 2002.
- [19] Inman, D.J., **Vibration with control, measurement and stability**, Chapter 2: Lumped parameter models, Prentice-Hall, Inc., New Jersey, 1989.

- [20] Jei, Y.G. and Kim, Y.J., "Modal testing theory of rotor-bearing systems", Transactions of the ASME Journal of Vibration and Acoustics, vol. 115, no. 2, pp. 165-176, April 1993.
- [21] Jei, Y. G. and Lee, C.W., "Modal analysis of continuous asymmetrical rotor-bearing systems", Journal of Sound and Vibration, vol. 151, no. 2, pp. 245-262, January 1992.
- [22] Joh, Y.D. and Lee, C.W., "Excitation methods and modal parameter identification in complex modal testing of rotating machinery", International Journal of Analytical and Experimental Modal Analysis, vol. 8, no. 3, pp. 179-203, July 1993.
- [23] Kammer, D.C., "Sensor placement for on-orbit modal identification and correlation of large space structures", Journal of Guidance, Control and Dynamics, v 2, n 15, March-April 1991, pp 251-259.
- [24] Kessler, C., **Complex modal analysis of rotating machinery**, Ph. D. Thesis, Department of Mechanical, Industrial and Nuclear Engineering, College of Engineering, University of Cincinnati, 1999.
- [25] Kimball, A. L., "Internal friction theory of shaft whirling", General Electric Review, vol. 27, no. 4, pp. 244-251, April 1924.
- [26] Kraemer, E., **Dynamic of rotors and foundations**, Chapter 6: Oil-film bearings, pp. 77-96, Springer-Verlag, Berlin 1993.
- [27] Lancaster, P., **Theory of matrices**, Academic Press, New York 1969.
- [28] Lathi, B.P., **Signals, systems and communications**, Wiley, John & Sons, Incorporated, New York , January 1965
- [29] Lee, C.W., "A complex modal testing theory for rotating machinery", Mechanical Systems and Signal Processing, vol. 5, no. 2, pp. 119-137, March 1991.
- [30] Lee, C.W., **Vibration analysis of rotors**, Kluwer Academic Publishers, 1993.
- [31] Maxwell, J.C., "On the calculation of the equilibrium and stiffness of frames", Philosophical Magazine, vol. 27, pp. 294-299, 1864.

- [32] Meirovitch, L., "A new method for the solution of the eigenvalue problem for gyroscopic systems", *AIAA Journal*, vol. 12, no. 10, pp. 1337-1342, October 1974.
- [33] Muszynska, A., "Modal testing of rotor/bearing systems", *International Journal of Analytical and Experimental Modal Analysis*, vol. 1, no. 3, pp. 15-34, July 1986.
- [34] Newkirk, B.L., "Shaft whipping", *General Electric Review*, vol. 27, no. 3, pp. 169-178, March 1924.
- [35] Nordmann, R., "Identification of the modal parameters of an elastic rotor with oil film bearings", *Transactions of the ASME Journal of Vibration, Acoustics and Reliability in Design*, v 106, n 1, pp 107-112, January 1984.
- [36] Nordmann, R, **Dynamics of Rotors, Stability and System Identification**, Chapter 4.3: Identification of Modal Parameters of Rotors, Springer Verlag, pp. 371-393, 1984.
- [37] Peeters, F., Pintelton, R., Schoukens, J., Rolain, Y., Gutierrez, E.S. and Guillaume, P., "Identification of rotor-bearing systems in the frequency domain part I: Estimation of frequency response functions", *Mechanical Systems and Signal Processing*, vol. 15, no. 4, pp. 759-773, July 2001.
- [38] Penny, J.E.T., Friswell, M.I. and Garvey, S.D., "Automatic choice of measurement locations for dynamic testing", *AIAA Journal*, v 32, n 2, February 1994, pp 407-414.
- [39] Randall, R.B., **Frequency analysis**, Section 2.4.3 – Pseudo-random signals, Naerum 1987.
- [40] Rogers P.J. and Ewins, D.J., "Modal testing of an operating rotor system using a structural dynamics approach", *Proceedings of the 7th International Modal Analysis Conference*, Las Vegas, Nevada, vol. 1, pp. 466-473, January 1989.
- [41] Sawicki, J.T. and Genta, G., "Modal uncoupling of damped gyroscopic systems", *Journal of Sound and Vibration*, vol. 244, no. 3, pp. 431-451, July 2001.
- [42] Schedlinski, C. and Link, M., "An approach to optimal pick-up and exciter placement", *Proceedings of the 14th International Modal Analysis Conference*, Dearborne, Michigan, February 1996.

- [43] Shieh, R. C., "Effects of damping and circulatory forces on dynamic instability of gyroscopic conservative continuous systems", Transactions of the ASME Journal of Structural Mechanics, vol. 11, no. 2, pp. 197-213, 1983.
- [44] Strutt, J.W., "Some general theorems relating to vibrations", Proceedings of the London Mathematical Society, vol. 4, June 1873.
- [45] Tondl, A., **Some problems of rotor dynamics**, Chapter I: The effect internal damping on the stability of rotor motion and the rise of self-excited vibrations, Chapman and Hall Limited, London 1965.
- [46] Tondl, A., op. cit., Chapter III: The effect of journal bearings on the stability of rotor motion and the onset of self-excited vibrations, pp. 114-207.
- [47] Tuchinda, A., Hoffmann, N. P., Ewins, D. J. and Keiper, W., "Mode lock-in characteristics and instability study of the pin-on-disc system", Proceedings of the 19th International Modal Analysis Conference, vol. 1, pp. 71-77, Kissimmee, Florida, February 2001.
- [48] Wang, W. and Kirkhope, J., "New eigensolutions and modal analysis for gyroscopic/rotor systems, part 1: undamped systems", Journal of Sound and Vibration, vol. 175, no. 2, pp. 159-170, August 1994.
- [49] Zhang, Q., Lallement, G. & Fillod, R. "Relations between the right and left eigenvectors of non-symmetric structural models. Applications to rotors", Mechanical Systems and Signal Processing, vol. 2, no. 1, pp. 97-103, January 1988.
- [50] Zhang, X., Shinshi, T., Li, L. and Shimokohbe, A., "A combined repetitive control for precision rotation of magnetic bearing", Precision Engineering, vol. 27, no. 3, pp. 273-282, July 2003.
- [51] Zheng, Z., Ren, G. and Williams, F.W., "The eigenvalue problem for damped gyroscopic systems", International Journal of Mechanical Sciences, vol. 39, no. 6, pp. 741-750, June 1997.